Predicting the sea surface from high resolution multi-beam FMCW radar data

Gerald van der Geugten

TU Delft RADAC

Predicting the sea surface from high resolution multi-beam FMCW radar data

by

Gerald van der Geugten

to obtain the degree of Master of Science
at the Delft University of Technology,
to be defended publicly on February 11, 2020 at 3:00 PM.

Student number:	4107063	
Thesis committee:	Prof. dr. ir. A.W. Heemink,	TU Delft, supervisor
	Dr. ir. M. B. van Gijzen,	TU Delft
	Dr. J. L. A. Dubbeldam,	TU Delft
	Ir. R. van der Vlugt,	Radac B.V., company supervisor

An electronic version of this thesis is available at `http://repository.tudelft.nl/`.

TU Delft

Abstract

In this thesis a deterministic wave model is used to reconstruct and predict the sea surface motion from FMCW (Frequency Modulated Continuous Wave) radar data, produced by Radac. The deterministic model that is used to do this is based on the linear wave theory. The radar is looking horizontally straight towards the waves in 5 separate beam directions of -40,-20,0, 20 and 40 degrees. Using the FMCW principle the backscatterd signal is converted into velocity and spatial range information. After some compensations (current for example) this velocity data can be treated as horizontal component of the orbital velocity of the wave. By using a least-squares solving approach (the trust-region reflective algorithm) on these orbital velocities and the expression that holds for them in the linear wave theory the model can be fitted to the measurements. The result of the least squares solver consists of a set of parameters for wave amplitude, phase and frequency. With these parameters the deterministic motion of the sea surface can be computed. This method is tested using artificial data and a generalized one directional case (using information from 1 beam under assumption of infinitely long-crested waves).
For the experiments with artificial data consisting of waves with $H_s = 2$ meters (significant waveheight) the results are promising. A prediction time of 30 seconds over a range of 150 meters with an average error of 15 cm in the one directional model (fitted on 10 second data over 384 meters) can be achieved. For the multi directional model this lies between 20 and 30 seconds with an average error of 25 cm, depending on the spreading of the waves. Experiments with real data show less impressive results, an accurate reconstruction of the surface can be given, but the predictive capability is very limited.

Preface

In front of you lies the master thesis "*Predicting the sea surface from high resolution multi-beam FMCW radar data*", which concludes my MSc. Applied Mathematics at TU Delft. The thesis work started in the beginning of 2019 and was a collaboration of the TU together with the company Radac, also located in Delft. My project was started as derivation of a larger project, called Do-it. This subsidised project was done in a cooperation between Radac, Damen Shipyards, Next Ocean, the Royal Netherlands Sea Rescue Organisation KNRM and Marin. This project aimed to increase the operability of small boat operations by the forward prediction of vessel motions using radar remote sensing of the waves.

At Radac I was warmly welcomed with a personal spot and during my time there I also really felt a part of the team by attending the weekly team meetings, going for a 'Do-it' sea trial with the new radar on a KNRM boat, and being part of several nice celebrations of company milestones (especially the awesome Cirque du Soleil show!). Therefore I would like to thank all (former) employees. Special thanks go to Rolf (who was my supervisor during my time at Radac) for helping me going towards the right direction, providing me with practical insights, critical notes and useful tips. I also valued your special interest regarding my progress and your support during the project. The same holds for prof. dr. ir. A.W. Heemink, who was my supervisor from the university, providing me with valuable input and feedback on my work. Also thanks to Dr. ir. M.B. van Gijzen and Dr. J.L.A. Dubbeldam for taking place in the graduation committee.

Besides the people involved in the project I would also like to express my gratitude towards the people from my social life. Firstly a big thanks to my parents, step-parents and sister for all the years of support leading to this milestone. Also I would like to thank my friends, especially the group known as 'De Trein', for their support and cheering me up when I was struggling.

Gerald van der Geugten
Delft, January 2020

Contents

1 Introduction

This thesis is about the reconstruction and prediction of the sea surface based on radar velocity data coming from a forward looking, phase steered FMCW radar. This data is unique in it's kind since this specific measuring technique is only recently implemented in a future commercial product by the company Radac B.V. from Delft. For this unique data a linear wave model will be constructed to obtain a deterministic description of the current sea state, whereas statistical descriptions are more common (but also less accurate). With this deterministic model there is the possibility to not only reconstruct an entire sea surface but also predict what will happen in the domain at later times.

1.1. Motivation of the thesis

This precise real-time sea description of the sea state which the deterministic wave model provides can be highly valuable for several sensitive offshore operations. These operations include offshore crew transfers, float-over installations and helicopter take-offs and landing. With the crew transfers for example, people are transported from a vessel to an offshore platform (oil, gas or wind farm). These need to happen in a safe manner. One of the crucial steps in this process is the moment where a crew member enters the platform by getting off the boat and onto the platform or vice versa (as seen in figure 1.2). Casualties could happen in terms of personal injuries or damage to the equipment when the surface motion is suddenly very big. This limits the factor of operability quite a lot so this should be prevented. To be certain that this transfer happens in a safe way the wave conditions are checked before the transit leaves the shore, where a threshold of 1.5 meters significant wave height (the average height of the highest one-third of all waves measured which is equivalent to the estimate that would be made by a visual observer at sea) is now taken to determine whether it is safe to do a transfer and travel there or not. These wave conditions are quite common as can be seen in figure 1.1, where a month of data is displayed with the significant waveheight near a dutch wind farm. With a precise deterministic short-term wave prediction this boundary can be pushed, by avoiding the big waves.

1.2. Data

Conventional wave measurements are mostly done by using a wave buoy, pulse radar or X-band radar. The data that is used for this thesis comes from a phase steered FMCW radar which is quite unique and is part of the X-band radar-type since it operates at 10 GHz. The difference with the other radars is that it measures a smaller region with an approximate 10 times higher spatial resolution as compared to a conventional X-band radar (0.75 meters and 5-10 meters). Thus it is able to capture more details from the waves. The difference with the pulse radar is that FMCW is considered more accurate since the signal is continuously send out as opposed to pulse, where a single signal is send out and received. The FMCW radar from Radac is forwardly looking into the waves over a beam range of 384 meters and thus faces them almost horizontally in the far grid cells (depending on the mounting height). The set-up of the radar is that sends out a signal over 5 beams with a total resolution of 50 Hz, this delivers 10 Hz data over the entire spatial grid of the 5 beams. From the back-scattered signal the velocity and position of the measured object can be extracted. These velocities mainly represent the orbital

Figure 1.1: Significant waveheight near the Princess Amalia wind farm (Taken from [14])

Figure 1.2: A crew transport vessel positioning itself to a wind turbine (Taken from [16])

motion of the water particles at the sea surface but also captures noise and some other velocities that are not directly related to the orbital motion. In this thesis the radar itself is in a fixed position, so for movements of the radar (when placed on a ship) do not have to be accounted for. One of the objectives of the thesis (before the model can be used) will be to capture the measured phenomena and account for them as well as possible. With the processed data a model will be used to give a representation of the surface.

1.3. Models

The sea can be represented in several ways which have been researched for many years. A rough separation can be made between models that produce the same outputs given the input (deterministic) and models that that give different outputs in repeated cases (stochastic). Ocean physics can be described by both kinds of models. Given the setting of this thesis the focus will lie on the deterministic modeling. For these deterministic models the analysis of the problem has led to lots of nonlinear wave equations, which have also been simplified to a linear representation. A recent example of computation with the nonlinear waves is performed by Simanesew [15] where several representations are used, especially including the Modified Non linear Schödinger (MNLS) equation. These showed some promising results in predicting the surface for long crested waves as opposed to the solution using linear wave theory.

For matching the model to the data inverse modelling is needed, Simanesew presented least squares techniques and covariance matrix methods to do this. Use of this linear wave theory is common for a lot of commercial systems in recent days. An advantage of this representation is that for the link to the statistical description of the sea it is convenient to use the linear wave theory. These statistical descriptions are set-up by a random phase/amplitude model which can be naturally linked to the linear wave theory. With this approach several statistical parameters can be extracted from the model, including the wave spectrum and significant wave height.

Other research in this field has been done by Wijaya [17] using X-band radar data. This research proposed a model with a dynamic averaging procedure that uses evolved images from past time steps to reconstruct and predict the surface displacement. By doing so it was able to limit the effects of shadowing (high waves blocking the signal, leaving holes in the measurements), which has significant influence due to the nature of the data (having larger time steps and range steps in the data set as opposed to the FMCW radar data). The idea of averaging solutions will be used in one of the solution strategies in which a low time resolution is taken.

The deterministic model that will be used in this thesis is based on the linear wave theory. This is done for both a (generalized) situation in one spatial direction as in a multi directional case in space. To test this model also artificial data will be used. To generate this also linear wave theory will be used together with statistical parameters found in the JONSWAP project.

1.4. Objectives

The main goal of this thesis is thus to combine the radar measurements with a deterministic mathematical wave model to give a reconstruction and prediction of the wave surface. To get to this main goal a number of steps need to be taken to achieve this. These can be grouped as follows.

Main Goals:

- Reconstruct the sea surface by applying linear wave theory
- Predict the sea surface with the parameters found by the reconstruction

Sub Goals:

- Identify the information that is contained by the radar data
- Create an artificial data set which resembles radar data
- Build a deterministic linear wave model in one and multiple directions that can reconstruct the water surface
- Find the predictive capabilities of this deterministic model

1.5. Thesis structure

The strategy towards these goals is to first describe the mathematical equations that appear in the hydrodynamic theory together with the statistical properties of the ocean waves. This is done in chapter 2 to get an understanding on how the water surface can be described and what the relevant parameters are in this case. The linear wave theory will be derived from the hydrodynamic equations. This will first be considered for a case where wave travel in one direction and is then extended to multiple directions. The second part of this chapter is dedicated to the statistical description of the sea state, which is centered around the random phase/amplitude model. Also some effects of waves in coastal areas is treated which may be relevant for the data set produced by the radar.

In chapter 3 the data that will be dealt with is presented. First a brief explanation is given of the measuring principle of the FMCW radar. This is followed by some explanation of the effects that are likely to be captured by the radar signal. These include the water current and shadowing effects. Besides this real data also an artificial data set is built for the testing of the model.

After this chapter 4 is dedicated to the description of the mathematical model that is used to reconstruct and predict with the radar data. The methods that are used include inverse modelling by a least squares criterion to fit the model to the data.

The results of the modelling methods that are presented in chapter 4 are then discussed in chapter 5 for the one directional and multi directional case. In chapter 6 the most important conclusions are gathered together with some recommendations for further research.

2

Basic concepts of wave models

In this chapter the basic concepts that are relevant for the research are presented. These involve the movement (and shape) of the ocean surface, which is essentially the free boundary between water and atmosphere. There are two ways to describe the state of an ocean. The first way is to apply the available knowledge about particle movements and interactions by forces of nature. The second way is to observe the ocean and track the behaviour of it in statistical sense.

This is started by going into the hydrodynamic theory which captures the elementary properties of water and it's behaviour when in motion. These are primarily based on the conservation laws that hold not only for water, but any kind of volume of mass, so this is very broad. This is made more specific for the ocean by making some assumptions and neglect non linear terms to make the problem linear. Here the linear wave theory comes up and is discussed further by setting the boundaries of the problem and solving the system of equations. An important distinguishing here is the splitting of the problem into a one-directional and a multi-directional situation. The one-directional situation is a simplification of the multi-directional by assuming that waves travel as infinitely long crests in the other dimension. The mathematical solution of the water surface and particle velocity can be given for both these dimensions. This done in sections 2.1 to 2.3.

Besides this hydrodynamic theory a lot of useful information regarding the way in which oceans and seas behave come from measurements that are done over the years. Based on these researches a lot of statistical information about characteristics of oceans is gathered. Some of the most important information that can be gained and applied from this is treated in section 2.4.

2.1. Hydrodynamic theory

In this section the equations that describe the sea state will be derived (based on [4][6][7] and [11]). These equations are based on the conservation laws to respect the physical conditions. Some assumptions and idealisations of the ocean water are necessary when considering these conservation laws to make use of the linear wave theory in a later stage. This is done by neglecting the viscosity frictions and Coriolis forces, whilst their impact is relatively small compared to other forces. Furthermore it is assumed that the flow is irrotational (water particles may not rotate around their own axes), the water is incompressible and has constant density. In the next section The linear wave theory itself will be treated (for both one and multi directional wave systems).

2.1.1. Conservation of mass

As a starting point the condition that describes the conservation of mass is formulated. So consider a volume of water V in the (x, y, z)-space that is bounded by its boundary ∂V. Then the change in time of the mass enclosed by V is equal to the mass that traverses the surface through ∂V. This can be described by the following equation:

$$\frac{\partial}{\partial t}\rho_w + \frac{\partial}{\partial x}(\rho_w u) + \frac{\partial}{\partial y}(\rho_w v) + \frac{\partial}{\partial z}(\rho_w w) = 0 \tag{2.1}$$

where $\mathbf{u} = (u, v, w)$ represents the velocity in the x, y and z-direction resp. and ρ_w is the seawater density. So in a more compact way the equation can be rewritten as:

$$\frac{\partial}{\partial t}\rho_w + \nabla \cdot (\rho_w \mathbf{u}) = 0 \tag{2.2}$$

Since it is assumed that the flow of water is incompressible (which is often assumed in ocean modelling), the following holds: $\frac{\partial \rho_w}{\partial t} = 0$. So therefore 2.2 reduces to a simple expression:

$$\nabla \cdot \mathbf{u} = 0 \tag{2.3}$$

2.1.2. Conservation of momentum

To derive the conservation of momentum equations the second law of Newton is taken as starting point, this states that the sum of forces acting on a volume equals the mass times the acceleration. This is written as $F = m\mathbf{a}$. For a volume of ocean water this law can be expressed as follows:

$$\mathbf{a} = \frac{D\mathbf{u}}{Dt} = \mathbf{p} + \mathbf{g} + \mathbf{c} + \mathbf{m} \tag{2.4}$$

where $\mathbf{p}$ represents pressure force per unit mass, $\mathbf{g}$ represents gravity force per unit mass, $\mathbf{c}$ represents Coriolis force per unit mass and $\mathbf{m}$ represents frictional force per unit mass. Furthermore it should be noticed that the acceleration $\mathbf{a}$ of a body is equal to the total derivative of it's velocity $\mathbf{u}$. The contributions by $\mathbf{c}$ and $\mathbf{m}$ can be neglected since these are small in comparison to the others. So equation 2.4 reduces to:

$$\frac{D\mathbf{u}}{Dt} = \mathbf{p} + \mathbf{g} \tag{2.5}$$

This equation 2.5 can be explored further. This is done by interpreting the total derivative $\frac{D}{Dt}$, which gives the following set of equations for the left-hand side of equation 2.5:

$$\begin{cases} \dfrac{Du}{Dt} = \dfrac{\partial u}{\partial t} + (\mathbf{u} \cdot \nabla)u = \dfrac{\partial u}{\partial t} + u\dfrac{\partial u}{\partial x} + v\dfrac{\partial u}{\partial y} + w\dfrac{\partial u}{\partial w} \\ \dfrac{Dv}{Dt} = \dfrac{\partial v}{\partial t} + (\mathbf{u} \cdot \nabla)v = \dfrac{\partial v}{\partial t} + u\dfrac{\partial v}{\partial x} + v\dfrac{\partial v}{\partial y} + w\dfrac{\partial v}{\partial w} \\ \dfrac{Dw}{Dt} = \dfrac{\partial w}{\partial t} + (\mathbf{u} \cdot \nabla)w = \dfrac{\partial w}{\partial t} + u\dfrac{\partial w}{\partial x} + v\dfrac{\partial w}{\partial y} + w\dfrac{\partial w}{\partial w} \end{cases} \tag{2.6}$$

This expression can be written more compact as

$$\frac{D\mathbf{u}}{Dt} = \frac{\partial \mathbf{u}}{\partial t} + \frac{1}{2}\nabla(\mathbf{u}^2) + (\nabla \times \mathbf{u}) \times \mathbf{u} \tag{2.7}$$

The term rot$\mathbf{u} = \nabla \times \mathbf{u}$ is called vorticity. If it is unequal to zero, the motion is defined as rotational. As mentioned in the beginning of this chapter it is assumed that the motion is irrotational, so therefore let rot$\mathbf{u} = 0$. Then equation 2.7 can be expressed as:

$$\frac{D\mathbf{u}}{Dt} = \frac{\partial \mathbf{u}}{\partial t} + \frac{1}{2}\nabla(\mathbf{u}^2) \tag{2.8}$$

This allows that the velocity $\mathbf{u}$ can represented as the gradient of a scalar function, which is the velocity potential Φ:

$$\mathbf{u} = \nabla\Phi \tag{2.9}$$

Now still remains to find an expression for the right hand side term $\mathbf{p} + \mathbf{g}$ in 2.5. For the pressure force the following expression holds: $\mathbf{p} = -\frac{1}{\rho_w}\nabla p$. For the gravity $\mathbf{g}$ it can be assumed that it only works in the z-direction, so this gives only a $-g$ contribution there (where $g = |\mathbf{g}|$). So this results in the following rewriting of 2.5:

$$\begin{cases} \dfrac{Du}{Dt} = -\dfrac{1}{\rho_w}\dfrac{\partial p}{\partial x} \\ \dfrac{Dv}{Dt} = -\dfrac{1}{\rho_w}\dfrac{\partial p}{\partial y} \\ \dfrac{Dw}{Dt} = -\dfrac{1}{\rho_w}\dfrac{\partial p}{\partial z} - g \end{cases} \tag{2.10}$$

Above equations are called the inviscid *Euler equations for incompressible flow*. In the compact form that was used earlier they become:

$$\frac{D\mathbf{u}}{Dt} = -\nabla\left(\frac{p}{\rho} + gz\right) \tag{2.11}$$

When the results of the rewriting of $\frac{D\mathbf{u}}{Dt}$ in 2.7 and $\mathbf{p}+\mathbf{g}$ in 2.11 are put together the following equation arises:

$$\frac{\partial \mathbf{u}}{\partial t} = -\nabla\left(\frac{p}{\rho_w} + gz\right) - \frac{1}{2}\nabla(\mathbf{u}^2) \tag{2.12}$$

Using the notation with the potential in 2.9, which is allowed by the earlier stated assumption of irrotational motion allows to make a further simplification:

$$\frac{\partial}{\partial t}(\nabla\Phi) = -\nabla\left(\frac{p}{\rho_w} + gz - \frac{1}{2}(\nabla\Phi)^2\right) \tag{2.13}$$

Above equation can still be seen as a form of the inviscid Euler equations for incompressible flow. By taking the integral over the spatial domain this equation can be further reduced to:

$$\frac{\partial\Phi}{\partial t} = -\frac{p}{\rho_w} - gz + \frac{1}{2}(\nabla\Phi)^2 \tag{2.14}$$

This above equation is better known as the *Bernoulli equation for unsteady motion*, which thus is valid for time-dependent flows. This is an alternative version of the classical Bernoulli equation which is only valid for steady motions, and thus independent of time. Due to the assumption of constant density and irrotational motion the presented version holds. The *linearised Bernoulli equation for unsteady motion* is obtained by (obviously) linearising the result of 2.14:

$$\frac{\partial\Phi}{\partial t} + \frac{p}{\rho_w} + gz = 0 \tag{2.15}$$

2.2. Linear wave theory

In this section the linear wave theory for a single space dimension is derived. Therefore it is assumed that the waves are periodic with infinitely long crests in the y-direction. This reduces the wave to be described by a periodic *two-dimensional wave* (i.e., there exist only variations in the x- and z-directions; there is no variation in the y-direction). This will help a lot in simplifying the problem of describing the sea surface and will be a good starting point to get familiar with some of the basic concepts.

So, starting from the conservation laws that were seen in the previous sections it can be concluded that by conservation of mass should hold that:

$$\nabla\mathbf{u} = 0 \tag{2.16}$$

And by conservation of momentum under the assumptions of irrotational flow and zero contribution from Coriolis and frictional force as in section 2.1.2. should hold that the velocities have a potential Φ:

$$\mathbf{u} = \nabla\Phi \tag{2.17}$$

Combining these two gives the equation that should hold in the whole domain of water:

$$\Delta\Phi = 0 \tag{2.18}$$

To complete the system that needs to be solved the remaining boundaries to be considered are the water surface and the bottom. These will be derived and described in the following section.

2.2.1. Determining boundary conditions

For a realistic model it is assumed first that there is no flow of water going through the solid bottom. So this means that the vertical velocity component equals zero. This can be realized by setting:

$$\frac{\partial \Phi}{\partial z} = 0 \text{ at } z = -d \tag{2.19}$$

Another boundary condition arises at the water surface (where $z = \eta(x,t)$), namely that the velocity of the surface η at (x,t) should match the velocity $\mathbf{u}$ of the water at (x,η,t) in vertical direction. This is done by letting:

$$\frac{\partial \Phi}{\partial z} = \frac{\partial \eta}{\partial t} \text{ at } z = \eta(x,t) \tag{2.20}$$

This condition is posed on a varying and yet unknown boundary, so therefore it is helpful to make an approximation at a boundary that is known, like $z = 0$. Herefore the assumption is made that η is relatively small compared to the depth d and that the velocity potential is sufficiently smooth. Then the term $\frac{\partial \Phi}{\partial z}$ can be approximated by it's Taylor series at $z = 0$:

$$\frac{\partial \Phi}{\partial z}|_{z=\eta(x,t)} = \frac{\partial \Phi}{\partial z}|_{z=0} + \frac{\partial}{\partial z}\frac{\partial \Phi}{\partial t}|_{z=0}\eta + \cdots \tag{2.21}$$

$$\approx \frac{\partial \Phi}{\partial z}|_{z=0} \tag{2.22}$$

$$\tag{2.23}$$

And therefore the boundary condition is set to:

$$\frac{\partial \Phi}{\partial z} = \frac{\partial \eta}{\partial t} \text{ at } z = 0 \tag{2.24}$$

Furthermore, to ensure that the waves in the model are only subject to gravity (so called *free waves*) the pressure at the water surface is taken constant, equal to zero. This is called the *dynamic surface boundary condition*:

$$p = 0 \quad \text{at } z = 0 \tag{2.25}$$

The final boundary condition is the one that imposes that the *Bernouilli equation for unsteady motion* 2.14 should hold on the surface. The linearized version is taken by assumption that the velocities are relatively small (so the terms of $\nabla\Phi$ can be discarded). The boundary condition therefore becomes:

$$\frac{\partial \Phi}{\partial t} + g\eta = 0 \quad \text{at } z = \eta(x,t) \tag{2.26}$$

Which again is defined on the unknown boundary, so by using Taylor expansion as for the vertical velocity boundary condition the condition can be defined on $z = 0$:

$$\frac{\partial \Phi}{\partial t} + g\eta = 0 \quad \text{at } z = 0 \tag{2.27}$$

2.2.2. The boundary value problem

When putting together the Laplace equation and the boundary conditions the problem that needs to be solved looks as follows (also visually presented in 2.1):

$$\begin{cases} \nabla^2\Phi = 0, & -d < z < \eta(x,t) \\ \dfrac{\partial \Phi}{\partial z} = \dfrac{\partial \eta}{\partial t}, & z = 0 \\ \dfrac{\partial \Phi}{\partial z} = 0, & z = -d \\ p = 0, & z = 0 \\ \dfrac{\partial \Phi}{\partial t} + g\eta = 0, & z = 0 \end{cases} \tag{2.28}$$

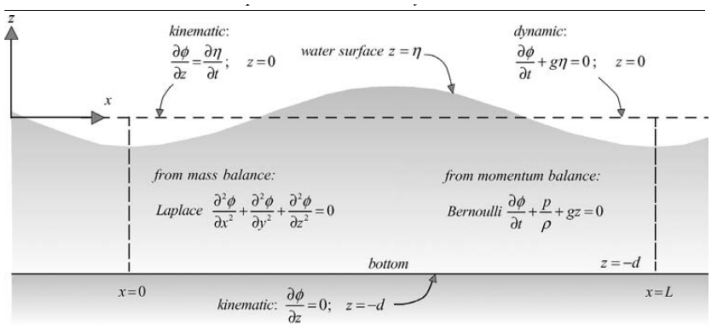

Figure 2.1: Visual representation of the 1-D linear wave theory equations (taken from [4])

This system has an analytical solution for the surface $\eta(x,t)$ in the following form:

$$\eta(x,t) = A\cos(\omega t - kx + \psi) \tag{2.29}$$

which is a long-crested harmonic wave travelling in the positive x-direction. Here $k = \frac{2\pi}{L}$ is called the *wave number*, $\omega = \frac{2\pi}{T}$ is called the *radian* or *angular frequency* and $A = \frac{H}{2}$ is called the amplitude. See also figure 2.2

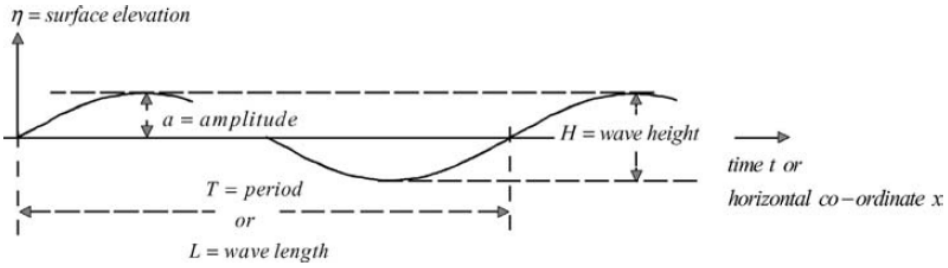

Figure 2.2: An overview of the characterising units a wave mode (taken from [4])

To find an expression for the potential a separation of variables is required:

$$\Phi(x,z,t) = F(x,t)Z(z) \tag{2.30}$$

This expression should hold for the boundary conditions, so check for: $\Phi_z = \eta_t$ at $z = 0$:

$$F(x,t)Z'(0) = -\omega A\sin(\omega t - kx + \psi) \tag{2.31}$$

This implies that $Z'(0) = \omega A$ and $F(x,t) = \sin(\omega t - kx + \psi)$. So the separation of variables becomes:

$$\Phi(x,y,t) = Z(z)\sin(\omega t - kx + \psi) \tag{2.32}$$

When this expression 2.32 is substituted into the Laplace equation $\Phi_{xx} + \Phi_{zz} = 0$ it results in:

$$-k^2\sin(\omega t - kx + \psi)Z(z) + \sin(\omega t - kx + \psi) = 0 \tag{2.33}$$

From which can be concluded that $Z(z)$ should satisfy the following differential equation:

$$Z'' - k^2 Z = 0 \tag{2.34}$$

So $Z(z) = c_1 e^{kz} + c_2 e^{-kz}$, by standard theory of ordinary differential equations. From the boundary at $z = -d$ (where $\Phi_z = 0$) it can then be concluded that the following holds:

$$Z'(-d) = kc_1 e^{-kd} - kc_2 e^{kd} = 0 \tag{2.35}$$

such that $c_1 = c_2 e^{2kd}$ and thus:

$$Z(z) = c_2(e^{2kd}e^{kz} + e^{-kz}) \tag{2.36}$$

To solve this expression for the remaining unknown constant c_2 the boundary $\Phi_z = \eta_t$ at $z = 0$ is needed again. This now gives:

$$\omega a \sin(\omega t - kx + \psi) = [c_2 k(e^{2kd} - 1)] \sin(\omega t - kx + \psi) \tag{2.37}$$

Hence:

$$c_2 = \frac{\omega A}{k(2e^{2kd} - 1)} \tag{2.38}$$

and this gives the expression for $Z(z)$:

$$Z(z) = \frac{\omega A}{k(2e^{2kd} - 1)}(e^{2kd}e^{kz} + e^{-kz}) \tag{2.39}$$

This concludes the derivation of the potential function $\Phi(x, y, t)$, which thus equals:

$$\Phi(x, y, t) = \sin(\omega t - kx + \psi) \frac{\omega A}{k(2e^{2kd} - 1)}(e^{2kd}e^{kz} + e^{-kz}) \tag{2.40}$$

Which can be reduced in a nice way using hyperbolic trigonometric functions to obtain:

$$\Phi(x, t) = \frac{\omega A}{k} \frac{\cosh[k(d + z)]}{\sinh(kd)} \sin(\omega t - kx + \psi) \tag{2.41}$$

Remarkable is that for this derivation none of the dynamic aspects coming from the Bernoulli equation were necessary. So from this it can be concluded that the potential function Φ holds for forced waves as well (when the surface wave is harmonic at least).

From the potential function Φ the particle velocities can also be derived by realizing that $\frac{\partial \Phi}{\partial x} = u$ and $\frac{\partial \Phi}{\partial z} = w$. This gives expressions:

$$u(x, t) = -\omega A \frac{\cosh[k(d + z)]}{\sinh(kd)} \cos(\omega t - kx + \psi) \tag{2.42}$$

$$w(x, t) = \omega A \frac{\sinh[k(d + z)]}{\sinh(kd)} \sin(\omega t - kx + \psi) \tag{2.43}$$

What is remarkable about these velocities is that they describe a closed circular motion for the water particles. Depending on the depth d this motion is circular or elliptic of shape. The smaller the depth, the bigger the motion in the horizontal plane will be, see also figure 2.3 for this effect.

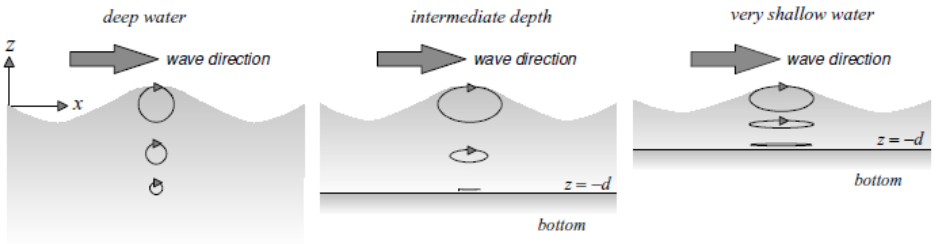

Figure 2.3: The effects of shallow water conditions on the orbital motion of water particles (taken from [4])

For deep water it holds that $kd \to \infty$, meaning that the $\frac{\cosh[k(d+z)]}{\sinh(kd)}$ term for u and $\frac{\sinh[k(d+z)]}{\sinh(kd)}$ term for v will drop from 2.42 and 2.43. This results in:

$$u(x, t) = -\omega A \cos(\omega t - kx + \psi) \tag{2.44}$$

$$w(x, t) = \omega A \sin(\omega t - kx + \psi) \tag{2.45}$$

2.2.3. Dispersion relation

A special relation that holds in the linear wave theory is called the *dispersion relation*. This gives a relation between the wave number and the radian frequency of the waves. It is derived by imposing the dynamic boundary condition on the general solution Φ with $\eta(x,t) = A\cos(\omega t - kx + \psi)$. This gives the following, starting from the dynamic boundary condition:

$$\frac{\partial \Phi}{\partial t} + g\eta = 0 \quad \text{at } z = 0 \tag{2.46}$$

Substituting the known expressions for $\frac{\partial \Phi}{\partial t}$ and η gives:

$$\frac{\omega^2 A}{k}\frac{\cosh(kd)}{\sinh(kd)}\cos(\omega t - kx + \psi) + Ag\cos(\omega t - kx + \psi) = 0 \tag{2.47}$$

Thus should hold that:

$$\frac{\omega^2}{k}\frac{\cosh(kd)}{\sinh(kd)} = g \tag{2.48}$$

This results in the dispersion relation:

$$\omega^2 = gk\frac{\sinh(kd)}{\cosh(kd)} = gk\tanh(kd) \tag{2.49}$$

Note that this relation is implicit in terms of the wave number, but for cases where the water is very deep or shallow the dispersion relation can be expressed in explicit way. This can be done since $\tanh(kd) \to 1$ for $kd \to \infty$ and $\tanh(kd) \to kd$ for $kd \to 0$. The dispersion relation is then expressed by $\omega = gk$ and $\omega = k\sqrt{gd}$ respectively. To put it more intuitively, deep water means that the wave length is relatively small compared to the water depth and shallow water waves have a relatively large wavelength compared to the water depth. This also effects the orbital motion of the water particles as shown in figure 2.3

To overcome the situation when there is an intermediate depth there are alternative explicit expressions to denote the relationship between ω and k, this was done by Eckhart [2]:

$$kd \approx \frac{\alpha}{\sqrt{\arctan(\alpha)}}, \tag{2.50}$$

where $\alpha = \frac{\omega^2 d}{g}$. This term is exact for the limits of deep and shallow water and for all other cases the error for the wave number k is below 5%.

When a constant current is present in the water the linear wave theory will still hold. The waves will travel in the same manner but faster due to the current. It has a influence on the dispersion relation:

$$\omega = \sqrt{gk\tanh(kd)} + kU, \tag{2.51}$$

here U represents the current velocity (which in this one dimensional case is in the same direction as the waves travel)

2.3. Linear wave theory in multiple directions

In this section the linear wave theory is expanded to the multiple direction case with an extra space dimension (so the assumption of infinitely long crests coming from the y-direction is discarded and replaced by any direction in the (x,y)-space). As a result the equations that were found in the one directional situation described up until now need an extra entry for the y-coordinate. Since the conservation laws will still hold the Laplace equation is also still present, but with an extra contribution:

$$\Delta\Phi = \frac{\partial^2\Phi}{\partial x^2} + \frac{\partial^2\Phi}{\partial y^2} + \frac{\partial^2\Phi}{\partial z^2} = 0 \tag{2.52}$$

Also the rest of the derived boundary conditions only need a small modification by replacing the single x-coordinate into a $\mathbf{x} = (x,y)$-coordinate. So this leads to the same boundary value problem, but with

an extra dimension:

$$\begin{cases} \nabla^2\Phi = 0, & -d < z < \eta(x,y,t) \\ \dfrac{\partial\Phi}{\partial z} = \dfrac{\partial\eta}{\partial t}, & z = 0 \\ \dfrac{\partial\Phi}{\partial z} = 0, & z = -d \\ p = 0, & z = 0 \\ \dfrac{\partial\Phi}{\partial t} + g\eta = 0, & z = 0 \end{cases} \tag{2.53}$$

As a consequence of the problem having similar equations it can be concluded that the same solutions as to the wave equation in one direction will hold. To generalize this for a wave with an extra dimension the assumption is made that each wave mode is infinitely crested into a particular direction (so not necessarily into x-direction, but some direction in (x, y)-space). Let s be the coordinate of the travelling direction of the wave mode. Then holds:

$$s = x\cos(\theta) + y\sin(\theta) \tag{2.54}$$

Where θ represents the angle in the (x, y)-plane to get to s. And thus along this travelling direction it holds:

$$\eta(s,t) = A\cos(\omega t - ks + \psi) \tag{2.55}$$

This gives a general solution:

$$\eta(x,y,t) = A\cos(\omega t - k(x\cos(\theta) + y\sin(\theta)) + \psi) \tag{2.56}$$

When doing the derivation with coordinate s for the potential as in last section for the 1-D case the result becomes:

$$\Phi(x,y,t) = \frac{\omega A}{k}\frac{\cosh[k(d+z)]}{\sinh(kd)}\sin(\omega t - k(x\cos(\theta) + y\sin(\theta)) + \psi) \tag{2.57}$$

From this potential function the orbital velocities can easily be obtained as before by letting $\frac{\partial\Phi}{\partial s} = u$ and $\frac{\partial\Phi}{\partial z}$. Where the orbital motion is towards s with angle θ, which denotes the propagation direction of the wave mode (instead of x or y):

$$u(x,y,t) = -\omega A\frac{\cosh[k(d+z)]}{\sinh(kd)}\cos(\omega t - k(x\cos(\theta) + y\sin(\theta)) + \psi) \tag{2.58}$$

$$w(x,y,t) = \omega A\frac{\sinh[k(d+z)]}{\sinh(kd)}\sin(\omega t - k(x\cos(\theta) + y\sin(\theta)) + \psi) \tag{2.59}$$

Alternative descriptions of the wave number can be given by $\mathbf{k} = (k_x, k_y)$, where:

$$k_x = k\cos(\theta) \qquad k_y = k\sin(\theta) \tag{2.60}$$

Note that in 2.58 and 2.59 the terms for $\frac{\cosh[k(d+z)]}{\sinh(kd)}$ and $\frac{\sinh[k(d+z)]}{\sinh(kd)}$ drop when $kd \to \infty$ in deep water conditions, resulting in . For deep water it holds that $kd \to \infty$, meaning that the $\frac{\cosh[k(d+z)]}{\sinh(kd)}$ term for u and $\frac{\sinh[k(d+z)]}{\sinh(kd)}$ term for v will drop from 2.42 and 2.43. This results in:

$$u(x,y,t) = -\omega A\cos(\omega t - k(x\cos(\theta) + y\sin(\theta)) + \psi) \tag{2.61}$$

$$w(x,y,t) = \omega A\sin(\omega t - k(x\cos(\theta) + y\sin(\theta)) + \psi) \tag{2.62}$$

When the cosine components of 2.56 are added together they can represent a sea surface. This is illustrated in figure 2.4.

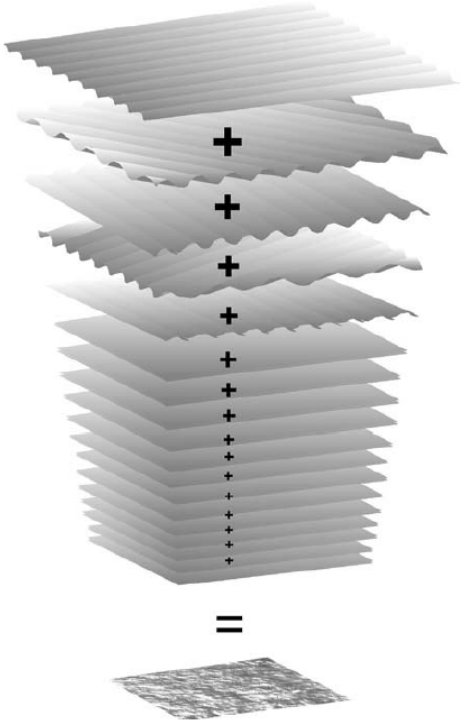

Figure 2.4: Representation of a sea surface made up as a superposition of individual long-crested waves

2.3.1. Dispersion relation

The dispersion relation still holds in the same way as with the one-dimensional space when current is absent:

$$\omega^2 = gk \tanh(kd), \tag{2.63}$$

But with (constant) current it is altered a bit from equation 2.51. This is due to the assumption that the current $\mathbf{U} = (U_x, U_y)$ travels along one direction. So the effect of this current on each wave mode is different depending on the direction of the wave mode (determined by angle θ). This is expressed as follows:

$$\omega = \sqrt{gk \tanh(kd)} + \mathbf{k} \cdot \mathbf{U}, \tag{2.64}$$

When the wave mode travels in the same direction as the current the dot product equals kU as in the one dimensional case.

2.4. Ocean characteristics

In this section the general aspects of the statistical description of oceanic waters are discussed. These will give some more insights and limitations to the model parameters for them to be feasible in a practical sense. Over the years lots of research has been done to understand the motions of oceanic waters (see also [4]). These have resulted in a detailed description of the statistics that oceans follow. The aspects that will be treated are the wave spectrum, wave breaking, shoaling and refraction.

2.4.1. Wave spectrum

One of the things that are really useful to characterize an ocean with (and different opposed to the deterministic approach presented until now) is called the *wave spectrum*. The aim for this is to statistically describe the state of the sea surface, making an observation of the sea surface a realisation of a stochastic process. This treatment (as described in [4]) is based on the *random-phase/amplitude model*, which states that the ocean surface at any point x (in a one-dimensional space for now) is considered

as a sum of harmonic waves:

$$\underline{\eta}(t) = \sum_{i=1}^{N} \underline{a}_i \cos(2\pi f_i t + \underline{\alpha}_i) \tag{2.65}$$

The underlined terms represent random variables and also N should be taken sufficiently large here. The wave spectrum then relates the frequency to the amplitudes and phases that are present. Since for most wave records any value between 0 and 2π is obtained for the phases, this spectrum is often ignored and assumed to be uniformly distributed. Thus the spectrum will be characterized by the amplitudes. For this the quantity that is taken, is not the amplitude itself, but the variance of each wave component $\frac{1}{2}\overline{a_i^2}$ (where the overline means that the average is taken over multiple realizations M for this wavemode i). This is done since it is statistically more meaningful, since the sum of variances equals the variances of the sum which is not the case when using the amplitudes (and also in the linear wave theory this variance is proportional to the energy of the waves $E_{energy}(f) = \rho g E_{variance}(f)$). The variance $E\left\{\frac{1}{2}\underline{a}_i^2\right\}$ alone is not enough tough, since this only uses discrete frequencies, whilst a real sea would have all frequencies present. Therefore the density is taken over every frequency interval, when letting this frequency interval go to zero a continuous spectrum is obtained. The continuous (one-dimensional) variance density spectrum can be expressed as:

$$E(f) = \lim_{\Delta f \to 0} \frac{1}{\Delta f} \frac{1}{2} \overline{a}^2 = \lim_{\Delta f \to 0} \frac{1}{\Delta f} E\left\{\frac{1}{2}\underline{a}^2\right\} \tag{2.66}$$

The actual distribution of these $\underline{a}_i$ is yet undetermined. In the random phase/amplitude model a Rayleigh distribution is taken for the amplitudes:

$$p(a_i|\sigma) = \frac{a_i}{\sigma^2} \exp\left[-\frac{a_i^2}{(2\sigma)^2}\right], \tag{2.67}$$

where $\sigma = \sqrt{\frac{pi}{2E(\underline{a}_i)}}$ as in [4]. For the frequencies a uniform distribution is taken between 0 and 2π. To get a link with the real wave records it is more useful to base the values of the amplitudes on a observed spectrum from this. One of the most well-known spectra is called the *JONSWAP spectrum* [3] (which is an abbreviation of 'Joint North Sea Wave Project'), which showed that the waves in the North Sea (under (near-)idealised conditions) fit the same spectrum. This can be expressed as follows:

$$E_{JONSWAP}(f) = \alpha g^2 (2\pi)^{-4} f^{-5} \exp\left[-\frac{5}{4}\left(\frac{f}{f_{peak}}\right)^{-4}\right] \gamma^{\exp\left[-\frac{1}{2}\left(\frac{f/f_{peak}-1}{\sigma}\right)^2\right]}, \tag{2.68}$$

with parameters α (energy scale parameter), f_{peak} (frequency scale parameter) and γ, σ (shape parameters). The values of these parameters have been researched and re-calibrated in many studies over the years, including [cite sources]. Furthermore it should be noticed that the terms left of the γ-term form what is called the *Pierson-Moskowitz spectrum* and the γ-term itself is called the *peak-enhancement factor* to sharpen the spectral peak that occurs in the Pierson-Moskowitz spectrum. A visualization of the spectrum is shown in figure 2.5.

Frequency direction spectrum

When the extra space dimension is added to define the spectrum again a large number of propagating waves is taken. These are represented in the random

$$\underline{\eta}(x, y, t) = \sum_{i=1}^{N} \sum_{j=1}^{M} \underline{a}_{ij} \cos(\omega_i t - k_i x \cos(\theta_j) - k_i y \sin(\theta_j) + \underline{\alpha}_{ij}) \tag{2.69}$$

Due to the dispersion relation the same index can be used for ω and k, which makes the random phase/amplitude model a two dimensional model in terms of frequency and direction. The model represents a Gaussian process which is stationary in time and homogeneous in x, y-space. As in the case with the single space dimension the variance density spectrum can be derived in a similar way, resulting in:

$$E(f, \theta) = \lim_{\Delta f \to 0} \lim_{\Delta \theta \to 0} \frac{1}{\Delta f \Delta \theta} E\left\{\frac{1}{2}\underline{a}^2\right\} \tag{2.70}$$

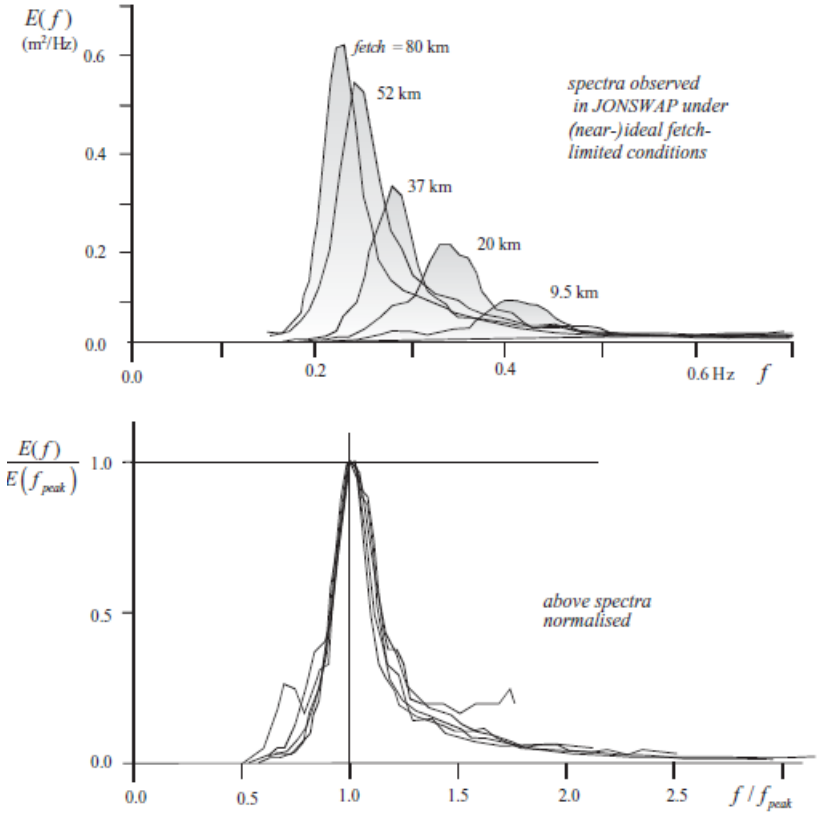

Figure 2.5: Observed spectra in the JONSWAP study, where fetch indicates the distance to the coast (above) and the spectra normalised with the peak frequency (below) (taken from [4])

This expression can be linked to the one dimensional spectrum by introducing the *wave direction spreading function*:

$$D(\theta) = \frac{E(f,\theta)}{E(f)} \tag{2.71}$$

The wave direction spreading function is a function that expresses how the total energy of the earlier encountered one dimensional spectrum is spreaded out over the extra space dimension. So it also holds that the integral over the total domain of θ (from 0 to 2π) of this spreading function equals one to make sure the total energy remains the same. An illustration of this can be found in figure 2.6.
The best-known and probably most widely used spreading function is defined by the $\cos^2\theta$-model [13], which is given by:

$$D(\theta) = \begin{cases} \frac{2}{\pi}\cos^2(\theta), & |\theta| \leq \frac{\pi}{2} \\ 0, & |\theta| > \frac{\pi}{2} \end{cases} \tag{2.72}$$

For this model it is important to note that the direction θ is always taken relative to the mean overall wave direction.

2.4.2. Wave breaking/white-capping

An other important concept is called white-capping (for deep waters) or wave breaking (for shallow waters). This is a phenomenon that is difficult to theoretically understand due to highly non-linear hydrodynamics and also has no precise general definition. This makes it hard to really understand, but the most reasonable explanation is that it is influenced by wave steepness. This has been theoretically captured in [12] by stating that the horizontal particle velocity u cannot exceed the forward speed of the wave c. The formula for this is (where H_{max} represents the maximum wave height and L the wave

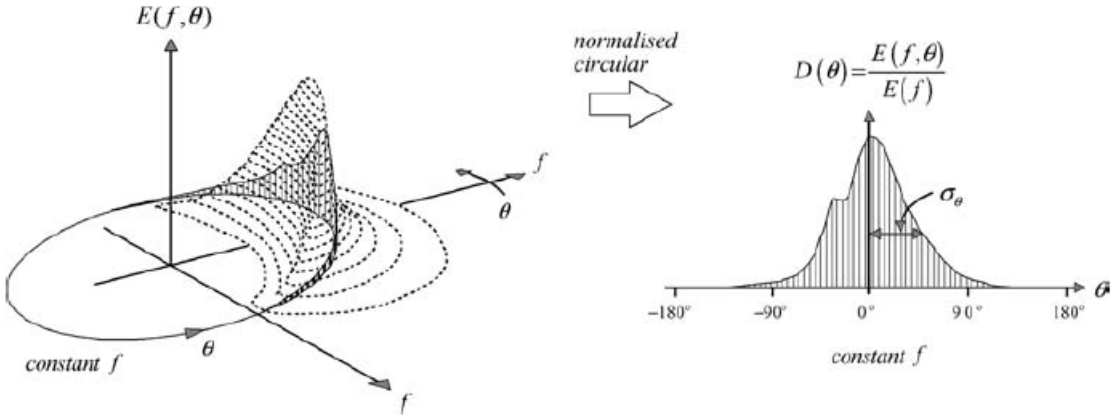

Figure 2.6: The energy directional spectrum

length):

$$H_{max} \approx 0.14L \tanh\left(\frac{2\pi d}{L}\right) \tag{2.73}$$

For deep waters (where $d \to 0$) the tanh term will drop, so it can be concluded that for these waters a ratio of 1:7 exists for a feasible wave height compared to wave length. This concept can be used as an upper bound for the relation between the frequency and the corresponding amplitude in the wave model.

2.4.3. Shoaling, Refraction

The following effects will appear when waves coming from deep water enter more shallow water. For the first effect that will take place assume that a wave is travelling straight towards the coast. Then the effect that will happen is called *shoaling*. Shoaling is the effect that occurs due to the the dispersion relation.

$$\omega^2 = gk \tanh(kd) \tag{2.74}$$

Since the wave will progress with the same frequency it had before entering shallow water the phase speed c will also decrease as a consequence of the decrease of the water depth.

$$c = \sqrt{\frac{g}{k} \tanh(kd)} \tag{2.75}$$

When the wave reaches the coast this will mean that the phase speed will go to zero. However the energy that is contained by the wave should remain equal. As a consequence of this the amplitude of the wave will rise when the depth of the water becomes smaller. This result is obtained by working out the energy conservation, which gives as a result:

$$a_{sh} = \sqrt{\frac{c_{g,\infty}}{c_g}} a_\infty, \tag{2.76}$$

where the ∞ index implies the deep water situation, and c_g denotes the group velocity:

$$c_g = \frac{1}{2}\left(1 + \frac{2kd}{\sinh(2kd)}\right) \tag{2.77}$$

Let the waves now have a direction with an oblique incidence angle towards the coast. A second effect that is encountered then is called *refraction*. This is the effect that the wave will change it's direction to go perpendicular to the coast due to the decrease in depth and thus decrease in phase speed (due to shoaling).
It can be explained as follows, since wave crests travel faster in deep water than shallow water a wave mode will travel over a larger distance in deep water than in shallow water at a given time interval. As

a consequence of this the wave mode will turn towards the region with shallower water, which is the coast. This is an universal effect for any kind of wave and also holds in case of an ambient current. A challenge lies in determining the rate of the directional turning. To determine the angular change several techniques have been developed, one of them makes use of *Snel's law* for a situation with parallel depth contours. This gives:

$$\sin\theta = \frac{c}{c_{deepwater}} \sin\theta_{deepwater} \tag{2.78}$$

As a result of this it can be concluded that all waves reach the shore at an angle of zero degrees (which is only theoretical, this not true in general).
What can be concluded for applying the knowledge about shoaling and refraction in a model though is that for it to work a precise description of bottom topography is needed to find to calculate the impact it will have.

2.5. Chapter summary

As a conclusion to this chapter the most important concepts for the further proceedings of the thesis are discussed in this section. With the introduction of the concepts used in linear wave theory a basis is formed for the solution that will need to be matched with the data. The formulations for the heave and orbital velocity together with the dispersion relation will mainly be used from this framework.

In the second part of the chapter the statistical description of the ocean is given. This will help limit the solution space for the parameters used in the linear wave theory, especially to limit the amplitudes to prevent the event of breaking waves in the model. Also the random/phase amplitude model and JONSWAP spectrum with the directional spreading will be used for recreating an artificial ocean surface which is needed when performing a twin experiment.

3

FMCW radar data

The data that will be used to reconstruct the sea surface is coming from a phase steered forward looking FMCW (which stands for 'Frequency Modulated Continuous Wave') radar, which is newly manufactured by Radac (for the purpose of wave measuring). In cooperation with TNO this product has been developed in aim to measure wave characteristics with higher precision then was possible before with conventional downward looking radars or pulse radars. This makes the data that is available for this thesis state-of-the-art.

3.1. FMCW measuring principle

With this measuring technique the positions and velocities of the reflections are measured within a radar bundle. It consists of a part that transmits a signal and one that receives the back-scattered energy of this signal. This transmitted signal consists of a known stable (sinusoidal or sawtooth-like) frequency continuous wave that varies in frequency for a period of time. This is done by sending out waves that start at a prior set minimum frequency and then increase to a set maximum frequency (this is called a *chirp*). In some other uses this frequency then also gradually decays back down again in the same manner. The increase and decrease are then called *up-* and *down chirp* and together they form the chirp. So formally the chirp that is used in the FMCW radar of Radac is only the up-chirp.
Next the transmitted signal is bouncing off the wave surface and returned to the receiving part of the radar. For a 'frozen' wave (so without any velocity) the *beat frequency* f_b (frequency difference between the transmitted and received signal at the same time t) is then computed by doing a (fast-)Fourier transform on the received signal and then pick the frequency with maximum amplitude. With this frequency the distance towards the radar can be calculated.

With a propagating wave there is an extra factor that should be taken care of, which is the Doppler frequency shift. This occurs due to the movement of the wave, which adds an extra frequency contribution to the returned signal. To deal with this the beat frequency and the Doppler frequency shift need to be superimposed. From these resulting frequencies the distance and velocity of the object towards the radar can be obtained. The velocity is obtained for each range cell by taking the velocity with the maximum reflection strength over the 1024 chirps. It is important to notice that this velocity is in the direction of the beam going from the surface towards the radar.

3.2. Data set

With this measuring technique a data set is obtained containing the distances to the radar and velocities towards the radar. The radar was mounted on the Pier in Scheveningen, Netherlands looking straight into the sea with no interfering objects (see also figure 3.2). Data was recorded during one of the trials on the 25th of March 2019, this means that it is safe to assume that the recorded data does not contain any extra movements from the radar itself but only the radar data of it's wave measurements. So the data set contains the velocities of the water surface towards the radar. The used radar setting can be found in table 3.1.

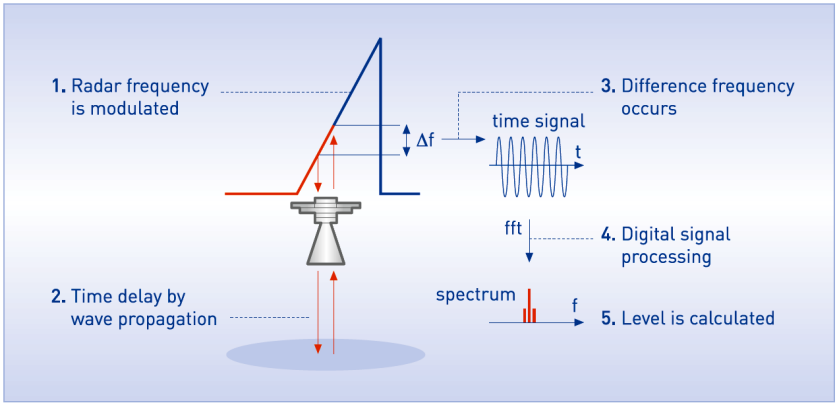

Figure 3.1: FMCW measuring principle (taken from [8])

Figure 3.2: Mounting of the FMCW radar on the Pier in Scheveningen (photo's taken by Filip Saad, Radac)

These velocities contain the orbital velocities u, but this is not the only information that is contained in the velocity data. A list of velocities/effects that are contained (and that need to be encountered for) are:

1. **Orbital velocity** u, this is the main component that is measured. Since this is also measured in the direction of the beam, it needs to be corrected for the angle between the beam and the horizontal plane. The multiple beam directions that are used require to correct for this azimuth angle as well. This can be done by choosing a polar grid.

2. **Shadowing**, this may be present in the data when a beam is not able to reach the through of a wave or possibly an entire wave because of a big wave in front of it which blocks the beam.

3. **Current**, as an effect of current the measured velocities will not be centered around a mean of zero. To effectively deal with the current it's direction and magnitude needs to estimated and subtracted from the signal.

4. **Wave direction**, this might cause the propagation speed of the velocities to be other than expected. The direction can be included by adjusting the wave numbers k_x, k_y

Parameter	Value	Unit
Sample rate	10	MHz
Frequency sweep per chirp	200	MHz
Samples per chirp	1032	
Processing blocksize	1024	
Bundle width	3.07	degrees
Bundle opening angle	19	degrees
Range resolution	75	cm
Range	384	m
Number of range cells	511	
Azimuth beams	-40,-20,0,20,40	degrees
Overall scan rate	50	Hz
Scan rate per beam	10	Hz
Mounting height	15	m

Table 3.1: Summary of the parameter settings of the radar

5. **Breaking waves**, as discussed in the previous chapter waves are able to break when the particle velocity exceeds the forward wave speed. In that case the radar will measure a relatively high velocity which is not part of a feasible wave in the linear wave theory
6. **Radar noise**, these are disturbance that are present due to the processing of the radar itself. They may cause some unpredictable fluctuations of the values in the data stream.

In the following sections the extra effects that are present in the data set are treated.

3.2.1. Orbital velocity

The set-up of the radar is that it measures in five different directions (-40, -20, 0, 20, 40 degrees) as seen table 3.1. For each radar scan an output for a fixed number (n) of fixed size (ΔR) range cells is obtained, let this be given by:

$$R_b = [1, 2, \dots, n]\Delta R \tag{3.1}$$

This radar beam is narrow in the horizontal plane and wide in the vertical plane. Where it hits the water surface it has a (mostly small) angle γ relative to the horizontal plane. This angle can be expressed in terms of the mounting height (H) and the radius of the beam hitting the water (R_w). This becomes:

$$\gamma = \sin^{-1}\left(\frac{H}{R_b}\right) \tag{3.2}$$

and thus the horizontal radius can be expressed like:

$$R_w = R_b \cos(\gamma) \tag{3.3}$$

As a consequence of this the grid will not be equidistant. Furthermore it can be concluded that for the first grid cells there is no useful measurement as the (real-valued) domain for the inverse sine lies between -1 and 1. Due to the mounting height of $H = 12$ meters it will cause $\frac{H}{R_b} > 1$ for the first 16 entries of R_b.

Besides this compensation for the range coordinates, also there needs to be a compensation for the model to deal with the data coming from these range cells. For the model the desired input is the horizontal component of the orbital velocity. For range cells that are located far from the radar in comparison to the mounting height this holds. For range cells closer to the radar the measured velocity does not represent the horizontal component of the orbital velocity due to the larger angle between the radar beam and the horizontal plane. To compensate for this effect the model formula or data needs to be projected on resp. the radar beam or the horizontal plane. An uncertainty arises here since the measured data itself is already a projection of the actual velocity onto the beam. For this model it is useful to transform the data such that is in the horizontal plane. By doing so it can be treated as the horizontal component of the orbital velocity (u_{meas}). So again consider γ, then we can transform the measured velocity for a particular beam (u_{beam})(where azimuth angle is not yet important) into:

$$u = u_{beam} \cos(\gamma) \tag{3.4}$$

3.2.2. Shadowing effects

The first effect that is present is called the shadowing effect. Shadowing occurs when a high wave blocks an area behind it such that the radar beams are not able to reach those areas. The size of shadowed areas depend on a few factors (or combinations of those). First one is the height of the wave blocking the radar beam, where a higher wave will block a larger area. Second is the distance of the wave that shadows an area towards the radar. When the high wave is located at a distance far from the radar it will block more area behind it. This is due to radar beam making less of an angle with the surface at distances further away. A third factor is that of the waves that are present behind the wave that shadows. E.g. if there is a pretty steep and high wave close behind the wave that creates a shadow the shadowed area is smaller than when the waves behind the wave that creates shadowing are small in amplitude.
When observing the data set that the radar gives, there is a value for each grid cell, so this would intuitively imply that there is no shadowing present. But when an inversion is done (by fitting a wave model to this data) it can be shown that shadowing is present. An example of this is give in figure 3.3, here it is visible that there are three shadowed areas. Hence, the data that the radar gives for these areas should not be trusted.

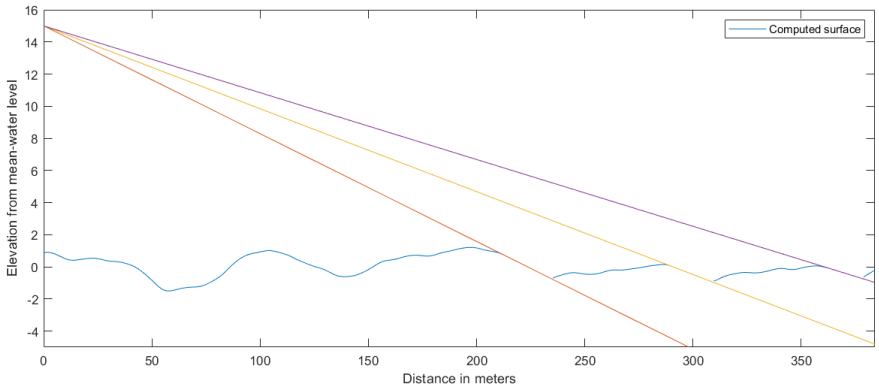

Figure 3.3: Example of the shadowing effect with the radar mounted at 15 meters above the surface. Rays indicating the beams from the radar where shadowing occurs.

These areas are identified by first finding the local peaks in the computed heave information since the cells behind those peaks are candidates for the shadowing effect. Then lines are drawn from the radar position towards each of these peaks. A few of these lines can be seen in figure 3.4.

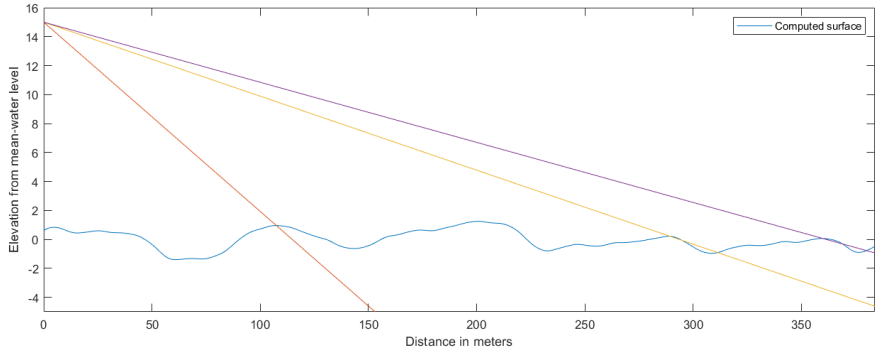

Figure 3.4: Beams from the radar towards some of the local maxima of the wave surface for shadowing identification

The number of crossings between the line and the surface then suggests whether shadowing is present, if the number of crossings is equal to one there is no shadowing effect from this wave (as with the red line in figure 3.4). If the number of crossings is higher than one there is a shadowed area behind this wave (as with the yellow and purple line in figure 3.4). For the waves where the presence of shadowing is identified the slope of the corresponding line is increased until the number of crossings becomes two.

The xgrid values between these two crossings form the shadowed area and is excluded from further computations.

3.2.3. Current velocity and other effects (due to coastal water)

When one takes a look at the velocities plotted over the spatial grid (see figure 3.5) it should be noticed that these velocities have a mean value that is higher than zero. If the radar would solely capture the orbital velocities it is expected that these would be centered around zero. There are multiple reasons that would explain why this occurs, which also makes it hard to distinguish what the contribution of one particular effect is.

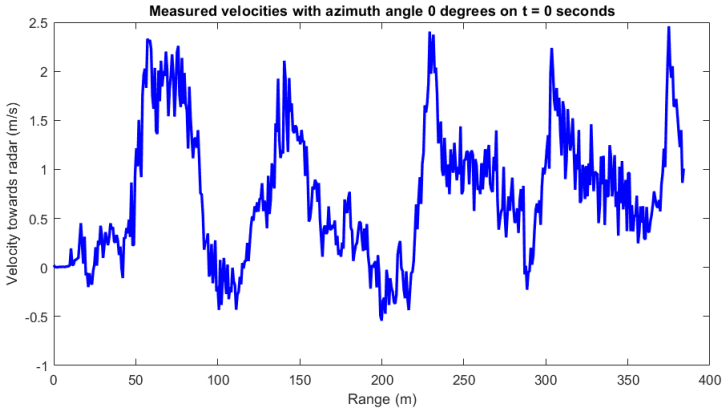

Figure 3.5: Example of the data coming from the beam with azimuth angle of zero degrees

The shadowing effect that is discussed in the previous subsection could be one of the reasons that contributes to the higher velocities, since data from a shadowed area is considered false and this information is often containing the negative velocities (since these are found in the wave trough). So since the velocities of these wave troughs are measured inaccurately it is hard to say whether they should actually be lower (or higher).
Another main contribution for the high mean velocity could be the current of the sea. With current direction towards the shore higher velocities are obtained by the radar. To estimate the effect the current has assumptions need to be made. If the area is assumed to have constant depth and the current itself is constant in space and time the waves will still behave according to the linear wave theory.

3.2.4. Disturbances by the radar itself

The data also has some disturbances that are due to the radar itself and not necessarily coming from the water surface. This can be seen in figure 3.6. The signal after about 4 minutes shows periodic behaviour for the mean velocity over the entire grid. This enhances the idea that the current during this period of time is constant. Therefore the linear wave theory is likely to still be valid in this case.

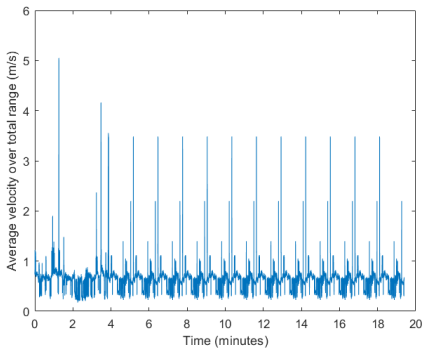

Figure 3.6: The average of the velocities over the entire spatial range plotted over time with azimuth angle equal to zero

3.3. Artificial data set

To test the model that will be built also an artificial environment needs to be created. By doing this the performance of the model can be evaluated in a precise way, whereas the real measurement data contains some irregularities, making it harder to distinguish whether the errors/faults are a consequence of the model performance or the data set. So there is a need for this artificial data set, and the more realistic it is, the better the model can be tuned before facing the real data. To do so a sea is created which resembles the North Sea, where the real data also comes from. To generate such a sea surface in a one dimensional case the JONSWAP spectrum [3] is used, which is also discussed in the previous chapter. When the extra space dimension is taken into account the $\cos^2\theta$ directional spreading is used. The waves are then generated by using a superposition of the solutions 2.29 and 2.58 of the linear wave theory derived in chapter 2. For this artificial data a deep water situation is used.

3.3.1. One directional data

This wave field is generated based on three input parameters: the significant wave height H_s (recall: mean of the highest one-third of waves in the wave record), peak period T_p and a frequency spectrum of the waves Ω. The code then generates amplitudes, phases and spectral values for the wave field. The number of wave components is determined by the number of input frequencies in Ω. Combining the input frequencies, amplitudes and phases into a sum of sine components allows one to recreate a (one-dimensional) sea surface and the corresponding orbital velocities as in the following equations. Here the wave numbers k_i are determined by the dispersion relation.

$$\eta(t) = \sum_{i=1}^{N} A_i \cos(w_i t - k_i x + \psi_i) \tag{3.5}$$

$$u(t) = \sum_{i=1}^{N} -\omega_i A_i \cos(w_i t - k_i x + \psi_i) \tag{3.6}$$

So this surface elevation and horizontal orbital velocity is in exact agreement with the derived formulas in the last chapter. This wave field is generated for a spatial grid and time steps equal to the real data. A realization of this surface can be found in figure 3.7. The realization of the orbital velocities is found in figure 3.8. These are generated with the parameter settings found in table 3.2.

Parameters	Values	Unit
T_p (peak period)	6	s
H_s (significant wave height)	2	m
ω_c (cut-off frequency)	$33T_p^{-1}$	Hz
ω (frequency spectrum)	linspace$(0.1, \omega_p, 200)$	Hz

Table 3.2: Summary of the input parameters for an one directional artificial data set

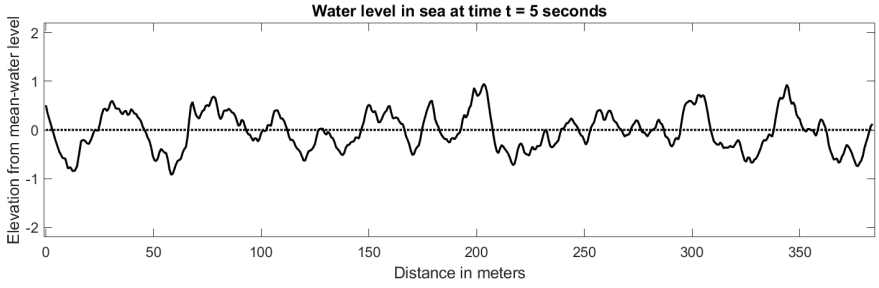

Figure 3.7: Realization of the water surface generated by the JONSWAP spectrum

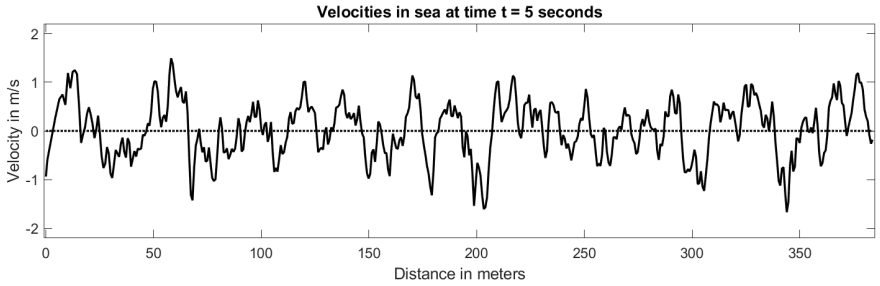

Figure 3.8: Realization of the horizontal orbital velocity generated by the JONSWAP spectrum

3.3.2. Multi directional data

For the data set with the extra space dimension also the JONSWAP spectrum is used, but with an added module to simulate the wave directions according to the $\cos^2\theta$-model. Then this wave field is generated based on four instead of three input parameters: the significant wave height H_s , peak period T_p, frequency spectrum of the waves Ω and directions θ for which the output needs to be generated (where the main direction is always with zero angle). The code then generates amplitudes, phases and spectral values for the wave field for the directions defined by θ. Combining these input frequencies, amplitudes and phases into a sum of sine components allows one to recreate a sea surface and orbital velocities as described below.

$$\eta(x,y,t) = \sum_{j=1}^{M}\sum_{i=1}^{N} A_{ij}\cos(\omega_i t - k_i(x\cos(\theta_j) + y\sin(\theta_j)) + \psi_{ij}) \tag{3.7}$$

$$u(x,y,t) = -\sum_{j=1}^{M}\sum_{i=1}^{N} \omega_i A_{ij}\cos(\omega_i t - k_i(x\cos(\theta_j) + y\sin(\theta_j)) + \psi_{ij}) \tag{3.8}$$

Here M denotes the number of wave directions that is taken by the user for θ and N denotes the number of cosine components per wave direction. For the situation to mimic the radar observations this above equation is not the best representation though. To improve this the switch is made to polar coordinates, where $x = r\cos(\gamma)$ and $y = r\sin(\gamma)$. This is a more natural choice since the measured data is coming from a radar at a fixed location where it measures over a 1-D distance range with a certain angle, which is naturally represented by polar coordinates. Let furthermore:

$$k_{x,ij} = k_i\cos(\theta_j) \qquad k_{y,ij} = k_i\sin(\theta_j) \tag{3.9}$$

Then the wave field is calculated as follows:

$$\eta(r,\gamma,t) = \sum_{j=1}^{M}\sum_{i=1}^{N} A_{ij}\cos[\omega_i t + \psi_{ij} - r(k_{x,ij}\cos(\gamma) + k_{y,ij}\sin(\gamma))] \tag{3.10}$$

$$u(r,\gamma,t) = \sum_{j=1}^{M}\sum_{i=1}^{N} -\omega_i A_{ij}\cos[\omega_i t + \psi_{ij} - r(k_{x,ij}\cos(\gamma) + k_{y,ij}\sin(\gamma))] \tag{3.11}$$

This is also done for a spatial grid and time steps equal to the real data. The other parameter settings can be found in table 3.3. A realization of this moving surface can be found in figure 3.9. This is a visualisation over a Cartesian grid which is nice to show the behaviour of the entire surface. For the model use it is more convenient to use the beam directions and make the plots in a dimension lower. Then the visualisation is used as in figure 3.10.

Parameters	Values	Unit
T_p (peak period)	6	s
H_s (significant wave height)	2	m
ω_c (cut-off frequency)	$33T_p^{-1}$	Hz
ω (frequency spectrum)	linspace$(0.1, \omega_p, 200)$	Hz
θ (directional spreading)	linspace$(-\frac{\pi}{8}, \frac{\pi}{8}, 5)$	radians

Table 3.3: Summary of the input parameters for the multi directional artificial data set

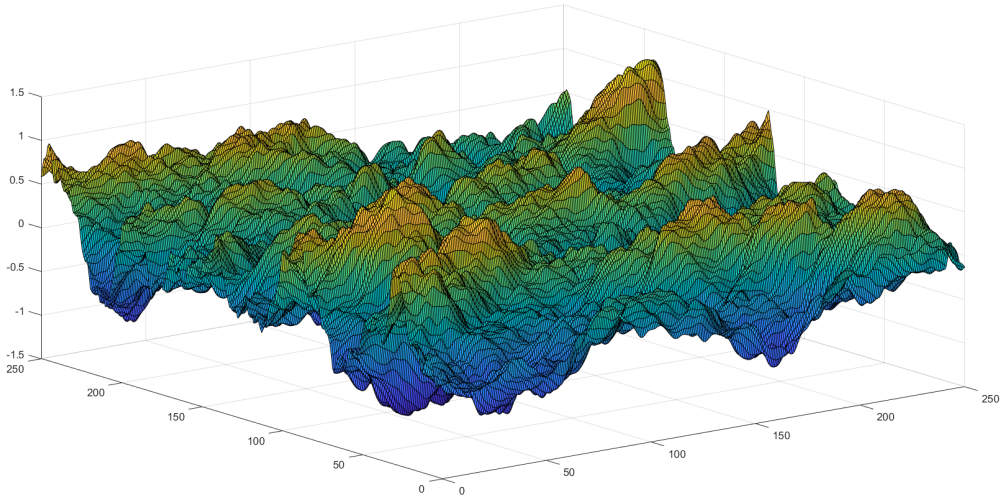

Figure 3.9: Realisation of an artificial sea surface with directional spreading

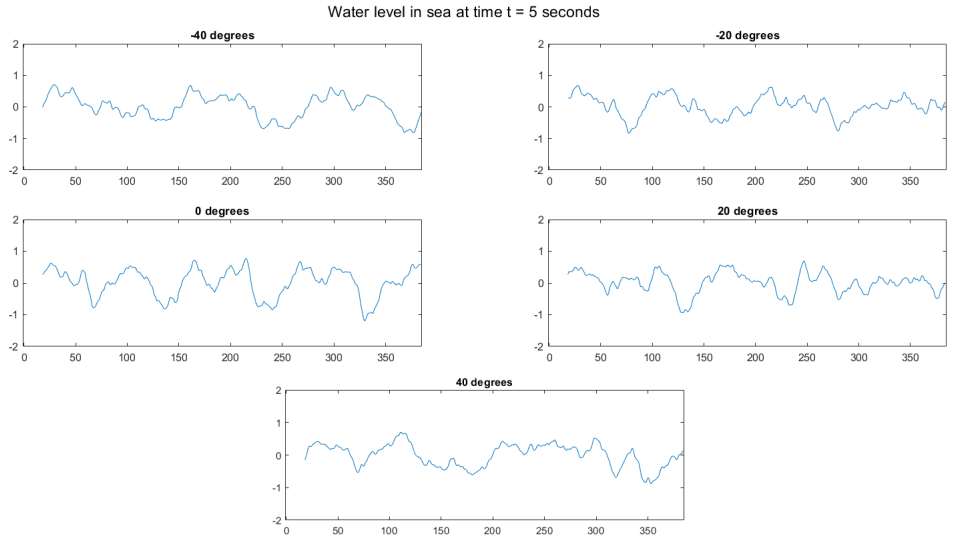

Figure 3.10: Realisation of an artificial sea surface with directional spreading in the 5 beam directions

3.3.3. Gaussian white noise

As a next step towards using the model on a real data set some Gaussian white noise is added to the signal. By doing so an extra challenge is added for the model to solve, in the real data the data also gets disturbed by multiple effects as discussed earlier this chapter.

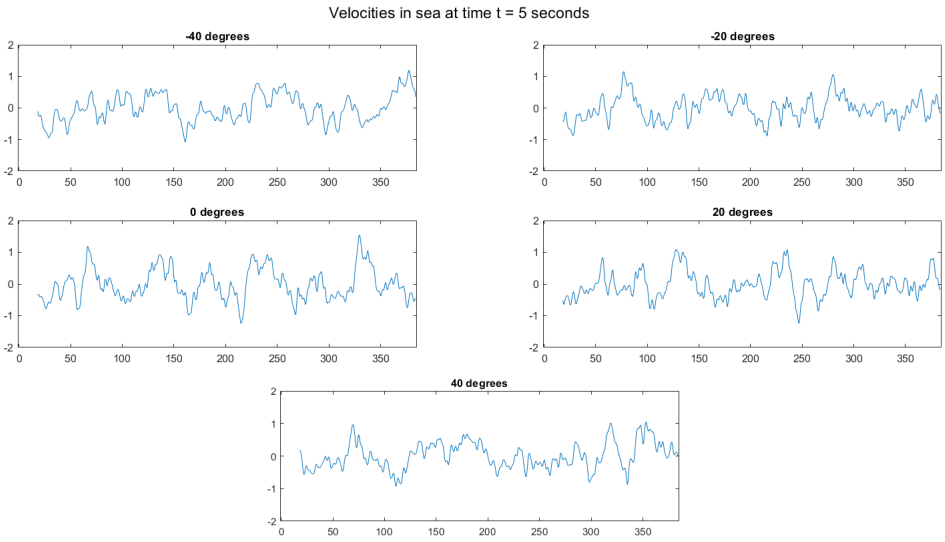

Figure 3.11: Realisation of an artificial sea surface with directional spreading in the 5 beam directions

White noise has the property that the mean of this signal is time independent and equal to zero for all timesteps, so $E[W(n)] = 0$. Furthermore the individual entries are normally distributed and uncorrelated.

This was implemented with the use of the MATLAB function *awgn*. This allows the user to input an incoming signal and a desired signal-to-noise ratio (SNR), which is the ratio of signal power to noise power, and produces an output of the original signal with the white noise added to it. A visualization of this sea in one direction can be found in figure 3.12. The orbital velocities are shown in figure 3.13 for the one directional model.

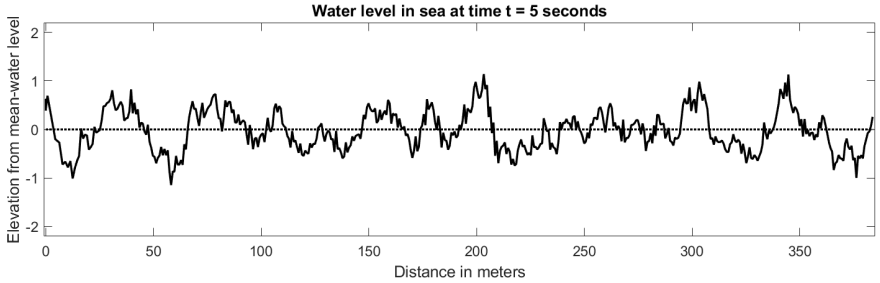

Figure 3.12: Realization of the water surface generated by the JONSWAP spectrum with Gaussian white noise (SNR 10)

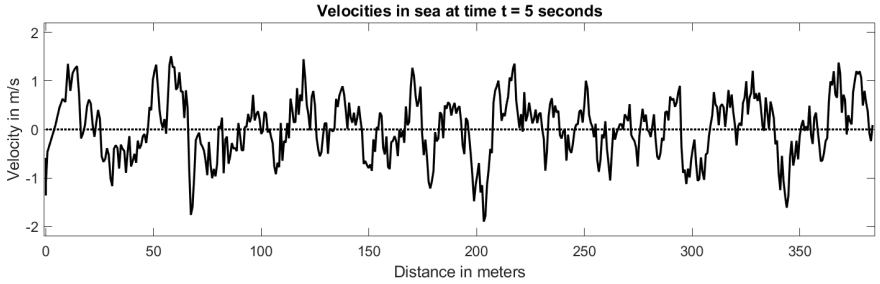

Figure 3.13: Realization of the horizontal orbital velocity generated by the JONSWAP spectrum with Gaussian white noise (SNR 10)

4

Reconstructing wave characteristics

The goal of this thesis is to able to reconstruct waves (and with that information predict incoming waves), based on the information the FMCW radar gives us from it's high frequency measurements in multiple directions (which are discussed in Chapter 3). The assumption that was made for this is that the waves can be characterized by using the linear wave theory that was treated in Chapter 2. This means that the data coming from the radar can be represented as a superposition of individual long-crested wave components:

$$\eta(\mathbf{x}, t) = \sum_{i=1}^{n} A_i \cos(\omega_i t - \mathbf{k_i} \cdot \mathbf{x} + \psi_i) \tag{4.1}$$

and thus that the orbital velocity is represented by a summation of individual components that have the same parameters as in equation 4.1:

$$u(\mathbf{x}, t) = -\sum_{i=1}^{n} \omega_i A_i \cos(\omega_i t - \mathbf{k_i} \cdot \mathbf{x} + \psi_i) \tag{4.2}$$

To retrieve these parameters whilst knowing what the result is from the measurements inverse modelling is used. To do this first the problem is reduced to an one directional situation to test the concepts of fitting to the data and is later expanded to the multi directional situation. Note that in 4.2 the deep water representation is taken, which holds for the artificial data by design.

4.1. Inverse modelling

In this section the mathematical methods of the modelling that were needed are discussed. These methods will be needed to match the mathematical formulation for the ocean waters to the data that will be available. By the linear wave theory it is assumed that the orbital velocity data coming from the radar can be represented as in 4.1.
Where the challenge lies in finding the best or 'true' parameter values of $A_i, \omega_i, \mathbf{k_i}$ and ψ_i to fit the sum of cosine components to the measured u_{meas}. Such problems of finding parameters whilst knowing the value that the function they appear in should equal is called inverse modelling. The method used to solve the problem is presented in this section. Besides the inverse modelling also dynamic averaging was used for the sequential modelling method, this is discussed in section 4.1.2.

4.1.1. Least squares solving algorithms

For this problem of parameter estimation a least squares solving method is one of the suited choices. Let β denote the vector containing the parameters that need to be fitted to the data set, so let $\beta = [A_1 ... A_n, \omega_1 ... \omega_n, k_1 ... k_n, \psi_1 ... \psi_n]$ in this setting. The goal of the methods then is to minimize the sum of squared residuals $S(\beta)$:

$$S(\beta) = ||\mathbf{r}(\beta)||_2^2 = \sum_{j=1}^{m} r_j^2(\beta), \tag{4.3}$$

where m represents the number of measurements the chosen function needs to fit on and where $\mathbf{r}(\beta) = [r_1(\beta), ..., r_m(\beta)]$ represents the vector containing residuals and where the residuals are given by:

$$r_j(\beta) = u_{meas}(\mathbf{x}_j) - u_{fit}(\mathbf{x}_j, \beta) \tag{4.4}$$

The input for $\mathbf{x}_j$ could be of various sizes and dimensions (including multiple space dimensions and with or without the time dimension), depending on the purpose of the fit. As long as there is a measured value for this $\mathbf{x}_j$ this will not give any complications.

In the following two subsections two kinds of least squares solving algorithms are treated. Both of them are contained in the Matlab curve fitting toolbox, making the execution of how there are implemented as efficient as it could be.

Levenberg-Marquardt algorithm

The first algorithm is the *Levenberg-Marquardt algorithm*[9][10]. This can be seen as an improved version of the basic *Gauss-Newton* algorithm, combining it with the *Gradient Descent* method. To understand the concept of Levenberg-Marquardt a brief explanation of this method is given first. Consider the problem described in the beginning of section 4.1.1.
The Gauss-Newton method finds an optimal β^* by updating it iteratively as follows:

$$\beta^{l+1} = \beta^l + (\mathbf{J}_u^\top \mathbf{J}_u)^{-1} \mathbf{J}_u^\top \mathbf{r}(\beta^l) \tag{4.5}$$

where $\mathbf{J}_u$ stands for the Jacobi matrix of u_{fit}, so this means:

$$(\mathbf{J}_u)_{ij} = \frac{\partial u_{fit}(\mathbf{x}_i, \beta^l)}{\partial \beta_j} \tag{4.6}$$

For the algorithm it is important that $m > 3n$ to find a (unique) solution, so the number of cosine terms is limited by the number of grid points that give data to fit on. The algorithm can be stopped when the difference in improvement becomes to small, so when:

$$|\beta^{l+1} - \beta^l| < \epsilon$$

or when a certain amount of iterations has been done. This could be a good option when the time that is reserved for calculating this optimization is limited.

The Levenberg-Marquardt algorithm is an improved version of the Gauss-Newton method, since this method uses a weighted step size (which results in faster convergence and makes it handle ill conditioned problems). This algorithm finds an optimal β^* by updating as follows:

$$\beta^{l+1} = \beta^l + (\mathbf{J}_u^\top \mathbf{J}_u + \lambda^l \operatorname{diag}(\mathbf{J}_u^\top \mathbf{J}_u))^{-1} \mathbf{J}_u^\top \mathbf{r}(\beta^l) \tag{4.7}$$

where λ represents the *damping* parameter. For large values of this λ this makes sure that:

$$\mathbf{J}_u^\top \mathbf{J}_u + \lambda^l \operatorname{diag}(\mathbf{J}_u^\top \mathbf{J}_u) \approx \mu \mathbf{I} \tag{4.8}$$

which as a consequence will make the update term for β^l similar to the one used in a gradient descent method. For small values of λ^l the following happens:

$$\mathbf{J}_u^\top \mathbf{J}_u + \lambda^l \operatorname{diag}(\mathbf{J}_u^\top \mathbf{J}_u) \approx \mathbf{J}_u^\top \mathbf{J}_u \tag{4.9}$$

which as a consequence will make the update term for β^l similar to the one used in a Gauss-Newton method. Also this algorithm combines the abilities of both methods (i.e., convergence from any initial state as in the case of gradient descent, and the rapid convergence near in the neighborhood of the minimum error as in the case of Gauss-Newton method) while avoiding their drawbacks. The disadvantage of this method however is that it cannot take lower and upper bounds into account for the parameters.

Trust-Region reflective algorithm

The algorithm that is used eventually is called the *trust-region reflective* algorithm, which itself can be seen as an evolution of the Levenberg-Marquardt method (with the possibility of setting bounds for the parameters). The idea of the Levenberg-Marquardt method is to handle possible ill-condition of $\mathbf{J}_u$ by introducing the damping parameter λ. This can also be seen as preventing that $||d||_2$ grows too large, where d equals the update term:

$$d = (\mathbf{J}_u^\top \mathbf{J}_u + \lambda \ \mathrm{diag}(\mathbf{J}_u^\top \mathbf{J}_u))^{-1} \mathbf{J}_u^\top \mathbf{r}(\beta) \tag{4.10}$$

This d is also a solution of the following minimization problem:

$$\min_{d \in R} ||\mathbf{r}(\beta) + \mathbf{J}_u d||_2^2 \tag{4.11}$$

$$\text{s. t.} \quad ||d||_2 \leq \Delta_l \tag{4.12}$$

where Δ_l is a positive scalar. The addition of the constraint 4.12 in this minimization problem makes that the Levenberg-Marquardt algorithm can be seen as similar to a trust-region algorithm. In every iteration the algorithm tries to improve within a bounded region from where the algorithm is at the current moment (like 4.12 (which will be called *the trust region*)). However a trust-region algorithm updates the bound Δ_l per iteration and not λ^l, making trust-region algorithms differ from what is treated so far.

The rough idea of the trust-region method goes as follows:

1. First a trust-region subproblem is formulated,
2. after this the trial step s is determined by solving this subproblem.
3. The current β then gets updated when $S(\beta + s) < S(\beta)$, if this is not the case then β remains the same.
4. The trust region radius Δ is updated

These steps are repeated until convergence of the 2-norm of the gradient of $S(\beta)$ is reached. Now the algorithm will be described in a bit more detail.

So first the subproblem needs to be formulated, this is set up as follows: Consider again the unconstrained minimization problem that was originally encountered, so minimize $S(\beta)$ (the squared sum of residuals $\mathbf{r}(\beta)$). Then at iteration l the trail step will be computed by solving this trust-region subproblem:

$$\min_{d \in R} \ \phi^l(d) = (g^l)^\top d + \frac{1}{2} d^\top B^l d \tag{4.13}$$

$$\text{s. t.} \quad ||d||_2 \leq \Delta_l \tag{4.14}$$

Here $g^l = \nabla S(\beta)$ represents the gradient and B^l represents the Hessian matrix of $S(\beta)$. Furthermore $\Delta_l > 0$ is called the trust region radius. $\phi^l(d)$ then represents a quadratic approximation of $S(\beta)$. Let s^l be a solution of this subproblem, then it needs to be decided whether this trial step is acceptable and if the trust region radius needs to be adjusted. The trial step is accepted when $S(\beta^l + s^l) < S(\beta^l)$, then the new parameter set becomes $\beta^{l+1} = \beta^l + s^l$; otherwise, the current parameter set β remains the same and Δ_l is shrunk and the trial step computation is repeated.

Solving the trust-region subproblem can be very challenging, and may require multiple factorizations of the Hessian matrix. This can be computationally expensive, thus an approximation technique is used. The approximation approach to compute the trial step s^l is to restrict the trust-region subproblem to a two-dimensional subspace S. The 2-dimensional search method is to minimize the objective function in the subspace S spanned by the steepest direction (let this be s_1) and the Newton step (let this be s_2) within the trust region. This 2-dimensional search method was first suggested by Schultz, Schnabel and Byrd[1].
The philosophy behind this choice of S is to force global convergence (via the steepest descent direction or negative curvature direction) and achieve fast local convergence (via the Newton step, when it exists).

Both the Levenberg-Marquardt and trust-region reflective algorithm are available in the Matlab *lsqcurvefit* routine. For the trust-region reflective algorithm the condition can be imposed that the parameters must be within certain bounds. This property will be very useful for the use of the model to exclude breaking waves from the solution.

4.1.2. Dynamic averaging method

Besides the inverse modelling another useful technique may be to average the solutions over time as suggested by Wijaya [17]. In that research a pulse radar was used, which has less updates over time, bigger grid cells and a larger area surrounding the radar itself where no measurements are available (compared to the FMCW radar data). Here an averaging of the reconstructed sea state was suggested to compensate for the shadowing and other inaccuracies of the measurements. This was done by evolving the reconstructions of two previous time steps and average them with the reconstruction of the current time step (where these time steps are in the range of 2 seconds). The weights that were chosen by Wijaya were not motivated in depth, though. The 3 evolved reconstructions were weighted equally and further averaged with an ongoing simulated sea multiplied with a characteristic function. This characteristic function denoted areas where the sea could not be observed, making the radar measurements useless for that area. This approach proved to be successful and therefore a similar approach for this problem could be beneficial when considering a model that generates solutions for several time steps that are further apart. The idea of Wijaya was taken and altered in a way that would suit the model of this thesis better. This is done by letting the weights depend on the quality of the evolved past reconstruction.

The averaging that is chosen for this thesis is to also take the two previous fits to measurement $t - dt, t - 2dt$ (to be referred to as t_{-1}, t_{-2}) and the current fit to a measurement t_0. The weight $w(t_{-1})$ of solution $u_{fit}(\mathbf{x}, t, \beta_{-1})$ with parameter set $\beta_{-1} = \beta(t_{-1})$ will depend on the MSE of that u_{fit} with u_{meas} at the current time (so evolved over one or two time steps (between the fits)). So this becomes:

$$\begin{aligned} w(t_{-2}) &= \frac{1}{\mathrm{MSE}(\beta_{-2}, t_0)} \\ w(t_{-1}) &= \frac{1}{\mathrm{MSE}(\beta_{-1}, t_0)} \\ w(t_0) &= \frac{1}{\mathrm{MSE}(\beta_0, t_0)} \end{aligned} \tag{4.15}$$

Where the MSE is computed for entries $j = -2, -1, 0$ as:

$$\mathrm{MSE}(\beta_j, t_0) = \frac{1}{M} \sum_{i=1}^{M} (u_{fit}(x_i, t_0, \beta_j) - u_{meas}(x_i, t_0))^2 \tag{4.16}$$

This gives the averaged solution:

$$\overline{u}_{fit}(\mathbf{x}, t, \beta_0, \beta_{-1}, \beta_{-2}) = \sum_{j=-2}^{0} \frac{w(t_j)}{w(t_{-2}) + w(t_{-1}) + w(t_0)} u_{fit}(\mathbf{x}, t, \beta_j) \tag{4.17}$$

This method will be used for the cosine-by-cosine sequential fit for the one directional model that is presented in the next section that describes the way in which the model used in Matlab works.

4.2. Fitting waves to measurements

In the last section the mathematical methods were presented to generate a fit to the data. In this section the structure of the model is discussed for the one direction and multi directional cases.

4.2.1. One directional model

To set-up the one directional model a division into smaller steps is useful. These will be broken down part-by-part in the following subsections. At first the data will be imported and processed. After this the precise formulas are set-up and the initial and boundary conditions are imposed. Then the model can be fitted to the data and afterwards the performance of it can be evaluated.

Data importing and processing

As a first step the measurement data is collected and corrected by some pre processing steps. This can be done for artificial data and the real measurement data. How this is done in both cases differs due to the nature of these data sets.

The pre processing for the artificial data is not too complicated as it is known how it is generated, only the white noise may cause issues in the fitting of wave modes. But it contains no extra hidden information that needs to be accounted for. For the processing of the real data some additional actions need to be taken, these are also discussed in chapter 3 in more detail. For the one directional model the assumption of infinitely long wave crests coming straight towards the radar is made, so the real data must be limited to information from one of the five (-40,-20,0,20,40 degrees) beams. Therefore the beam that is most aligned with the wave direction needs to be selected for the best result.
After this selection of the beam the grid over which this beam was obtained is corrected for the angle that the radar beam has towards the water and the velocities are adjusted as well to not represent velocities along the beam, but in the horizontal plane.
The next processing step of the real data is to remove the current velocity from the data. As shown in section 3.2 of chapter 3 it is reasonable to suggest that the current velocity is constant (which means that linear wave theory will still hold). For every time step the effect of the current is removed by subtracting the mean velocity over the grid from the measured velocities.

Problem formulation

Now that the data is imported (and corrected) it should be able to get represented by a linear wave theory model. As stated before it is assumed that this velocity data fits to the horizontal component of the orbital velocity of the wave. For the one directional model the assumption of infinitely long-crested waves in the direction of the radar holds. So let our model function be:

$$u_{fit}(x,t,\beta) = \begin{cases} -\sum_{i=1}^{N} \omega_i A_i \cos(\omega_i t - k_i x + \psi_i) & \text{if current is absent} \\ -\sum_{i=1}^{N} \omega_i A_i \cos((\omega_i - k_i U)t - k_i x + \psi_i) & \text{if (constant) current is present} \end{cases} \tag{4.18}$$

Where β is the collection of all parameters. Due to the dispersion relation the wavenumbers k_i will be expressed in terms of ω_i:

$$k_i = \frac{\omega_i^2 \tanh(k_i d)}{g} \tag{4.19}$$

By doing so the amount of parameters that need to be fitted is reduced and by this substitution the relation is automatically satisfied and does not need to be accounted for separately. Let the measured data be given by u_{meas}, then the sum of squared residuals $r = u_{meas} - u_{fit}$ becomes:

$$S(\beta) = \sum_{i=1}^{N} \sum_{j=1}^{M} r_{ij}(\beta)^2 \tag{4.20}$$

where j represents the points in space and time that are used from the measured data. Then this $S(\beta)$ can be minimized by applying the inverse modelling methods. For the artificial case the term the dispersion relation is altered by the deep water, which excludes the tanh-term from the equation.

$$\begin{aligned} \min_{\beta} \quad & S(\beta) \\ \text{s.t.} \quad & 0 \leq A_i \leq \frac{2\pi g \tanh(k_i d)}{7\alpha^2} \\ & 0 \leq \omega_i \leq \alpha \\ & 0 \leq \psi_i \leq 2\pi \end{aligned} \tag{4.21}$$

In the constraints there is a parameter α which links the constraints for the wave amplitude and the wave frequency. This is done since there is a physical limit for the relation between these two as described by 2.73.

Fitting strategies in Matlab

To solve the minimization problem a trust-region reflective algorithm is used. The execution of this algorithm can be done in a few ways, of which some use prior knowledge about the ocean to make further assumptions and some that give the algorithm some more freedom. These are combined into two sets of code which are discussed below.

Non-sequential fit

The first approach to solving 4.21 is by fitting the sum of cosine functions as one to the measured velocities. By doing so the algorithm adjusts all parameters A_i, ω_i, ψ_i each iteration to find an optimal fit to the measured velocity data. This approach has the advantage that the fitting algorithm has a lot of flexibility in adjusting all individual parameters.
This also means that the amount of parameters that should be adjusted becomes quite large ($3N$), when a lot of cosine functions are required to give an accurate fit, though. Consequence of this is that iterations could become very costly in terms of calculation time, since the algorithm needs to work with high dimensions. To reduce this amount of parameters the choice was made to exclude ω_i as a parameter in the fit. Instead the angular frequency values are fixed between a minimum and maximum frequency on a equidistant grid between those values. The number of frequencies is equal to the amount of cosine components that are used. So:

$$\omega = [\omega_1, \dots, \omega_N] \tag{4.22}$$

So only the amplitudes and phases are left to be fitted on the data, which reduces the amount of parameters in the model to $2N$. A downside of this fixed frequency bins could be that in general all frequencies occur in the sea and thus that this choice takes away some of the flexibility of the model to make use of this property.
An important notice is that a higher number of observations compared to the number of parameters is needed to make a fit. This is necessary to give the model sufficient degrees of freedom and to prevent it from overfitting. To do so the amount of time and range steps needs to be sufficiently large. Taking multiple time steps will also help to capture the dynamics of the waves. This gives this method an advantage over the sequential method that will be discussed next.
As an initial condition for the amplitudes the Rayleigh distribution as in equation 2.67 is taken and the phases are initially chosen constant.

Cosine-by-cosine sequential fit

A second way to execute the optimization is an alternative to fitting all cosines as one function, namely by fitting the A_i, ω_i, ψ_i cosine-by-cosine to the velocity information on a fixed point in time. Once the algorithm has found an optimal fit for a single cosine to the signal (which is bounded by a certain number of iterations or improvement ratio), it gets subtracted (using the found values for A_i, ω_i, ψ_i) from the measured velocity information. And then it starts the same fitting procedure for the next cosine. When an optimal fit is found for this cosine again it gets subtracted and so on until the last cosine is fitted to the original signal minus all the previously fitted cosine functions.

An advantage of this method is that only a small number of parameters is fitted per function, which makes it easy to solve for the trust region algorithm. Though the number of times this has to be done can become large and may hit the max iteration bound of the solver. Another advantage of the method

is that the shadowing effects can be explicitly taken into account when there are historical realizations of the fitted surface. Based on this information, grid cells that may contain shadowed data can be excluded from the next fitting procedure. Furthermore there are some downsides to this method, there is a risk of overfitting to the data or fitting to noise when the number of sines is taken too large. And the algorithm cannot change parameter values once it is fitted, this gives a limitation in the flexibility of the procedure. It will be harder to make up for a fitted cosine that was inaccurate. Besides this the model will generate a fit on the data of only one moment t in time. This is compensated by dynamically averaging the solutions from previous time steps where the model has been fitted to the data as described in section 4.1.2.

Performance metrics

To measure the performance of the fitted function a performance metric is helpful. For this there are multiple options. The most common measures are the mean absolute errors (MAE) and the mean squared error (MSE).

$$\text{MAE}(\beta) = \frac{1}{M}\sum_{i=1}^{M}|u_{fit}(\mathbf{x}_i,\beta) - u_{meas}(\mathbf{x}_i)| \tag{4.23}$$

$$\text{MSE}(\beta) = \frac{1}{M}\sum_{i=1}^{M}(u_{fit}(\mathbf{x}_i,\beta) - u_{meas}(\mathbf{x}_i))^2 \tag{4.24}$$

In the notation $\mathbf{x}_i$ refers to the points in (x,t)-space for which the fit is compared to the data. Besides these traditional measures a normalized averaged prediction error is suggested in [15]:

$$error(\beta) = \sqrt{\frac{\sum_{i=1}^{M}(u_{fit}(\mathbf{x}_i,\beta) - u_{meas}(\mathbf{x}_i))^2}{\sum_{i=1}^{M}(u_{meas}(\mathbf{x}_i)^2)}} \tag{4.25}$$

This last measure gives the magnitude of the error compared to the measured value. So an error of value 1 states that the discrepancy between measurement and fit has the same magnitude as the measured value. E.g. if the measured velocity is 0.5, the magnitude of the error is 0.5 and if the measured velocity is 3, the magnitude of the error is 3. But both are represented by value 1. A value close to 0 states that the fit and measured velocities are in agreement.

Statistical parameters

Due to the set-up of this model with linear wave theory a nice extra is that the possibility arises to subtract statistical information from the sea. This is possible since the linear wave theory solution for the water surface is similar to random phase/amplitude model used to gather sea statistics. The first statistical information that can be obtained is the (amplitude) spectrum of waves. This is done by taking the fitted A_i and plot them against the frequencies ω.
The second statistical parameter that can be obtained is the significant wave height H_s.

$$H_s \approx 4\sqrt{m_0} \tag{4.26}$$

where m_0 represents the zero-th order moment, where the moments m_n given by:

$$m_n = \int_0^\infty f^n E(f)df \tag{4.27}$$

and $E(f)$ can be computed as shown in section 2.4.1:

$$E(f) = \lim_{\Delta f \to 0} E\left(\frac{1}{2}\underline{a}^2\right) \tag{4.28}$$

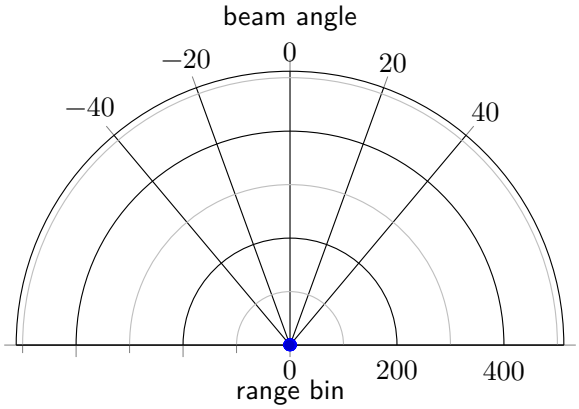

Figure 4.1: The polar grid representation of the data

4.2.2. Multi directional model

To set-up the multi directional model again a division into smaller steps is made. These will be broken down part-by-part in the following subsections. At first the data will be imported and processed. After this the precise formulas are set-up and the initial and boundary conditions are imposed. Then the model can be fitted to the data and afterwards the performance of it can be evaluated.

Data importing and processing

The importing of this data is similar as to the one directional case. The difference is that the data has an extra dimension due to the direction angle that is connected to the range bins. Furthermore the pre processing steps to let the velocities represent their horizontal component (by correcting for the angle between the radar beam and the surface) can be done as described in chapter 3.
For the multi directional waves one of the first challenges is to find the main wave direction (and a potential spreading of the waves round this) and to find the direction of the current. The current direction and magnitude are dealt with first. These can be represented as:

$$\mathbf{U}(\gamma) = U\cos(\xi - \gamma), \tag{4.29}$$

where U represents the magnitude of the current, ξ the current direction and γ the beam angle of the measurement. The direction and magnitude can be found by first averaging over the velocities along the range dimension. This leaves us with a single velocity per beam and time step. Then another averaging is done over the time domain, which leaves only a single average velocity per beam. In absence of current these values should be zero or at very close to zero. (A non-zero contribution occurs when a wave is not captured in it's entirety at the beginning and/or end of the data record). To obtain the current direction and magnitude the equation 4.29 is fitted to the beam/averaged velocity combinations. For this the trust-region reflective algorithm is used. The result of this fit gives the estimated magnitude U_{fit} and estimated current direction ξ_{fit}. These values are substituted in 4.29 and then this current gets subtracted from the velocity measurements for each beam direction.

After the current velocity direction the main wave direction needs to be determined from the data. This is not a straight forward procedure since the wave modes could come from several directions. But for a single long crested wave one can realize the following: since the data is naturally represented by a polar grid (see figure 4.1) a wave will be noticed in a certain grid cell first by the beam that is most in line with the direction of this wave. Then it will be noticed by the beam that is the next closest to the wave direction and finally by the beam which direction is the least in agreement with the actual wave direction. Thus this main direction can be estimated by picking the beam that sees the waves first and compare this with the other beams. If two beams see a wave at the same time in a grid cell this means that the wave is coming from the direction angle that is in the middle of the beam angles. To give the model enough flexibility there will be a few other wave directions allowed that surround this observed main wave direction for the fitting.

Problem formulation

The linear wave theory model can now be formulated as the data is processed in a way that only the orbital motion remains present. This leads to the following (comprehensive) formula:

$$u_{fit}(r,\gamma,t,\beta) = -\sum_{j=i}^{M}\sum_{i=1}^{N}(\omega_i - \mathbf{k}_{ij}\cdot\mathbf{U})A_{ij}\cos(-(\omega_i-\mathbf{k}_{ij}\cdot\mathbf{U})t - r(k_{x,ij}\cos(\gamma)+k_{y,ij}\sin(\gamma))+\psi_i) \quad (4.30)$$

Where β is the collection of all parameters and $\mathbf{k}_{ij} = [k_{x,ij}, k_{y,ij}]$ denotes the wave number vector over the number of sines per direction (N) and the number of wave directions (M) that are allowed. This means for each angular frequency ω_i there will be M wave numbers $k_{x,ij}$ and $k_{y,ij}$. Their entries are as follows:

$$k_{x,ij} = k_i\cos(\theta_j) \qquad k_{y,ij} = k_i\sin(\theta_j) \quad (4.31)$$

Due to the dispersion relation the wave numbers k_i will again be expressed in terms of ω_i:

$$k_i = \frac{\omega_i^2\tanh(k_i d)}{g} \quad (4.32)$$

By doing so the amount of parameters that need to be fitted is reduced and by this substitution the relation is automatically satisfied and does not need to be accounted for separately. Let the measured data be given by u_{meas}, then the sum of squared residuals $r = u_{meas} - u_{fit}$ becomes:

$$S(\beta) = \sum_{l=1}^{L}\sum_{i=1}^{N}\sum_{j=1}^{M} r_{lij}(\beta)^2 \quad (4.33)$$

where l represents the points in space and time that are used from the measured data. Then this $S(\beta)$ can be minimized by applying the inverse modelling methods.

$$\begin{aligned} \min_{\beta} \quad & S(\beta) \\ \text{s.t.} \quad & 0 \le A_i \le \frac{2\pi g\tanh(k_i d)}{7\alpha^2} \\ & 0 \le \omega_i \le \alpha \\ & 0 \le \psi_i \le 2\pi \end{aligned} \quad (4.34)$$

Furthermore the dispersion relation is altered due to deep water ($k_i d \to \infty$), dropping the tanh-term from the equation.

Fitting strategies in Matlab

To solve the minimization problem a trust-region reflective algorithm is used. The execution of this algorithm could be done in the two ways with sequential and non-sequential fitting as discussed in the one directional model. Due to the results found in the one directional case the choice is made to solely focus on the non-sequential way for the multi directional model.

Non-sequential fit

As with the one directional model this non-sequential method the amount of parameters is reduced by excluding ω_i as a parameter in the fit. Instead the angular frequency values are fixed between a minimum and maximum frequency on a equidistant grid between those values. The number of frequencies is equal to the amount of cosine components that are used per wave direction. So:

$$\omega = [\omega_1, \dots, \omega_N] \quad (4.35)$$

Besides these frequencies there is another parameter that needs to be considered. This is the wave direction, given by θ. As seen in the data processing section this can be derived by checking what grid cell notices a wave first. This is taken as main wave direction and in total 5 directions are taken surrounding this beam. So by doing this the wave direction is excluded from the fitting routine. So again only amplitudes and phases need to be fitted for each of the previous selected wave directions. This makes the amount of parameters that need to be fitted equal to NM.

Also for this model an important notice is that a higher number of observations compared to the number of parameters is needed to make a fit. This is necessary to give the model sufficient degrees of freedom and to prevent it from overfitting. To do so the amount of time and range steps needs to be sufficiently large. Taking multiple time steps will also help to capture the dynamics of the waves.
As an initial condition for the amplitudes the Rayleigh distribution as in equation 2.67 is taken and the phases are initially chosen constant.

Performance metrics

For this model the same performance metrics are taken as in the one directional case. This is then done for the five beam directions that are considered, which thus gives the performance of the fit in each of the directions.

$$\mathrm{MAE}(\beta) = \frac{1}{M}\sum_{i=1}^{M} |u_{fit}(\mathbf{x}_i, \beta) - u_{meas}(\mathbf{x}_i)| \tag{4.36}$$

$$\mathrm{MSE}(\beta) = \frac{1}{M}\sum_{i=1}^{M} (u_{fit}(\mathbf{x}_i, \beta) - u_{meas}(\mathbf{x}_i))^2 \tag{4.37}$$

In the notation $\mathbf{x}_i$ refers to the points in (ρ, θ, t)-space for which the fit is compared to the data. Besides these traditional measures a normalized averaged prediction error is suggested in [15]:

$$error(\beta) = \sqrt{\frac{\sum_{i=1}^{M} (u_{fit}(\mathbf{x}_i, \beta) - u_{meas}(\mathbf{x}_i))^2}{\sum_{i=1}^{M} (u_{meas}(\mathbf{x}_i)^2)}} \tag{4.38}$$

5

Inverse modelling results

In this chapter the modelling results are discussed. First this is done for the model in one direction with artificial data and real data. Later this is done for the multi directional model, also for artificial and real data. The results that are presented include visualizations of the fitting routines and the performance metrics that are defined in chapter 4. Besides this the amplitude spectrum is presented, which consists of the fitted parameter values A_i combined with the belonging frequencies ($f_i = \frac{w_i}{2\pi}$). This chapter only includes the main results, other results exploring variations in parameter settings can be found in the appendices A and B.

5.1. One directional model

In this section the results of the reconstruction and prediction of the wave model on the one directional data are presented. This is first done the artificial case for the non-sequential model and then for the sequential model.

5.1.1. Artificial data: non-sequential

Data without noise

The summary of the data inputs for the JONSWAP spectrum are found below in table 5.1, these are also discussed in chapter 3. For the creation of the artificial sea surface an amount of cosine components equal to 100 is chosen. As a first result a basic case is considered. From this result the effect of several

Parameters	Values	Unit
T_p (peak period)	6	s
H_s (significant wave height)	2	m
ω_c (cut-off frequency)	$33T_p^{-1}$	Hz
ω (frequency spectrum)	linspace$(0.1, \omega_c, 100)$	Hz

Table 5.1: Summary of the input parameters for the one directional artificial data set

adjustments of algorithm settings can be treated and compared to this basic case. The set-up for the basic model settings can be found in table 5.2. The motivation behind the chosen frequency spectrum is that with this choice the model can capture the longest wave length that can be measured as well as the smallest. This can be readily seen by using the dispersion relation (for deep water) and the definition for the wave number. The initial set up for the amplitudes and phases which are fitted are chosen Rayleigh distributed and constant as mentioned in the previous chapter. The lower and upper bounds for the amplitudes and phases are also mentioned there, for the amplitudes this lies between 0 and the wave breaking criterion shown in 2.73 and resp. 0 and 2π for the phases.

The results of the fitted function with the least-squares solver gives the results found in figs. 5.1 to 5.2. In these figs. 5.1 to 5.2 it can be seen that the fitted model performs the best in the first 10 seconds, which makes perfect sense since it is fitted to the data that was obtained in this period of time. After

Algorithm parameters	Values	Unit
Number of cosines	100	
Time range	10	s
Time stepsize	0.5	s
Spatial range	0 to 384	m
Spatial stepsize	0.75	m
ω (frequency spectrum)	linspace$(0.5, 5, 100)$	Hz
Function tolerance	10^{-6}	
Maximum iterations	10	
Maximum function evaluations	2000	

Table 5.2: Summary of the input parameters for the one directional fitted non-sequential model

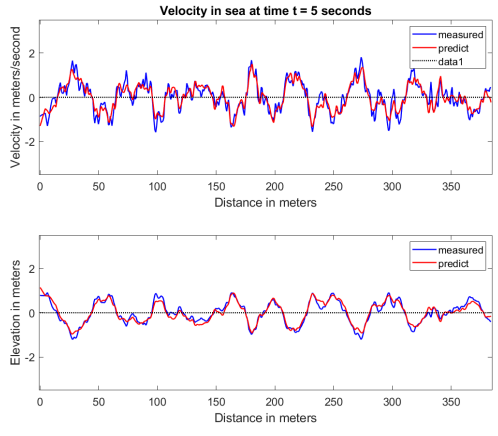

(a) Non-sequential fit with 100 cosines

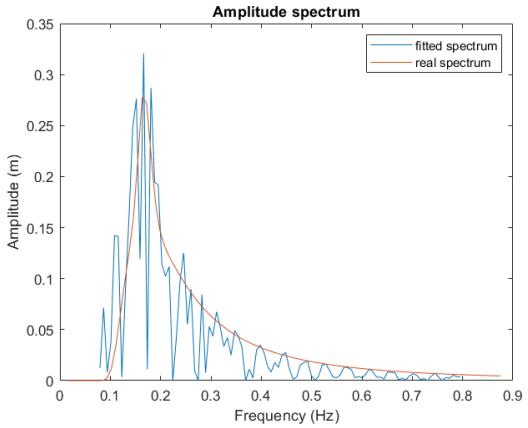

(b) Amplitude spectrum for a non-sequential fit

Figure 5.1: Results for the basis case: (a): visualisation of the fitted velocity function and computed surface, (b): fitted amplitudes plotted against the actual amplitudes of the data

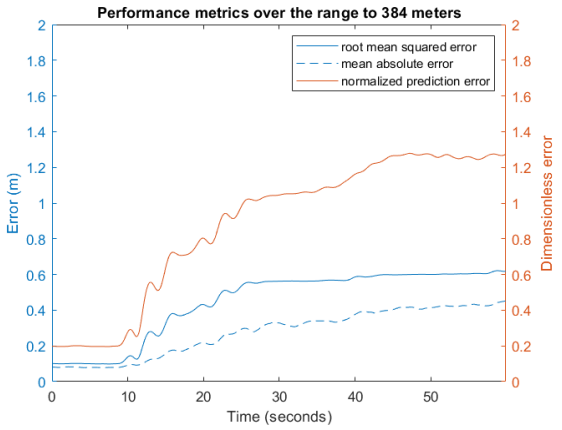

(a) 512 range bins (representing 384 meters)

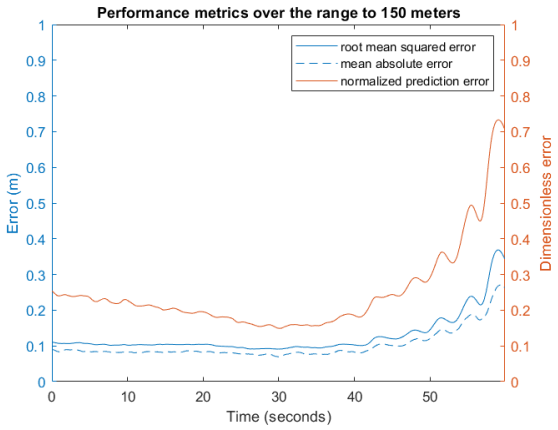

(b) 200 range bins (representing 150 meters)

Figure 5.2: Performance metrics for a non-sequential fit with 100 cosines

these 10 seconds the model is faced with new data coming from the boundary on the right which is flowing into the domain. Here the model starts to struggle with it's prediction as can be seen in fig. 5.3. This figure shows that the model cannot actually predict waves it has not measured before. It is quite capable though to predict the behaviour of the waves it has measured. This is visible in fig. 5.2b. For a range of 150 meters from the radar location (so 200 bins) the MSE and MAD remain (almost) constant around 0.1 meters The normalized error stays below 0.24 for a time of 40 seconds, this gives an accurate

prediction for 30 seconds. A remarkable result is that the error decreases in the 150 meters range during the first 35 seconds. This can be explained by realizing that the waves that come into this domain have been in the larger domain of 384 meter for a longer period of time than the waves that are very close to the observer at time $t = 0$. Hence, the model has fitted better to these waves that are further away since they are more present in the domain for a longer period of time. This effect is present in more of the experiments with artificial data.
The fitted amplitudes in figure 5.1b also resembles the actual spectrum of amplitudes quite well. It is important to note that most of these spectrum plots show spikes since the frequencies are fixed and the parameters are only fitted for one time record (so taking the A_i instead of $\overline{A_i}$). This is statistically not a correct thing to do (since the mean is estimated from a single value). Thus it is not entirely correct to treat this result the same way as a spectrum. If this experiment is repeated numerous times on multiple time records the combined result will resemble the spectrum more accurately. This can be seen in figure 5.4, where the peaks are smoothed out due to the averaging of the amplitudes per frequency bin. With these realizations the significant wave height H_s (defined in 4.26) can be calculated, this gives $H_s = 2.19$ meters for the amplitudes averaged over 8 time records and $H_s = 2.11$ meters for the amplitudes averaged over 16 time records.

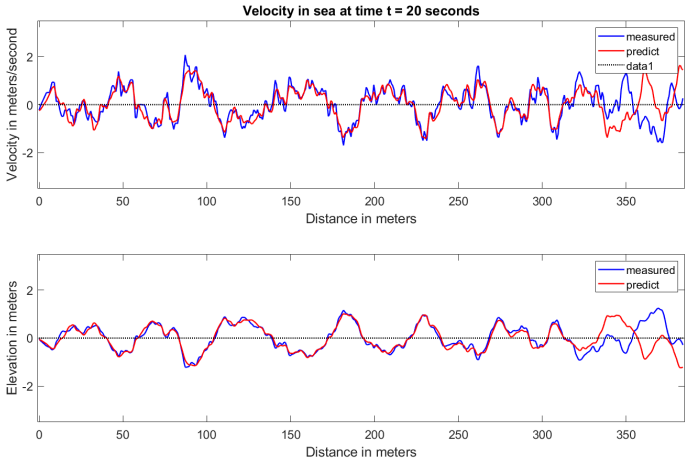

Figure 5.3: Visualisation of the fitted velocity function and computed surface at time $t = 20s$ where new waves enter the domain

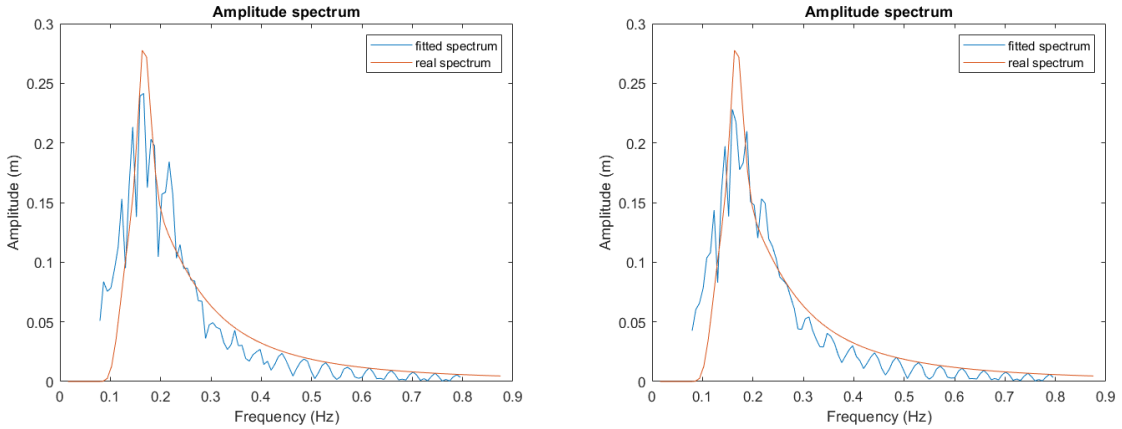

(a) Combined result of 8 fitted amplitudes sets (80 seconds of data)

(b) Combined result of 16 fitted amplitudes sets (160 seconds of data)

Figure 5.4: Amplitude spectrum for multiple non-sequential fits using the averaged fitted amplitudes per frequency against the actual amplitudes

Noisy data

When disturbance of Gaussian white noise is added to the signal the same routines are performed as with the clean data. The results can be found in figs. 5.5a to 5.6b. From these figures it can be concluded that the addition of the Gaussian white noise does not have a large effect on the results of the model in the time period that the model is fitted to the data. The prediction horizon of 30 seconds remains valid in this case but with a slightly higher error than in the clean data case with MSE and MAD below 0.12 meters and normalized error below 0.3. The amplitude spectrum is a bit less accurate for this realization, the high amplitudes are likely to cancel each other out at the given domain, but create a larger error at later stages, which is visible when comparing fig. 5.6a and 5.6b to figures 5.2a and 5.2b. From these findings it was decided to exclude the noise from further experiments.

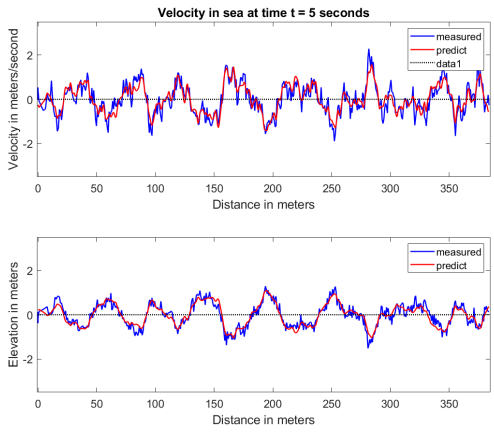

(a) Non-sequential fit on disturbed data

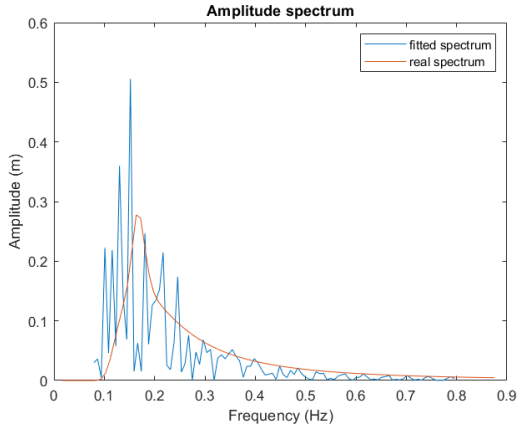

(b) Amplitude spectrum for a non-sequential fit on disturbed data

Figure 5.5: Results for data with added white noise: (a): visualisation of the fitted velocity function and computed surface, (b): fitted amplitudes plotted against the actual amplitudes of the data

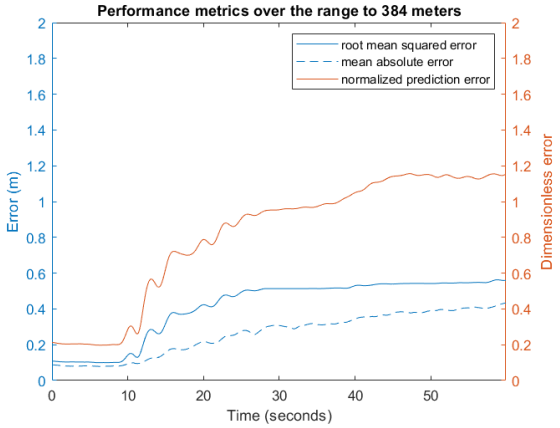

(a) 512 range bins (representing 384 meters)

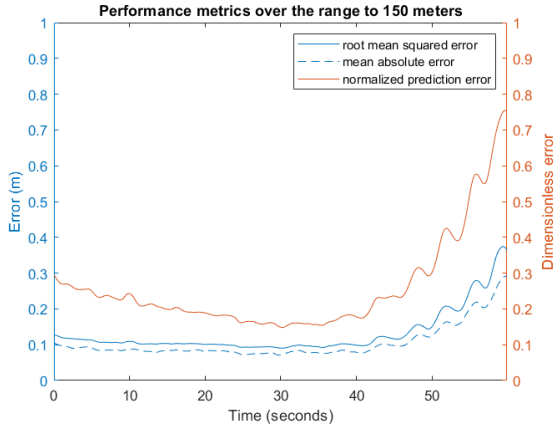

(b) 200 range bins (representing 150 meters)

Figure 5.6: Performance metrics for a non-sequential fit on disturbed data with 100 cosines

Changing model settings

In this section the effect of some of the adjustments that are possible are explored. There are several parameters that can be adjusted, the ones that are explored are the effects on number of cosine terms, number of measurements and the wave conditions.

Number of cosine terms

The amount of cosines taken into account has a linear effect on the computation time. This can be seen

in fig. 5.7. For the accuracy and spectrum it can be noticed that the normalized error when using less than 50 terms is consequently higher than 0.5 and the effect of the fit on the first 10 seconds becomes harder to notice. For simulations with 50 to 100 terms it is noticeable that the accuracy in the fitted time region keeps increasing with the number of terms, for the entire range the prediction performance decreases significantly as seen in the basis case. The full results that show this are available in Appendix A. An impression of the performance with 50 terms can be found in figure 5.8.

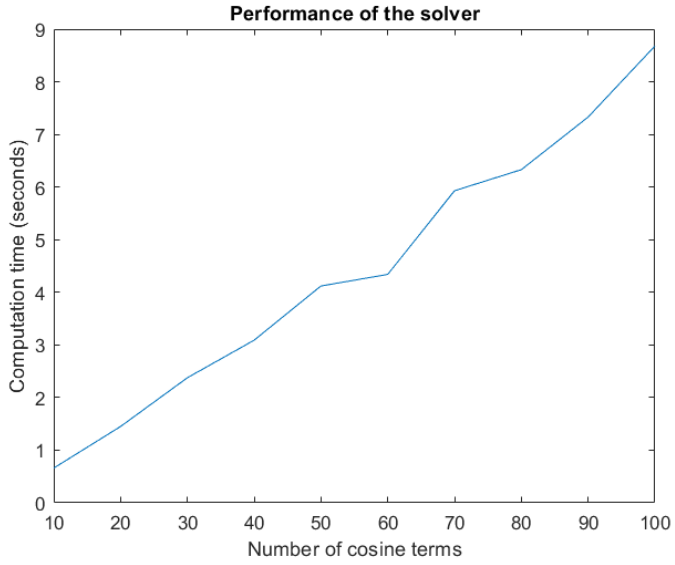

Figure 5.7: Performance of the solver in terms of computation time plotted against the number of cosine terms used to fit the data

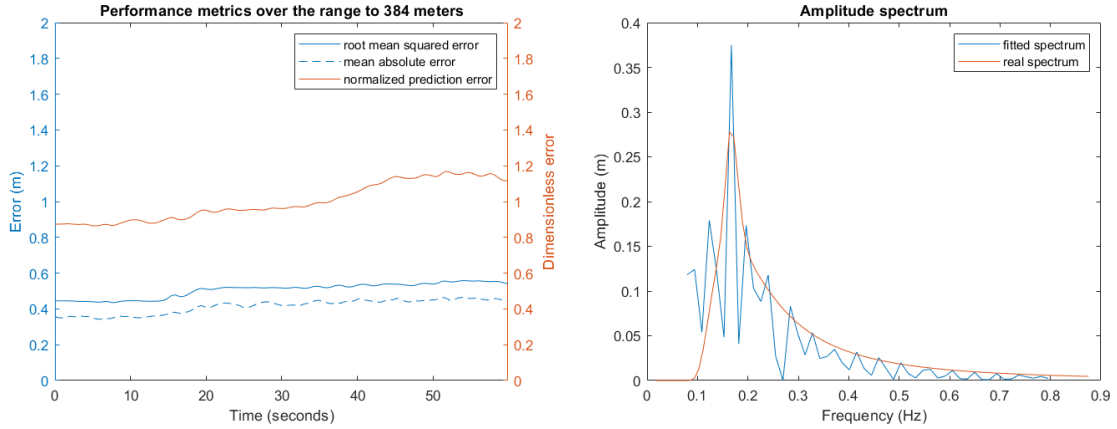

(a) 512 range bins (representing 384 meters) (b) Amplitude spectrum

Figure 5.8: Performance metrics for a non-sequential fit with 50 cosines

Number of measurements

Another variation can be done in the amount of measurements that is used to fit the cosine terms on the data. Variations for this can be done in the spatial and time range. Reducing the amount of grid cells to fit on leads to a linear decrease in computation time. Also it does not dramatically effect the performance of the solver in this artificial linear case. For applying these results to real data it should be noticed that part of the power of the real data lies in the high resolution.
A similar result in terms of computation time and performance is also obtained when limiting the amount of time steps that are used within these 10 seconds of data.

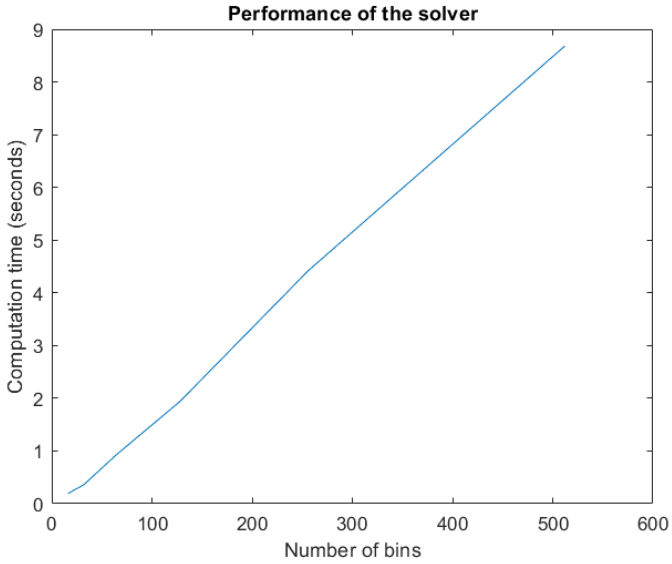

Figure 5.9: Summary of the solver performance in terms of computation time in relation to the number of bins that are chosen to fit on

Wave conditions

When changing the wave conditions of the artificial data set to the ones in table 5.3 the solver is tested again using the same algorithm settings as initially in table 5.2. This gives the results as visualized in figs. 5.10a to 5.11b. From this it can be seen that the performance remains very accurate for the period the model is fitted to the data. This is displayed in figure 5.11b, here the MSE and MAD remain below 0.2 meters in the first 32 seconds and the normalized error below 0.22. Thus this gives an accurate prediction for the first 32 seconds (so 22 seconds after the measurement). The errors grow more quickly in magnitude afterwards up to 1.2 meters for MSE and MAD as well as 1.2 for the normalized error.

Parameters	Values	Unit
T_p (peak period)	10	s
H_s (significant wave height)	5	m
ω_c (cut-off frequency)	$33T_p^{-1}$	Hz
ω (frequency spectrum)	linspace$(0.1, \omega_p, 100)$	Hz

Table 5.3: Summary of the adjusted parameters for the one directional artificial data set

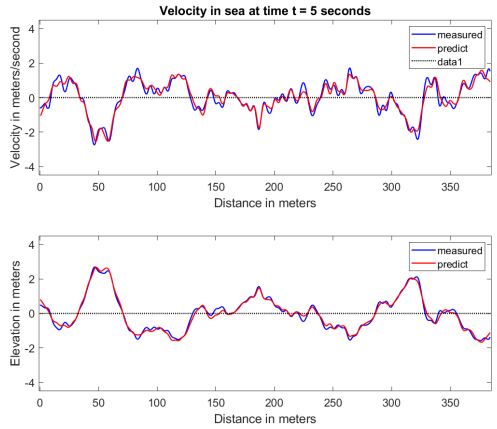

(a) Non-sequential fit with 100 cosines

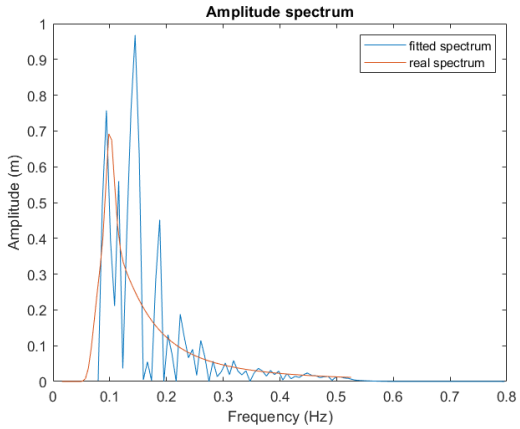

(b) Amplitude spectrum for a non-sequential fit

Figure 5.10: Results for the H_s: 5 m and T_p: 10 s case: (a): visualisation of the fitted velocity function and computed surface, (b): fitted amplitudes plotted against the actual amplitudes of the data

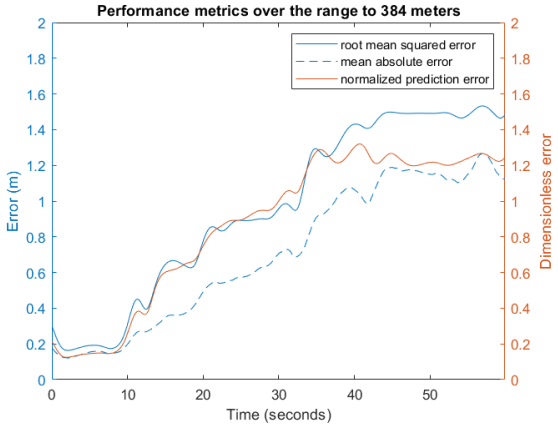

(a) 512 range bins (representing 384 meters)

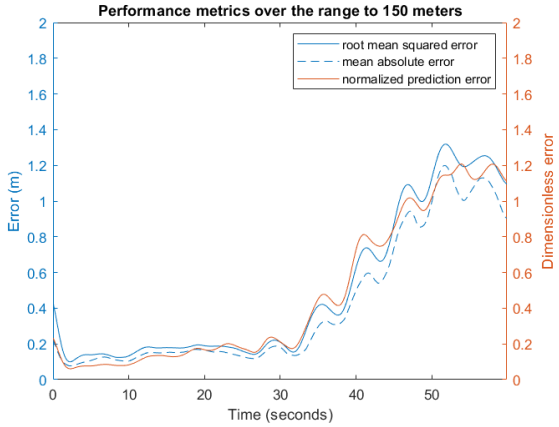

(b) 200 range bins (representing 150 meters)

Figure 5.11: Performance metrics for a non-sequential fit with 100 cosines

5.1.2. Artificial data: sequential

In this subsection the results of the sequential fitting approach are presented. The artificial data set that was used is the same as with the non-sequential model, it's parameters are available in table 5.1. The model parameters can be found in table 5.4. For this model there are some important differences compared to the non-sequential case. First mayor difference is that the angular frequencies ω are left as a parameter to fit. This will have effect on the spectrum acquisition, since there are no fixed frequency bins anymore. A second mayor difference is that the fit is done sequentially on a certain moment in time on only that measurement. This is then used to update the reconstruction/prediction by dynamically averaging with the two previous fits as described in the previous chapter. Lastly, before every fit happens the heave profile computed with the previous fitted parameters at that specific time is evaluated to check whether shadowing could be present. If so, these range bins will be excluded from the measured data for the new fit. An important parameter thus becomes the time that is left between those fits. Some realizations are done exploring this for various time gaps of 3,5 and 7 seconds. Results of this can be found in figs. 5.12a to 5.17b.

Algorithm parameters	Values	Unit
Number of cosines	100	
Time stepsize	3,5 or 7	s
Spatial range	0 to 384	m
Spatial stepsize	0.75	m
Lower bound ω	0.5	Hz
Upper bound ω	5	Hz
Function tolerance	10^{-6}	
Maximum iterations	75	

Table 5.4: Summary of the input parameters for the one directional fitted sequential model

The spectra of amplitudes of these fitting procedures match the actual spectrum reasonably well, remarkable are the small peaks for some higher frequencies around 0.45 Hz in figures 5.12b and 5.14b. The performance metrics of the sequential model in most cases shows some sharp decreases in value when the fitted function gets newly averaged with the latest data sample, which is positive. With the model that updates every 3 seconds it is visible that the new prediction fails to improve the current result though, this could be happening when a past fitted parameter set still provided a good fit to the current data, but had to be discarded since it was no longer part of the 3 latest updates. Over the entire range of 384 meters this sequential model is not able to outperform the non-sequential model for all 3 cases (regarding the time period it was fitted on). The same holds for the smaller range of 150 meters, but the sequential model does perform better there than it does on the full spatial range. In terms of predictive capability it is hard to determine the performance since the idea of this sequential model is to remain precise for all times by constantly updating the result every 3,5 or 7 seconds.

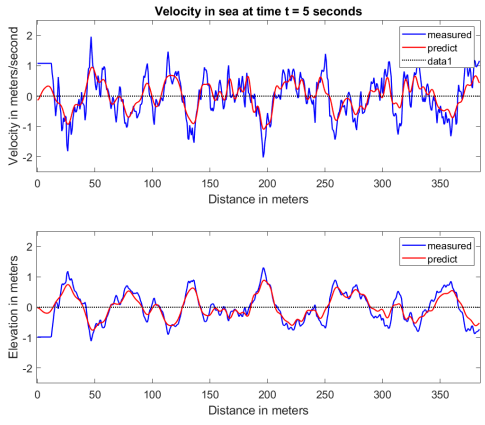

(a) Sequential fit with 100 cosines

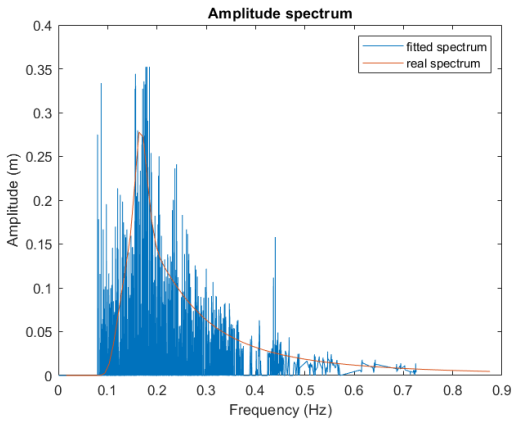

(b) Amplitude spectrum for a sequential fit

Figure 5.12: Results for the sequential fitting case with a gap of 3 seconds between fitted data: (a): visualisation of the fitted velocity function and computed surface, (b): fitted combined amplitudes plotted against the actual amplitudes of the data

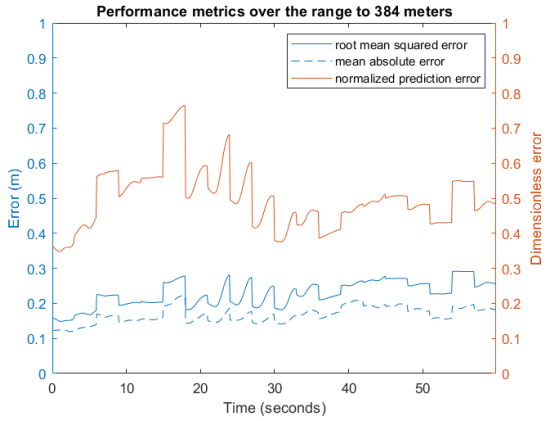

(a) 512 range bins (representing 384 meters)

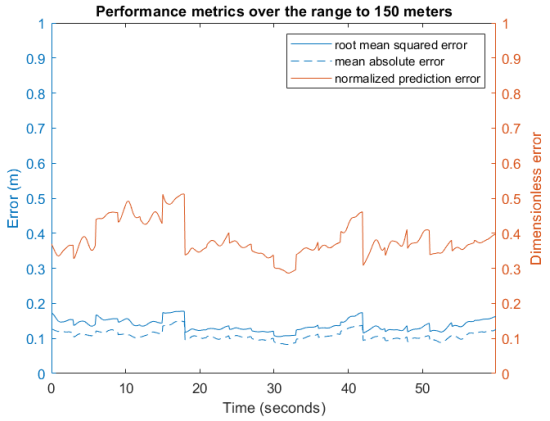

(b) 200 range bins (representing 150 meters)

Figure 5.13: Performance metrics for the sequential fit with 100 cosines and a time gap of 3 seconds

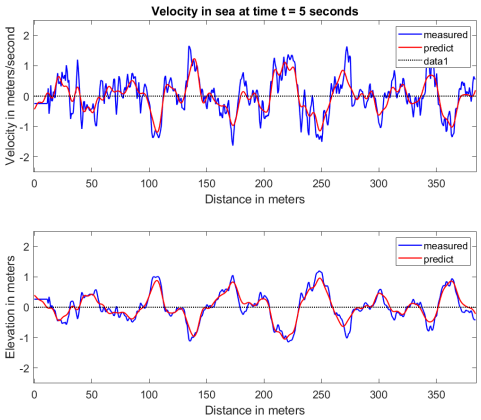

(a) Sequential fit with 100 cosines

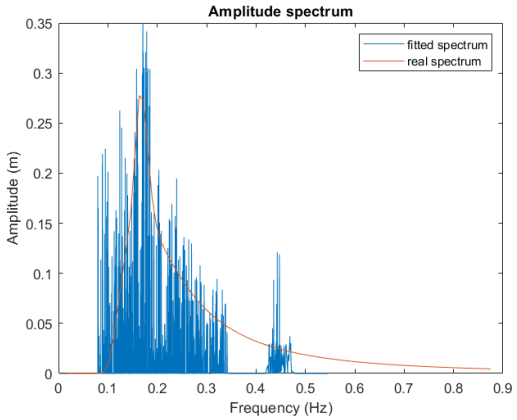

(b) Amplitude spectrum for a sequential fit

Figure 5.14: Results for the sequential fitting case with a gap of 5 seconds between fitted data: (a): visualisation of the fitted velocity function and computed surface, (b): fitted combined amplitudes plotted against the actual amplitudes of the data

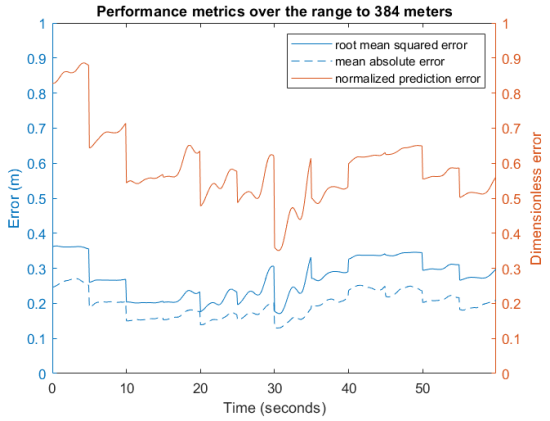

(a) 512 range bins (representing 384 meters)

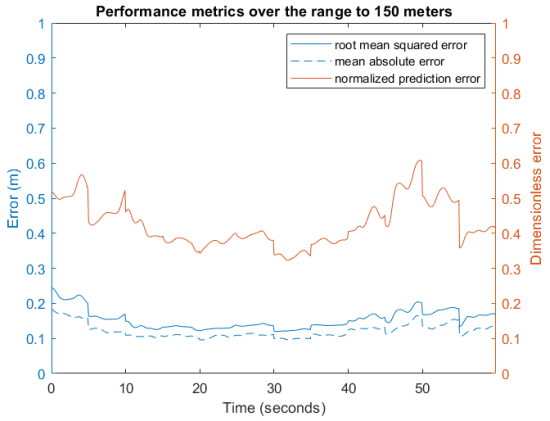

(b) 200 range bins (representing 150 meters)

Figure 5.15: Performance metrics for the sequential fit with 100 cosines and a time gap of 5 seconds

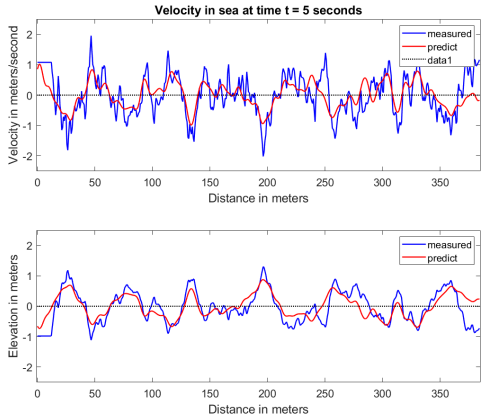

(a) Sequential fit with 100 cosines

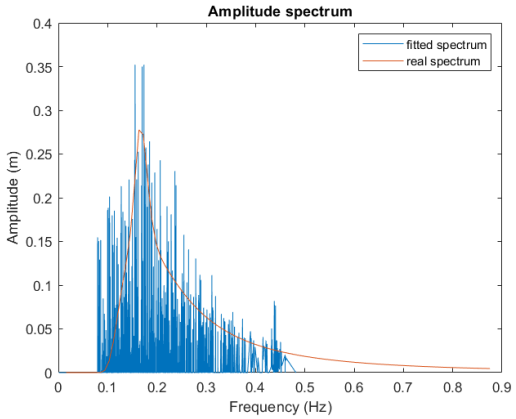

(b) Amplitude spectrum for a sequential fit

Figure 5.16: Results for the sequential fitting case with a gap of 7 seconds between fitted data: (a): visualisation of the fitted velocity function and computed surface, (b): fitted combined amplitudes plotted against the actual amplitudes of the data

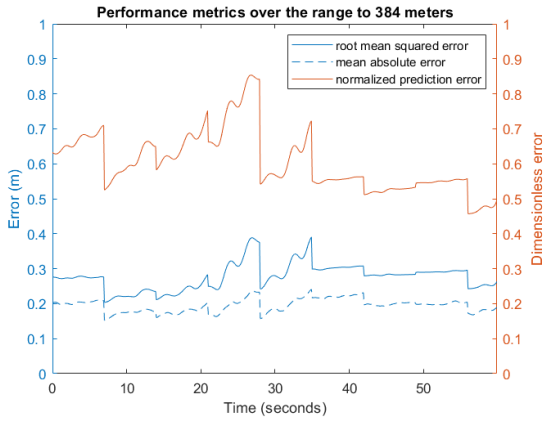

(a) 512 range bins (representing 384 meters)

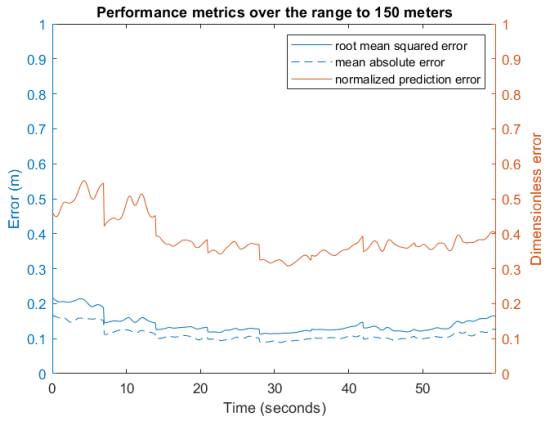

(b) 200 range bins (representing 150 meters)

Figure 5.17: Performance metrics for the sequential fit with 100 cosines and a time gap of 7 seconds

5.1.3. Real data

Pre processing

In contrast to the experiments with the artificial data there are some pre processing steps that need to be done before the model can work with the data set the same way as in the artificial case.
The first step of the pre processing is to correct the velocities for the beam angle with the water surface so they represent the horizontal component of the velocity.

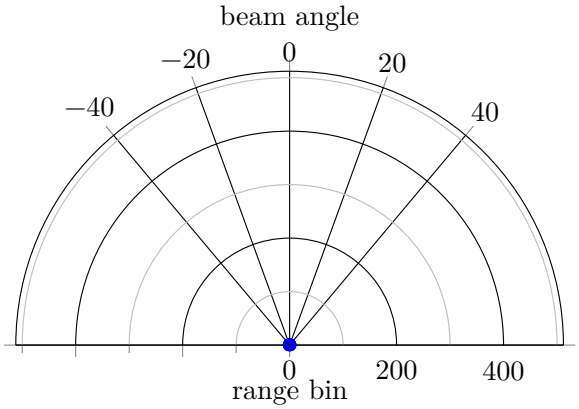

After this the beam that is most aligned with the wave direction needs to be selected. To select this one can realize the following: since the data is naturally represented by a polar grid a wave will be noticed in a certain grid cell first by the beam that is most in line with the direction of this wave. An example of this can be seen in figure 5.18a. This figure shows the measured velocities in bin 150, corresponding with range 112.5m, for the -20, 0 and 20 degrees beam for a period of time. It is visible that the same waves are measured by these beams with a small time delay between them. The wave is first measured by the red beam, then the blue beam and latest by the green beam. so it might be assumed that the wave are mainly coming from a direction surrounding the -20 degrees beam. This idea is supported by plotting the -40 and 40 degree beams instead of the -20 and 20 degree beams in figure 5.18b. The 40 degree hits the wave at a later moment then the 20 degree beam, supporting the thought that the wave mode is coming from the negative angle direction. Meanwhile the -40 degree beam notices the waves later then the -20 degrees beam. Thus from this analysis it can be concluded that the main wave direction will probably lie around the -20 degree beam direction. Thus this beam will be taken to do further computations with.

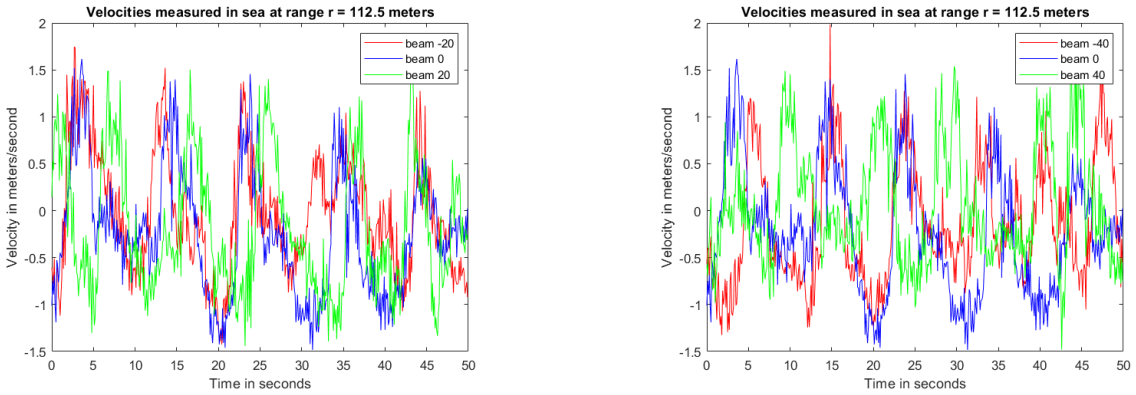

(a) -20,0 and 20 degrees beams

(b) -40,0 and 40 degrees beams

Figure 5.18: Measured data from range bin 150 (located at 112,5m from the radar) plotted for a period of 50 seconds

A last pre processing step is to supply an estimate of the depth of the sea along the spatial bins. This is not straightforward, but the best guess that could be made is by using [5]. This states that the water depth along the coastal region of the Netherlands within the spatial range of the radar will not exceed the 10 meter depth mark. The exact sea bed may have sand banks or other irregularities, but unfortunately these cannot be accounted for. As an input for the model a water depth of 8 meters was taken. Other parameter values can be found in table 5.5.

Algorithm parameters	Values	Unit
Number of cosines	100	
Time range	10	s
Time step size	0.5	s
Spatial range	7.73 to 384	m
Spatial step size	$0.75\cos(\gamma)$	m
Used spatial range bins	20 to 512	
ω (frequency spectrum)	linspace$(0.5, 5, 100)$	Hz
Water depth	8	m
Function tolerance	10^{-6}	
Maximum iterations	15	
Maximum function evaluations	2000	

Table 5.5: Summary of the input parameters for the one directional fitted model on real data

Fitting to measurements: non-sequential

The results of the non-sequential method of fitting on the real data is presented in figs. 5.19a to 5.20b. From these results it is visible that the model has some struggles to really accurately fit to the data. In the first 10 seconds the model is able to resemble the measured data quite good when looking at figure 5.19a. Though this is not explicitly expressed by the performance metrics, this may be due to irregular behaviour and noise in the data. After the 10 second where the model was fitted the normalized error does grow pretty rapidly from 0.8 to 1.8 in the range of 150 meters from the radar, but the RMSE and MAD grow less extreme, which is positive. Also remarkable is the decrease in error after 30 seconds. This is mainly due to the decrease in magnitude of the measured velocities, as can be seen in figs. 5.21a to 5.21b. An explanation for the mismatch between the model and the radar data could be the influence of waves with other directions travelling through the domain, which could cause an unexpected effect on the wave lengths of the waves that are measured by a single radar beam. This violates the assumption of infinitely long crests travelling towards the radar (in both current and wave direction), this does not come as a huge surprise since this would be a very idealised case. What also can be noted from figs. 5.21a to 5.21b is that the waves fitted by the model travel faster than the data. This could also be explained by the other wave directions or it could be caused by an alternative current direction/magnitude.
As a conclusion it can be stated that the model is quite able to reconstruct the measured data in the 10 second fitting period, though an accurate prediction cannot be given from this model.

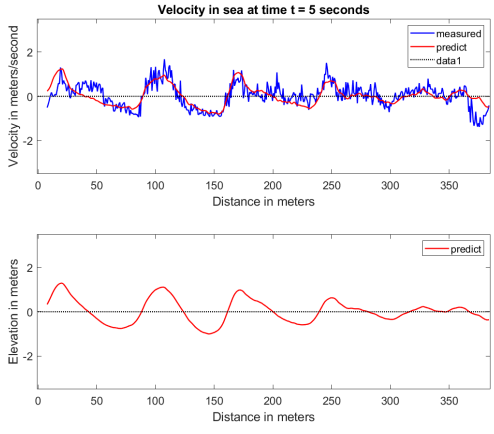

(a) Non-sequential fit with 100 cosines

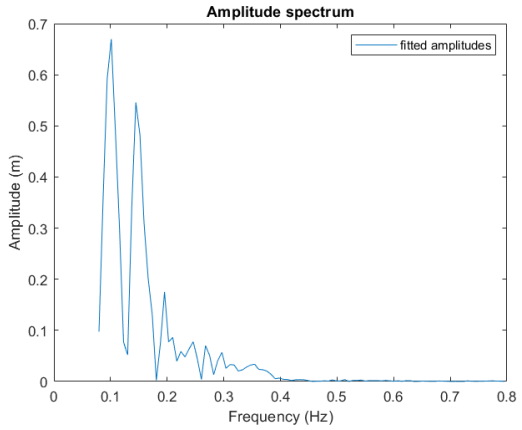

(b) Amplitude spectrum for a non-sequential fit

Figure 5.19: Results for the one directional model on real data: (a): visualisation of the fitted velocity function and computed surface, (b): fitted amplitudes of the model

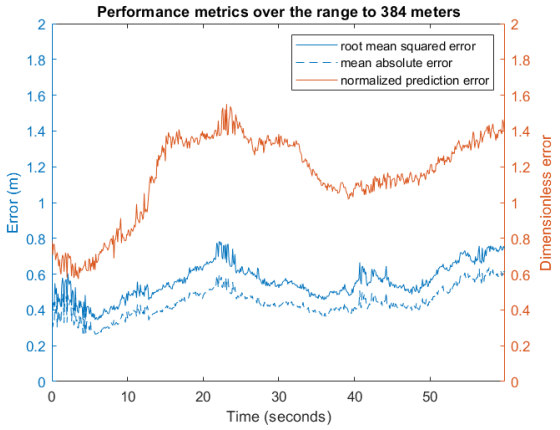

(a) 492 range bins (representing 384 meters)

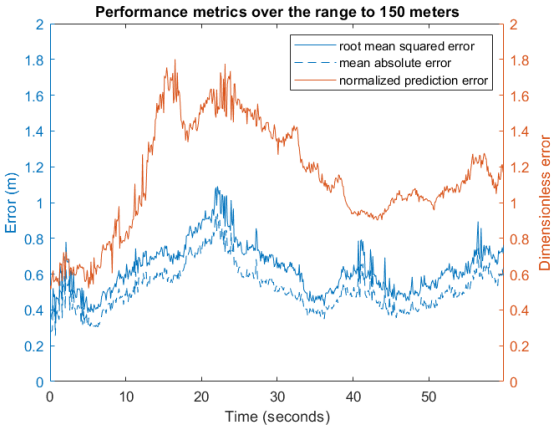

(b) 180 range bins (representing 150 meters)

Figure 5.20: Performance metrics for a non-sequential fit with 100 cosines taken from a starting point in bin 20 (at 7.73 meters from the radar)

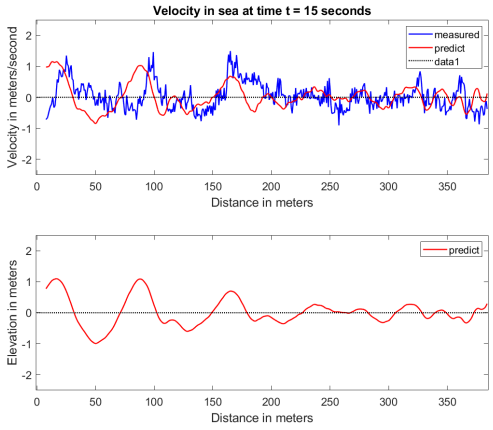

(a) Non-sequential fit with 100 cosines

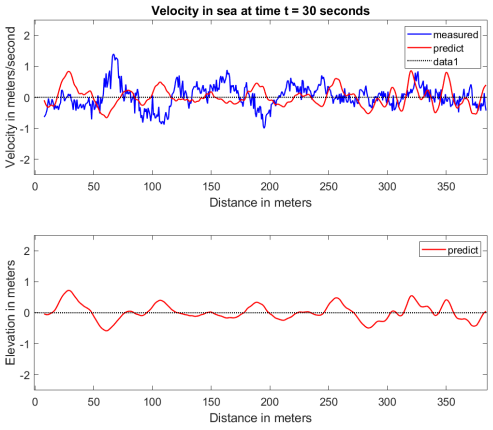

(b) Non-sequential fit with 100 cosines

Figure 5.21: Visualisation of the fitted velocity function and computed surface for the one directional model on real data at: (a): 15 seconds , (b): 30 seconds

Fitting to measurements: sequential

Besides the non-sequential model, also the sequential model has been used to fit on the real data coming from the -20 degrees beam. This has been done with the time step of 3 seconds between the fits. The results of this sequentially fitted model to the real data is presented in figs. 5.22 to 5.24.

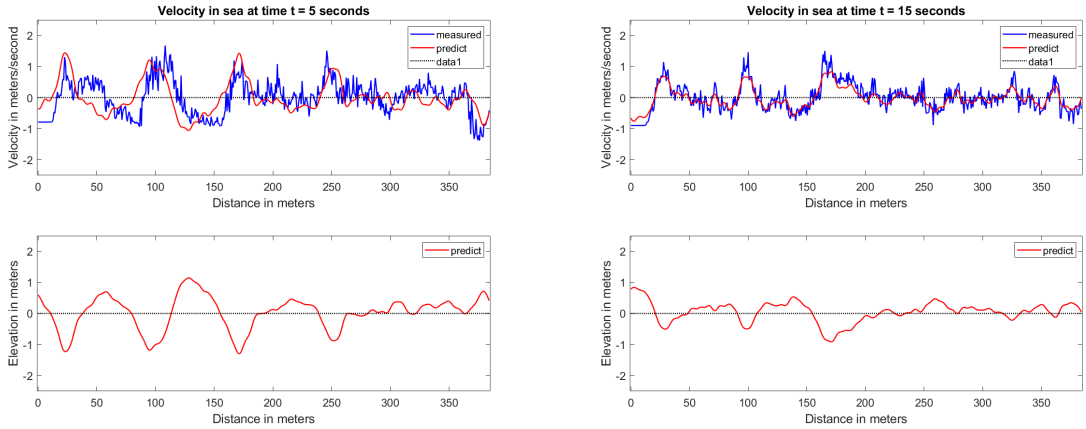

(a) Sequential fit with 100 cosines

(b) Sequential fit with 100 cosines

Figure 5.22: Visualisation of the fitted velocity function and computed surface for the sequential one directional model with time gaps of 3 seconds on real data at: (a): 5 seconds , (b): 15 seconds

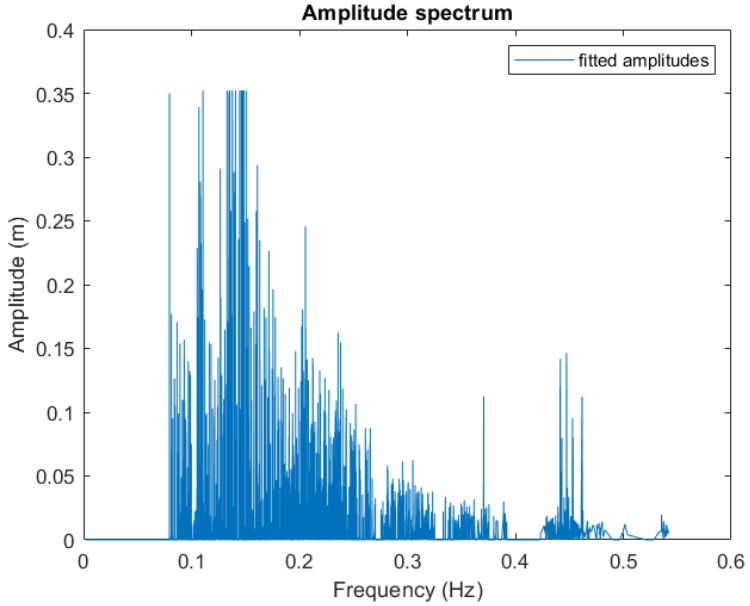

Figure 5.23: Amplitude spectrum for a sequential fit with a time gap of 3 seconds between fits

From these plots it is visible that every newly fitted set of parameters has big impact on the solution performance. The performance metrics show significant decrease up to 0.5 in terms of the normalized error when a new solution is averaged with the old ones. This also means that during the 3 seconds in which the data is not fitted to the model the errors grow rapidly. Over the entire time range the method is able to limit these errors between 0.75 and 0.2 meters in terms of MSE and MAD and between 1.24 and 0.4 in terms of normalized error in the 150 meters range from the radar. Overall it should be concluded that this model also does not represent the actual water surface in an accurate way. Explanations for this are similar to the statements that were given for the non-sequential fitting method on the real data.

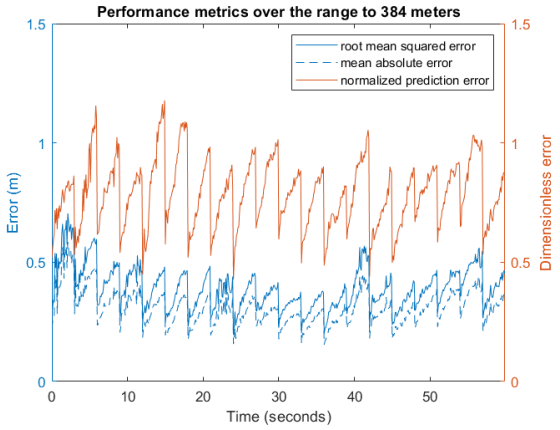

(a) 492 range bins (representing 384 meters)

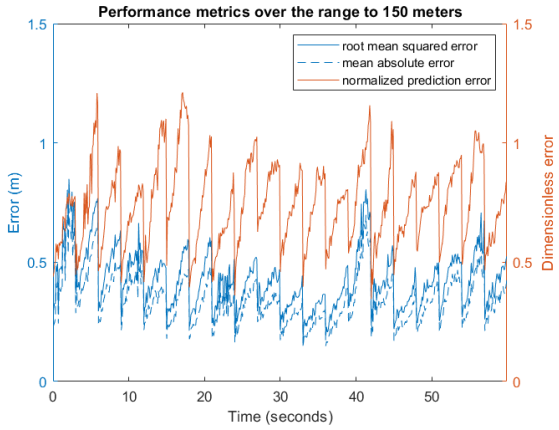

(b) 180 range bins (representing 150 meters)

Figure 5.24: Performance metrics for a sequential fit with 100 cosines taken from a starting point in bin 20 (at 7.73 meters from the radar) with time gaps of 3 seconds

5.1.4. Summary of results

In this section the most important findings of the modelling results for the one directional model are discussed. For the artificial case the non-sequential model is able to capture the behaviour of the sea very well, with an MAD and RMSE displaying similar behaviour. This means that the magnitude of the error that is made is not enormously large. For the fitted time period their magnitude lies around 0.1 meters, which grows over time when new waves enter the domain. For the artificial case it can be concluded that the prediction is accurate for 30 seconds in the domain that spans the first 150 meters from the radar. Here the MSE and MAD are below 0.15 meters and the normalized error between 0.3 and 0.15.

When applying this non-sequential model to the real data the performance decreases. It is able to reasonably reconstruct the waves that are measured, but (probably) due to the assumption of the waves/current travelling in one direction it fails to accurately predict for longer times. So the predictive capabilities are very limited.

For the sequential model a similar result was obtained. For the artificial data it's performance is a bit worse compared to the non-sequential model. On the long term it's results will be better due to the frequent amount of re-fitting to the data. This also makes it unfair to compare this aspect with the non-sequential modeling results since this only used the first 10 seconds of data. In terms of predictive capabilities this makes it also hard to draw a conclusion since it's set-up is done in a way that it should remain accurate the entire time. When looking at figure 5.17 it can be noted that the increase of the error in 7 seconds is limited on the 150 meters range. For the full range of 384 meters the increase of error can become large (increase of 20 % in terms of normalized error). This increase of error is also very visible in the results when the sequential model is fitted on the real data, supporting the earlier claim of assumptions that do not hold for this case. Based on the experiences and results of this one directional case the choice was made to solely proceed with the non-sequential model for the multi directional case. This will be treated next.

5.2. Multi directional model

In this section the results for the multi directional model are treated. This is first done on the artificial data and later on the real data. Also this is solely done for non-sequential model (thus leaving out the sequential model) as discussed in the results for the one directional model.

5.2.1. Artificial data

As for the one directional model first the model is used on artificial data. The summary of the data inputs for the JONSWAP spectrum are found below in table 5.6, these are also discussed in chapter 3. For the creation of the artificial sea surface an amount of cosine components equal to 50 in each of the directions is chosen. This directional distribution is based on the $\cos^2\theta$-model. As a build-up towards working with these multiple wave directions they are gradually added to the artificial data.

As a first result a basic case is considered with only $n = 1$ wave direction and also $n = 2, 3$ and 5 wave

Parameters	Values	Unit
T_p (peak period)	6	s
H_s (significant wave height)	2	m
ω_c (cut-off frequency)	$33T_p^{-1}$	Hz
ω (frequency spectrum)	linspace$(0.1, \omega_p, 50)$	Hz
θ (directional spreading)	linspace$(-\frac{\pi}{8}, \frac{\pi}{8}, n)$	radians

Table 5.6: Summary of the input parameters for the multi directional artificial data set

directions are considered. The set-up for this basic case on the model side is presented in table 5.7. The chosen frequency spectrum is the same as with the one directional case. This also has the same reasoning as the explanation given there.

Algorithm parameters	Values	Unit
Number of cosines per direction	50	
Number of directions	n	
Time range	10	s
Time stepsize	0.5	s
Spatial range	0 to 384	m
Spatial stepsize	0.75	m
ω (frequency spectrum) per direction	linspace$(0.5, 5, 50)$	Hz
Function tolerance	10^{-6}	
Maximum iterations	10	
Maximum function evaluations	2000	

Table 5.7: Summary of the input parameters for the multi directional fitted model on artificial data

The results when using the data set (containing only one wave direction at 0 degrees incidence angle) and applying the basic settings for the fitted function with the least-squares solver gives the results found in figs. 5.25 to 5.28. From these results it can be concluded that for the 150 range from the radar the fitted model performs very well, though it is not able to achieve the same accuracy as with the one directional case. The normalized error remarkably grows very fast during the first 10 seconds when considering the full range, though this is not the case in the -40 degrees beam. Reasons behind this phenomenon are not clear. Furthermore it can be stated that the RMSE and MAD of the model show no remarkable behaviour compared to the normalized error. As a conclusion to the situation with this one wave direction it can be stated that the model is able to reconstruct and predict the wave surface for 30 seconds in the 150 meters range (after it was fitted) within a precision range of 15 cm (MAD and RMSE) and 0.42 in terms of normalized dimensionless error (in the -40 degrees beam).

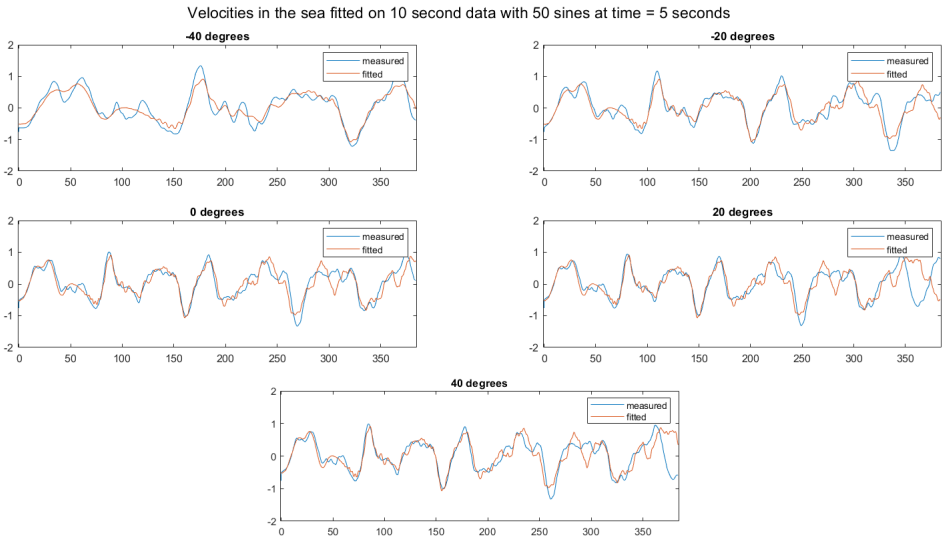

Figure 5.25: Velocities along the 5 beams fitted on a long crested sea containing one wave direction

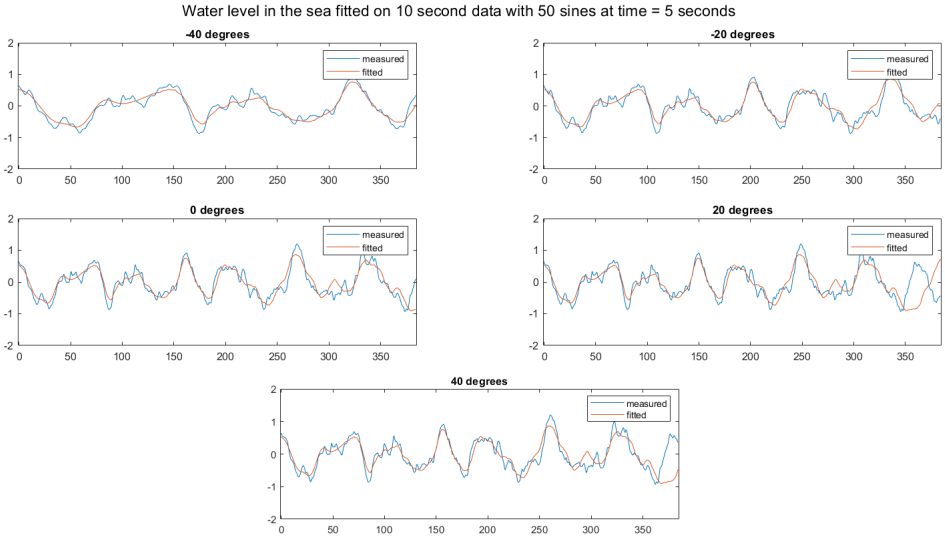

Figure 5.26: Water level along the 5 beams fitted on a long crested sea containing one wave direction

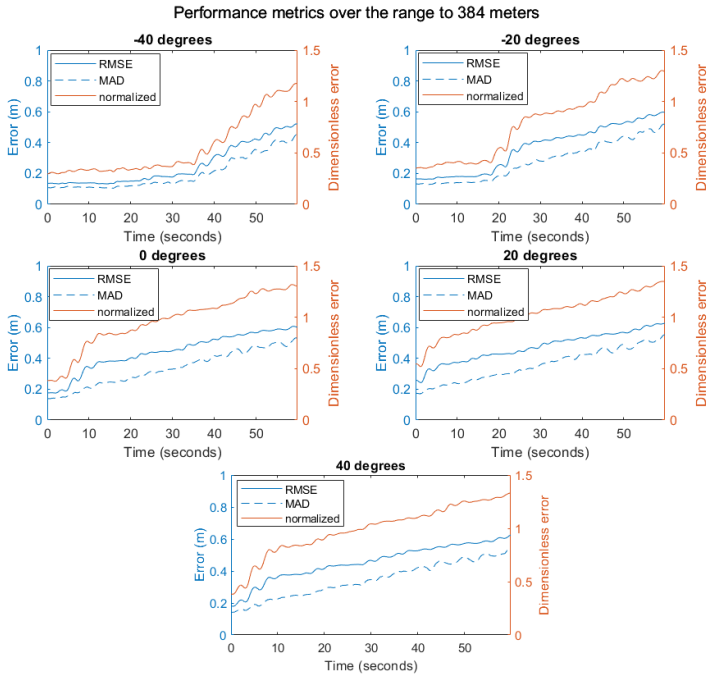

Figure 5.27: Performance metrics for a non-sequential fit over the wave directions over the full range of 384 meters from the radar fitted on a long crested sea containing one wave direction

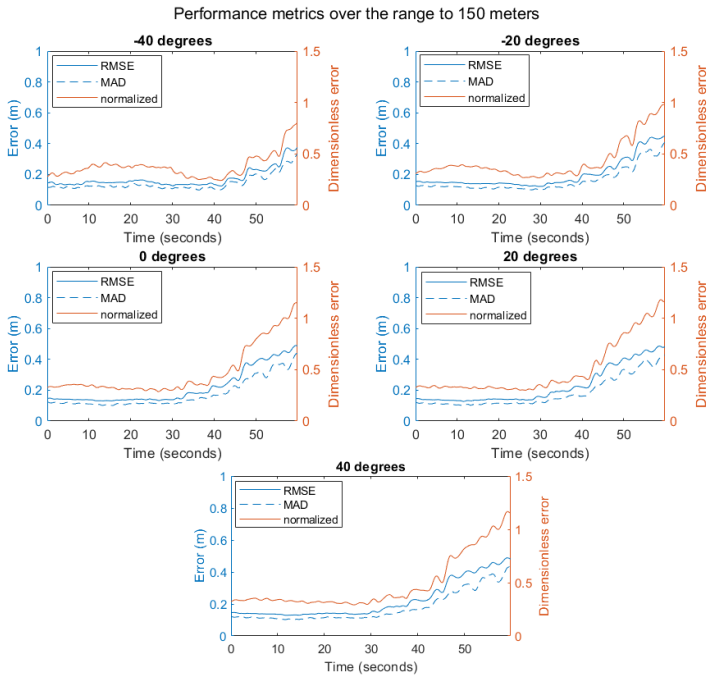

Figure 5.28: Performance metrics for a non-sequential fit over the wave directions over a range of 150 meters from the radar fitted on a long crested sea containing one wave direction

Next the case is treated where there are five wave directions in the artificial data (which are also known and given to the model) between $-\frac{\pi}{8}$ and $\frac{\pi}{8}$. From figures 5.29 and 5.30 it is visible that the model is able to capture the general behaviour of the sea surface quite well. This is not clearly visible in terms of the normalized error in figs. 5.32 to 5.33. For both the 150 meters as the 384 meters range this error is close to 1 for the time it was fitted on, meaning the average error would equal the magnitude of the total wave amplitude. The RMSE and MAD do not show an error that is that significantly large. For the 150 meters domain this remains about 0.3 meters. For a significant waveheight of 2 meters this still seems quite reasonable. With that in mind a precise prediction could be given for a time period of 20 seconds after the fitted time. Other results for the long crested waves can be found in appendix B.

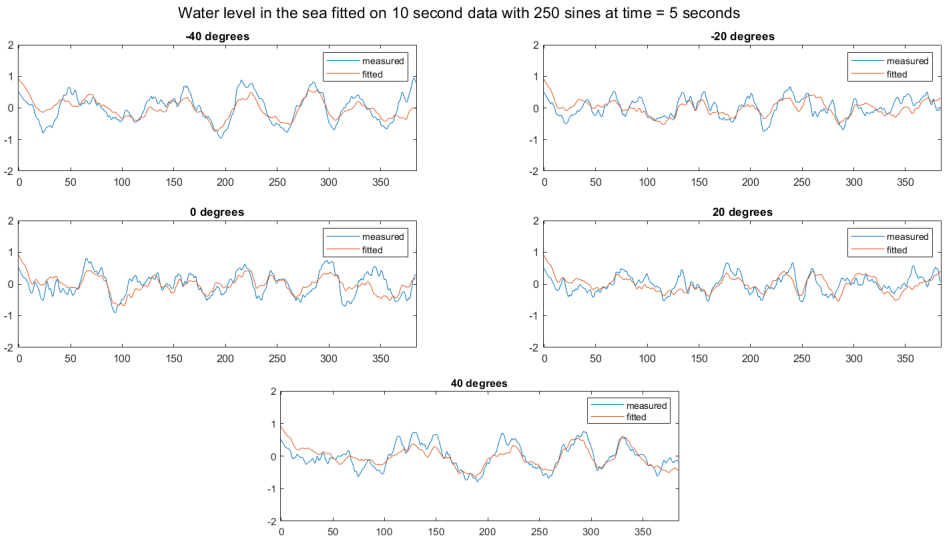

Figure 5.29: Water level along the 5 beams fitted on a long crested sea containing five wave directions

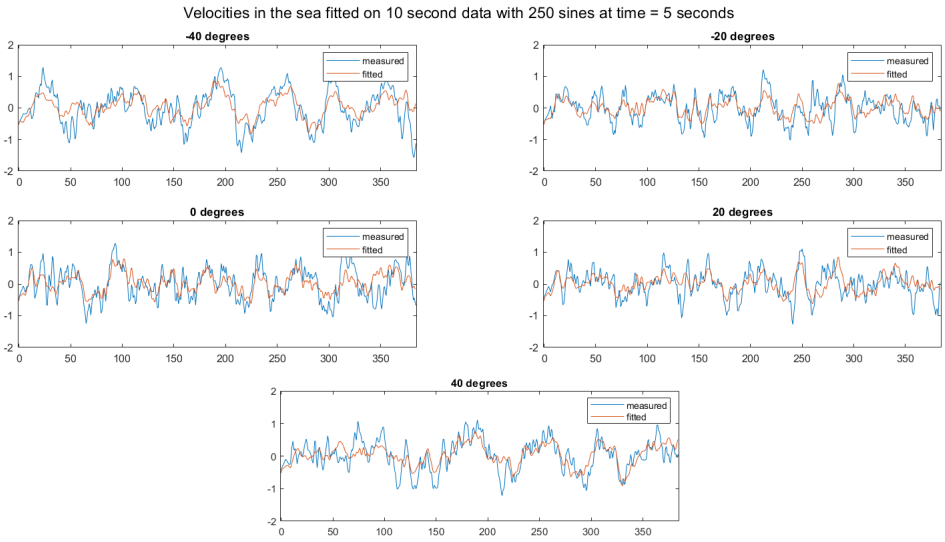

Figure 5.30: Horizontal orbital velocities along the 5 beams fitted on a long crested sea containing five wave direction

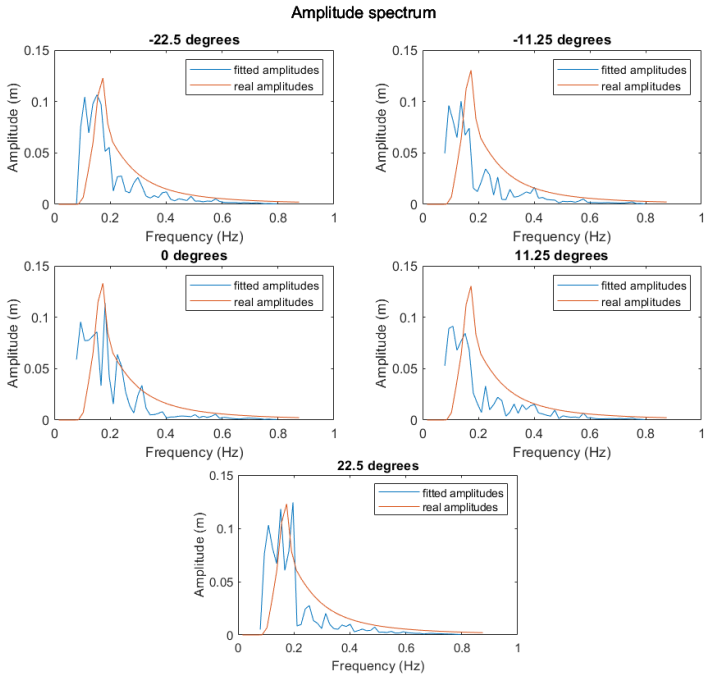

Figure 5.31: Amplitude spectrum for a non-sequential fit over the five wave directions computed with the directional JONSWAP spectrum

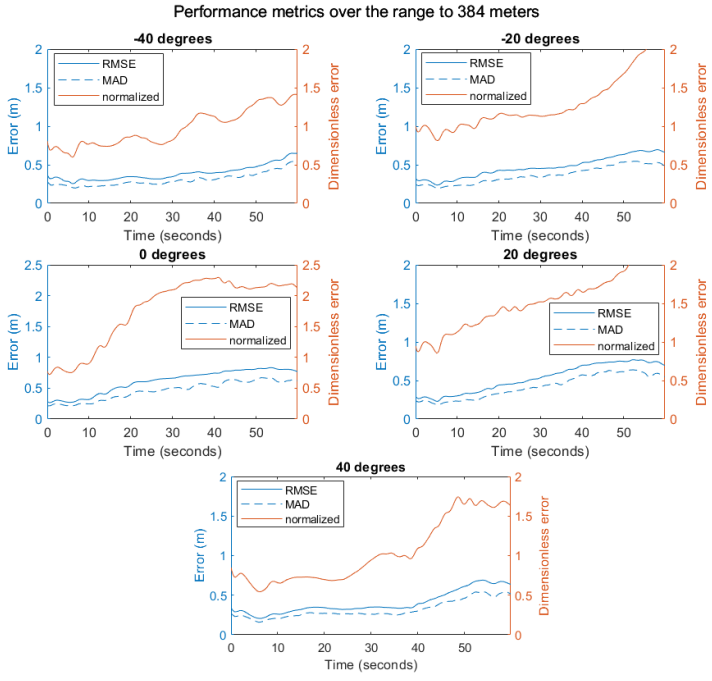

Figure 5.32: Performance metrics for a non-sequential fit over the wave directions over the full range of 384 meters fitted on a long crested sea containing five wave directions

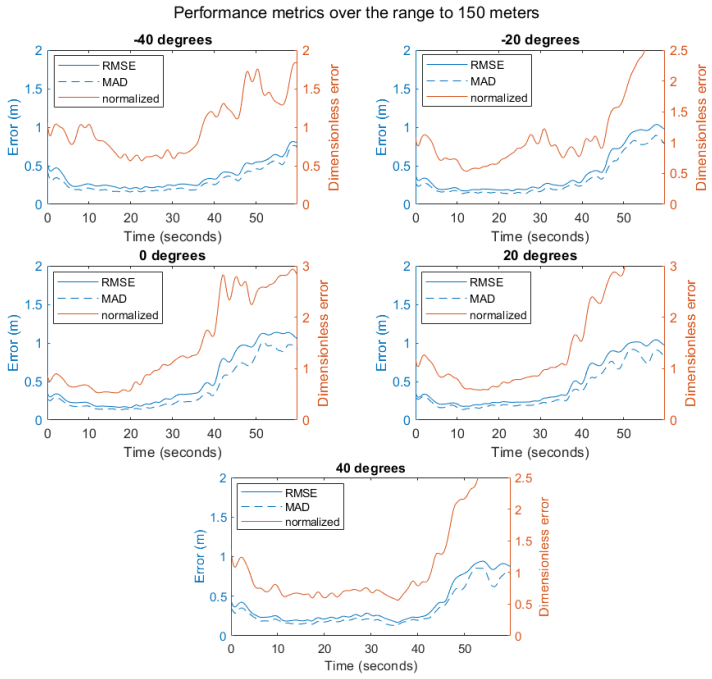

Figure 5.33: Performance metrics for a non-sequential fit over the wave directions over a range of 150 meters from the radar fitted on a long crested sea containing five wave directions

5.2.2. Real data

Pre processing

To do the experiments with the real data some pre processing steps need to be taken. Besides the corrections for the beam angle, grid and water depth as in the one directional case, the direction of the current and waves need to be estimated. This will be done first as a pre processing step. Selecting the main wave direction has also been done for the real data in the one directional model to choose the most suited beam. This gave the outcome that the wave direction was likely to be around the -20 degrees beam. This estimate will be taken as an initial point for the following experiments.

Then it remain to estimate the current direction. The velocities are therefore averaged over the range bins. These averaged velocities per beam are shown in figure 5.34 and the further averaged results over the time range can be found in table 5.8. These show that the average velocity is highest in the -20 degrees beam, with a slightly smaller velocity in the -40 degrees beam. This means that the current direction will probably be coming from somewhere between the -20 and -40 degrees incidence angle. For the first computation the angle of -20 degrees is taken as current direction. The method introduced in the previous chapter which would use these velocities and their incidence angles to least square fit the best suited current magnitude and direction did not give satisfactory results when tested in an artificial environment and was therefore discarded.

beam	average velocity
-40 degrees	0.89
-20 degrees	0.92
0 degrees	0.70
20 degrees	0.68
40 degrees	0.55

Table 5.8: The average velocity over the entire grid and time per beam direction

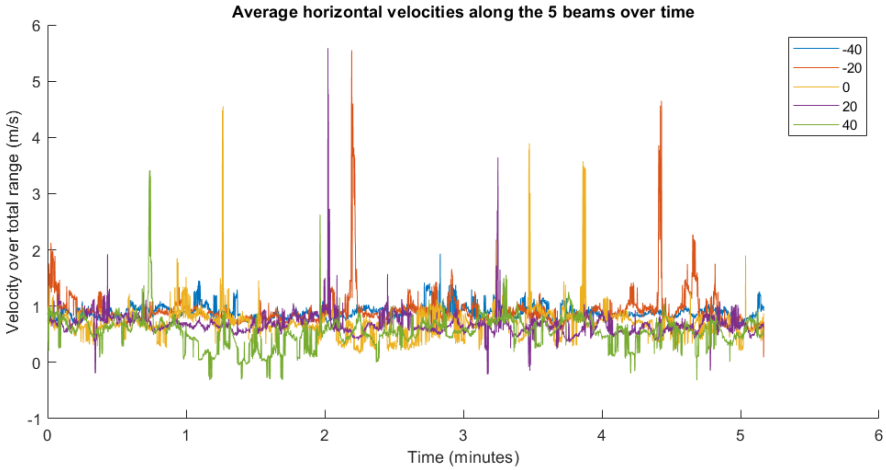

Figure 5.34: The average velocities of the entire grid over time

Fitting to measurements

As found in last section the input for the wave direction will be surrounding the -20 degrees beam. To give the model enough flexibility there are also 4 other wave directions for the model to fit with. These and other model parameters are found in table 5.9. With these parameters the non-sequential

Algorithm parameters	Values	Unit
Number of cosines per direction	40	
Number of directions	5	
Wave directions	$-38, -29, -20, -11, -2$	degrees
Time range	5	s
Time stepsize	0.5	s
Spatial range	0 to 384	m
Spatial stepsize	$0.75\cos(\gamma)$	m
ω (frequency spectrum) per direction	linspace$(0.5, 5, 40)$	Hz
Function tolerance	10^{-6}	
Maximum iterations	10	
Maximum function evaluations	2000	

Table 5.9: Summary of the input parameters for the multi directional fitted model on real data

model is fitted to the data. The results of this are displayed in figs. 5.35 to 5.39. The visualization in figure 5.35 shows that the fitted model resembles the recorded data nicely. Thus this means that the reconstruction of the waves is quite successful. The performance metrics show a different trend, stating that the normalized error is almost in the same order of magnitude as the waves themselves in the fitted period of the first 5 seconds with a value of 0.9. This then increases slowly when new waves enter the domain. The RMSE and MAD vary a lot when comparing them over the beams, in general they are about 0.45 meters/second for the 150 meters range. Remarkable is the behaviour of the performance metrics in the 40 degrees beam, it is unclear as to why this occurs. Thus the predictive capabilities seem limited.

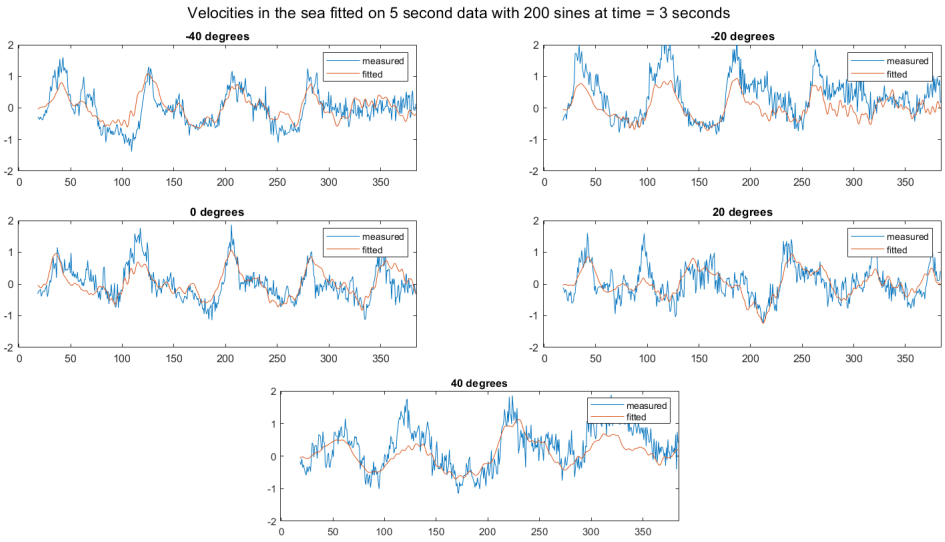

Figure 5.35: Velocities along the 5 beams fitted to real velocity data

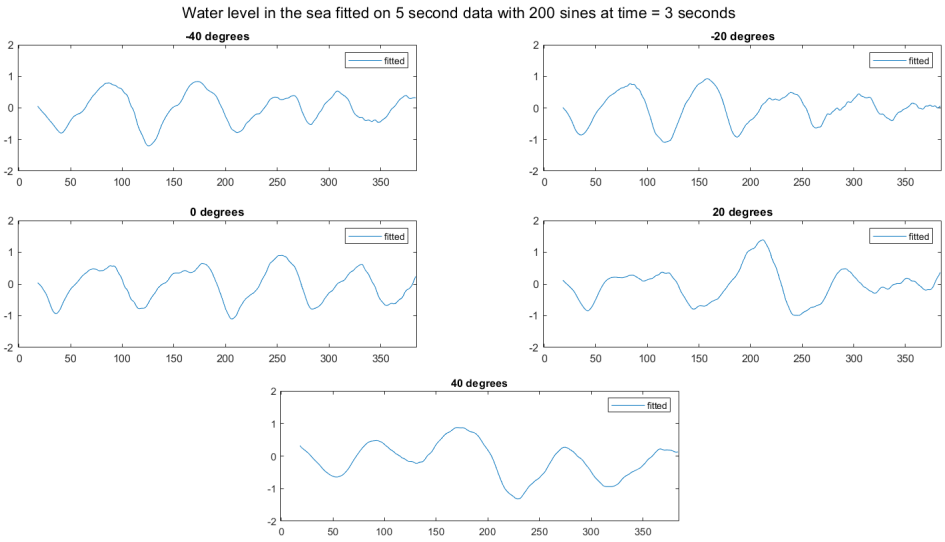

Figure 5.36: Water level along the 5 beams fitted to real velocity data

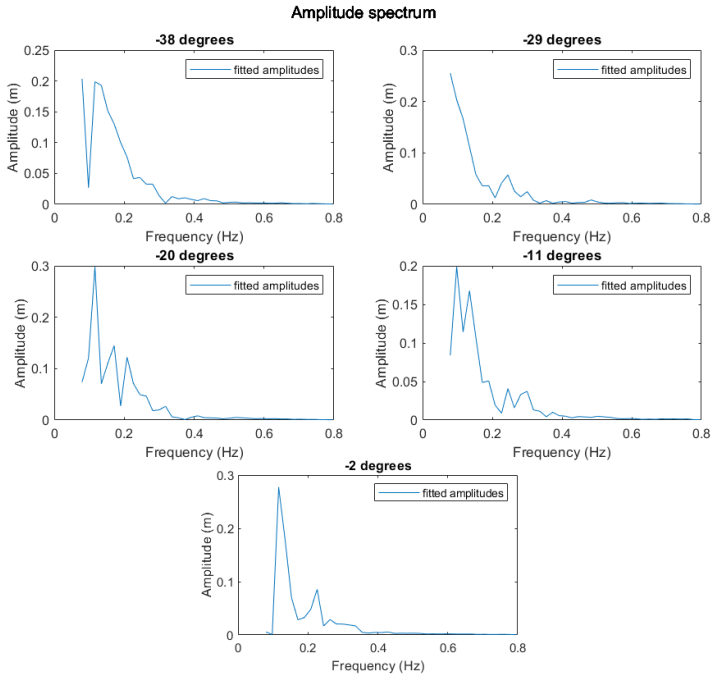

Figure 5.37: Amplitude spectrum for a non-sequential fit over the wave directions fitted to real velocity data

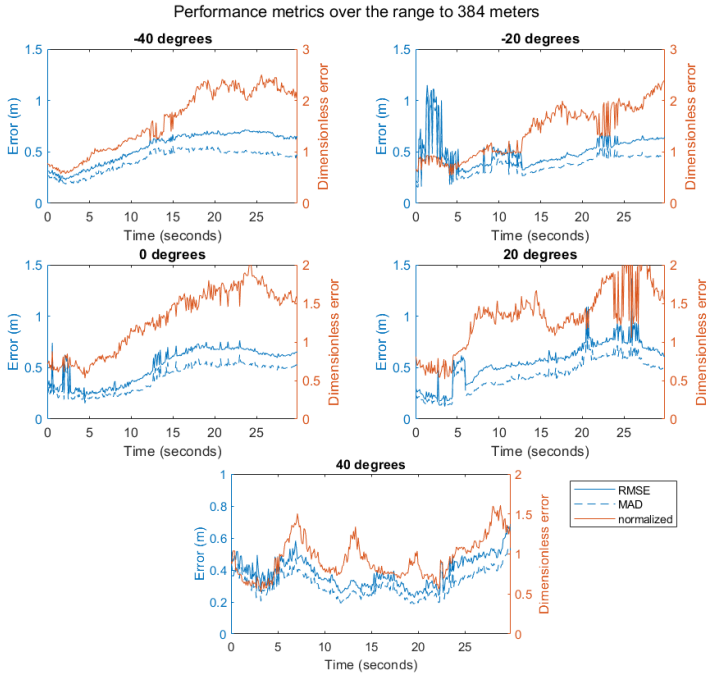

Figure 5.38: Performance metrics for a non-sequential fit over the wave directions over the full range of 384 meters fitted to real velocity data

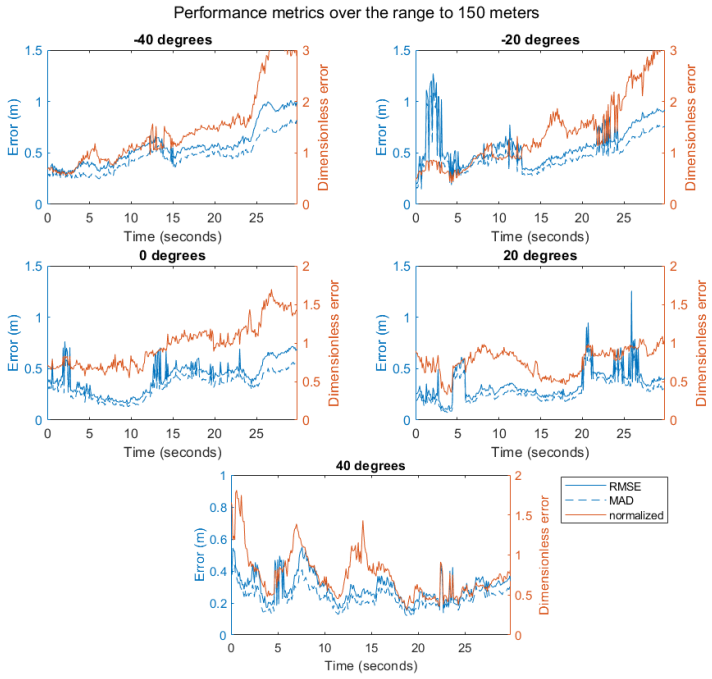

Figure 5.39: Performance metrics for a non-sequential fit over the wave directions over a range of 150 meters from the radar fitted to real velocity data

To exclude that the inaccuracies are caused by a wrong estimation of the current and/or wave directions some experiments have been done with alternative current and wave directions. These can be found in appendix B. When the results of these experiments are compared to the one presented in this section the following stands out. When changing the current direction from -20 degrees to +20 degrees incidence angle, the results are not influenced much. Both performance metrics show similar behaviour.
When the wave directions are centered around a +20 degrees incidence angle instead on the -20 incidence angle the performance metrics perform worse than in the -20 degrees case. Though this does not hold for the data coming from the -20 degrees beam remarkably enough.
A last alteration was made by changing the current direction and the main wave direction both from -20 to +20 degrees. This did not show improvement of the overall result compared to the -20 degrees case.
This thus rules out the possibility of the error being solely caused by very inaccurate estimation of current and wave directions.

5.2.3. Summary of results

In this section the most important findings of the modelling results for the multi directional model are discussed. For the artificial case the non-sequential model is able to capture the behaviour of the sea very well, with an MAD and RMSE displaying similar behaviour. The best performance is found here when using a limited amount of wave directions. Thus the more long-crested the waves are, the better the model can handle them. For artificial data with only one direction the prediction time of 30 seconds for the 150 meter range from the radar remains valid (as in the one directional case) within a precision range of 15 cm (MAD and RMSE) and 0.42 in terms of normalized dimensionless error (in the -40 degrees beam). For the data set with two directions this reduces to 20 seconds for the 150 meters range with a precision range of 25 cm (MAD and RMSE). In terms of the normalized dimensionless error the performance varies since in some beam directions (the 0 and 20 degrees beam) the quality of the performance first increases before it decreases which is the case since the waves closest to the radar are observed for a shorter time. Whilst for the other beams this is not the case. Though all errors remain within 0.67 in terms of normalized error within these first 30 seconds (thus 20 seconds prediction). For

a data set with three wave directions the predictive capability decreases to 15 seconds. This is best seen from the results in the 0 degrees beam.
When applying this non-sequential model to the real data the performance decreases. It is able to reasonably reconstruct the waves that are measured, but it fails to accurately predict for longer times. Though this is most likely not due to an inaccurate estimation of wave/current direction as altering them did not improve the results. The predictive capabilities are very limited.

5.3. Discussion on the results

To conclude this chapter a general discussion of the obtained results with the inverse modelling is done in this section. Main problems arise when using the real data, in both the one as multi directional model. The fit that is generated by the models resembles the measured data quite well from a visual point of view, but this is not readily shown by the performance metrics. These state that the error made by the model lies around 0.5 meters in mean absolute error and mean squared error, and is higher than the magnitude of the signal itself for the normalized error. Reasons for these inaccuracies of the fitted result can be:

1. Water depth estimation, when this is chosen wrongly it will have effect on the propagation speed of the wave. If the recorded data of the waves progresses faster or slower than the model this could be one of the causes.

2. Current/Wave direction mismatch, this could also explain inaccuracies in the progress of the model as compared to the data, a few other combinations of current and wave directions are found in the appendix B. Though these don't improve the reconstruction and prediction. Possibly there could also be refraction in the data, though this can only be really confirmed when the wave directions are determined precisely. For an incidence angle of 20 degrees the effect of this will also be limited.

3. Choice of frequency bins, it might be possible that the choice of frequency bins is not sufficient. Alternatives could be to reserve more bins for certain frequencies that are more present in the data.

4. Noise/quality of the dataset, the recorded data is quite noisy. When this noise is smoothed per time step the difference is not very big when computing the performance metrics. The same holds when the noise is smoothed out through time. Thus another reason could be that some data from the radar is inaccurately and does not contain water motion. It could be useful to therefore include the received signal strength from the radar to determine what is the high quality data.

5. Linear wave theory is not suited, to build the model the assumptions were made that the sea behaves according to the linear wave theory. Due to the advantage of the link that can be made with wave statistics and straightforward way of using it, this seemed a good option. The data that was used is very likely not suitable to get an exact match with a model using linear wave theory though. This is due to the shallow coastal water region near the Pier, which likely has some non linear phenomena taking place there.

For the multi direcional model it is also worth to note that the amount of computation time is very large now due to the large objects the MATLAB code needs to evaluate. These objects are 4-D matrices with entries for the number of cosines, spatial range, directional range and time range which uses a lot of memory. This could be speeded up by supplying the lsqcurvefit routine in MATLAB with a user defined gradient. This was implemented successfully for the one directional model (which did improve the calculation time), but not for the multi directional model.

6

Conclusions and discussion

As a conclusion to this thesis it is worthwhile to discuss the goals that were set in the introduction and the outcome that has been delivered in the past chapters. These will be treated one by one. After the conclusions that are drawn there will be some recommendations for future work.

The first main goal was to reconstruct the sea surface from the radar data by using the linear wave theory. To get to this goal there were some steps needed in between. The first one of these steps was to identify the information the information that is contained in the radar data. By studying literature on the subject and some discussions with experts from Radac and Marin the main components that are present in the data were identified. These consisted of (as discussed in chapter 3):

- Orbital velocity
- Shadowing
- Current/directionally spreaded waves
- Radar noise
- Breaking waves

Distinguishing which of the above is causing a particular effect in the data set remained hard to say. But by setting an upper bound for the amplitudes in terms of the frequency in least squares algorithm helped to prevent the model from creating breaking waves. Determining the actual current direction and wave directions proved to be hard since the results did not show significant decrease of performance when the estimated directions were altered.

Besides identifying the phenomena captured by the radar an important task was to create artificial data that resembles the radar data to have a controlled environment for the model to test. This data was created with the use of the JONSWAP spectrum and the $\cos^2\theta$ directional spreading function. This data helped the development of the model in both one and multiple directions enormously. These models could reconstruct the waves from the artificial data with high precision very well. Depending on the input and model parameter settings the water surface could also be predicted from the reconstructed surface. The time span for which these predictions would hold for a region consisting of the area located between 150 meters from the radar and the radar are 30 seconds for the one directional model with a precision of 15 centimeters (for waves that have significant waveheight of 2 meters) and between 20 and 30 seconds (depending on the artificial data) with a precision of 25 centimeters (also with waves that have significant waveheight of 2 meters) for the multi directional model. Thus for the artificial data it can be stated that the goal of reconstructing and predicting the sea surface has been reached successfully.

Applying the models to the real data coming from the FMCW radar proved to be more challenging. For this to work there needed to be several adjustments to deal with the shallow water conditions (by altering the dispersion relation), current and wave directions and adjusting for the angles for which

the data was recorded. These alterations made that the model was able to fit and reconstruct the measured radar data quite well, but predicting was not possible whilst maintaining an error that has lower magnitude as the waves themselves in terms of the normalized error. As mentioned in the previous chapter there are multiple reasons as to why this is the case. The most likely reasons will be the quality of the dataset and that the linear wave theory probably is not the best suited for fitting a model to this particular data. This is most likely due to the shallow coastal waters and the non linear behaviour near the Pier. But it is fair to state that the possibilities with the linear wave theory are limited computation-wise and that most of these possibilities have been explored.

6.1. Recommendations for future work

In this section some recommendations for future work are given. These might improve the performance of fitting a wave model to the real FMCW radar data. The first recommendation is to determine the high quality regions of data from the radar images and use these to fit the model on. By doing so the effect of noise can be reduced, and will also increase the reliability of the data. For this it might be useful to include the signal strength of the backscatter that the radar receives.
To further improve the performance of the model it is also recommended to find ways to speed up the computation of fit on the multi directional data. This process could take up to 15 minutes in Matlab, which is explained by the big amount of storage space that is needed to keep the orbital velocity function in- and output. This consisted of a large 4-D object containing entries for the amount of cosine terms besides the time, angular and spatial range. This can be done by supplying the least squares solver with an user defined gradient, which would not have to be generated by Matlab then. This was succesfully done for the one directional model, but not for the multi directional model.

Another recommendation is to explore some other non-linear/alternative wave models to fit the data on. This can be done using Cnoidal theory or possibly the Modified Non-linear Schrodinger equation (MNLS) that was used by Simanesew [15]. It can be expected that these models are better able to deal with non-linearities and are thus likely better suited to predict the surface than the linear wave theory that was used for this thesis for this particular data coming from a system mounted on the Pier.
Since the linear wave model that was used is best suited for deep water waves and more idealised conditions it would also be recommended to test the model with data that is obtained under these conditions. And maybe even more important, to have a clear understanding of what the precise conditions are in terms of water depth, current direction and roughly the wave direction(s). This would help with identifying where the model and/or the radar particularly struggles since there is more information available of what the outcome should be. So this motivates to use a more controlled set-up of the test environment to get more results and more detailed information on the performance.

A

One directional model

A.1. Artificial

A.1.1. Variation in number of terms

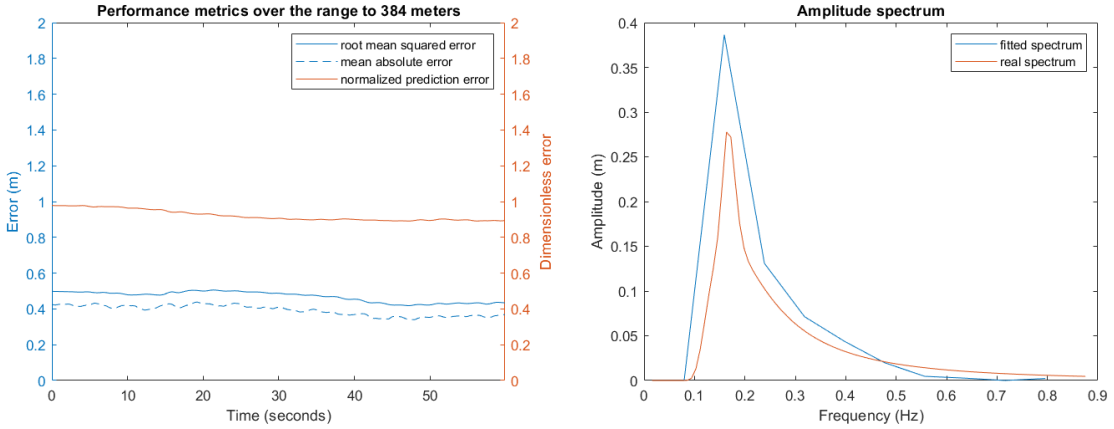

(a) 512 range bins (representing 384 meters) (b) Amplitude spectrum

Figure A.1: Performance metrics for a non-sequential fit with 10 cosines

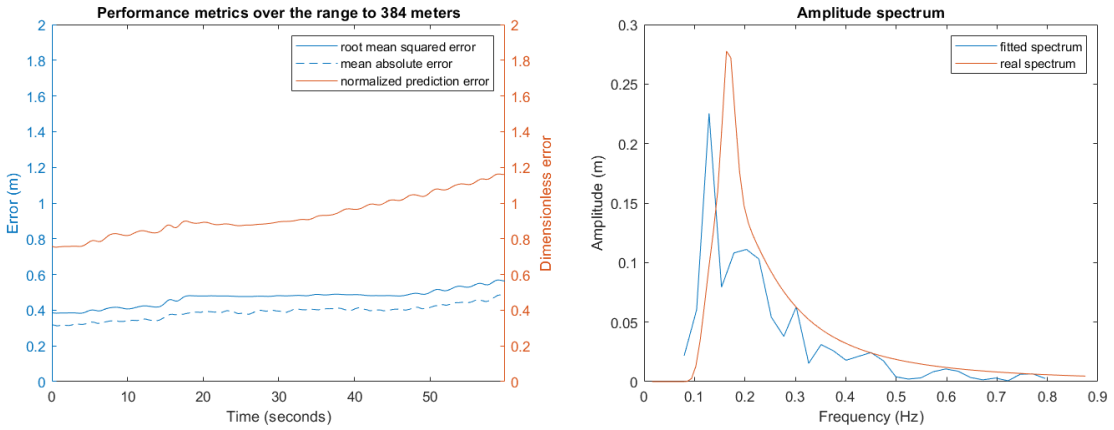

(a) 512 range bins (representing 384 meters) (b) Amplitude spectrum

Figure A.2: Performance metrics for a non-sequential fit with 30 cosines

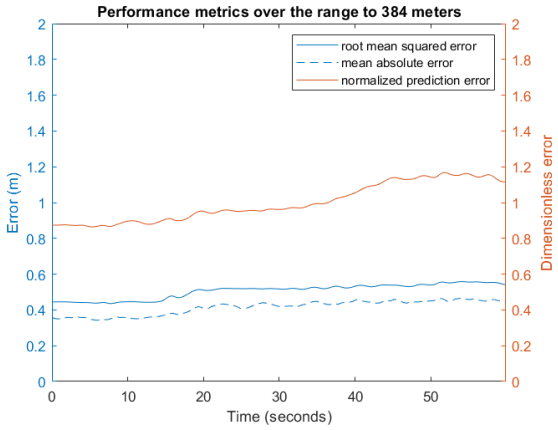

(a) 512 range bins (representing 384 meters)

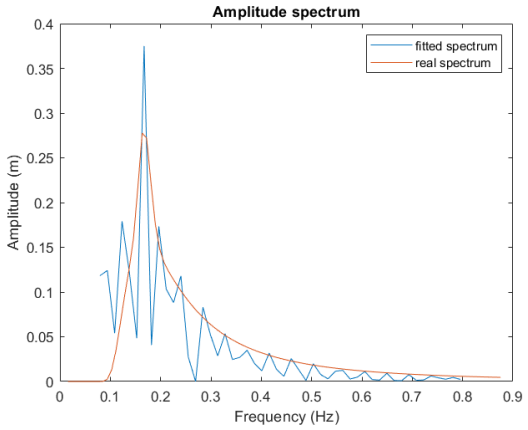

(b) Amplitude spectrum

Figure A.3: Performance metrics for a non-sequential fit with 50 cosines

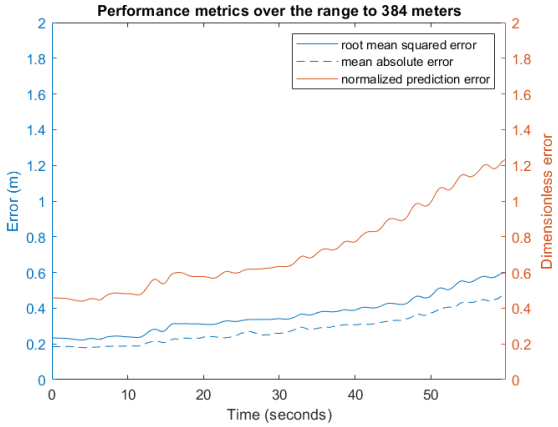

(a) 512 range bins (representing 384 meters)

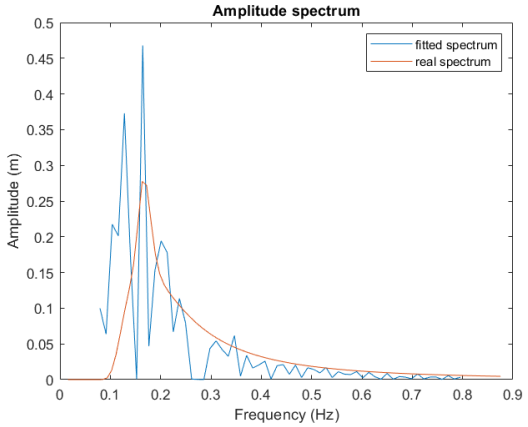

(b) Amplitude spectrum

Figure A.4: Performance metrics for a non-sequential fit with 60 cosines

(a) 512 range bins (representing 384 meters)

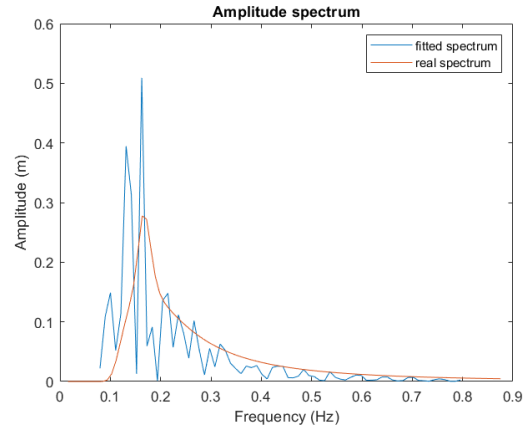

(b) Amplitude spectrum

Figure A.5: Performance metrics for a non-sequential fit with 70 cosines

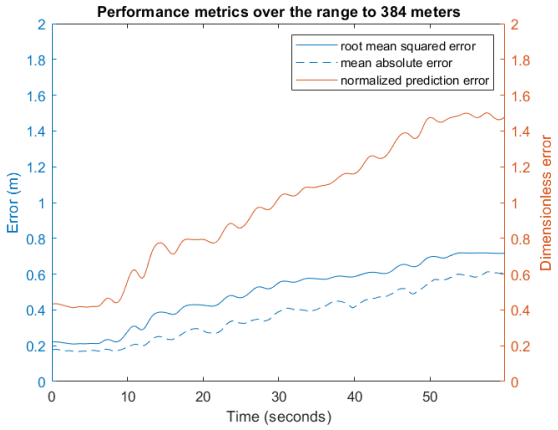

(a) 512 range bins (representing 384 meters)

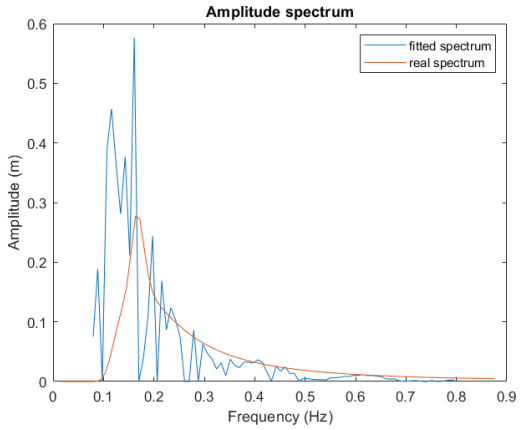

(b) Amplitude spectrum

Figure A.6: Performance metrics for a non-sequential fit with 80 cosines

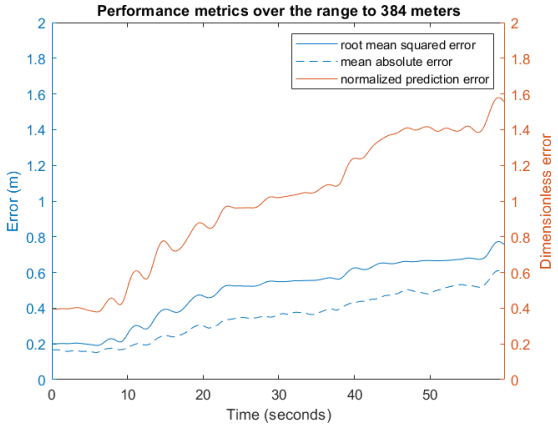

(a) 512 range bins (representing 384 meters)

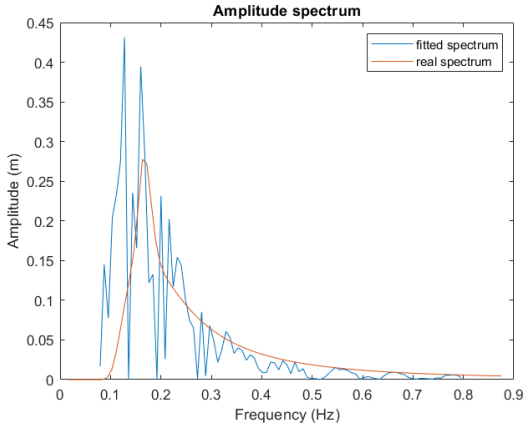

(b) Amplitude spectrum

Figure A.7: Performance metrics for a non-sequential fit with 90 cosines

A.1.2. Variation in spatial step size

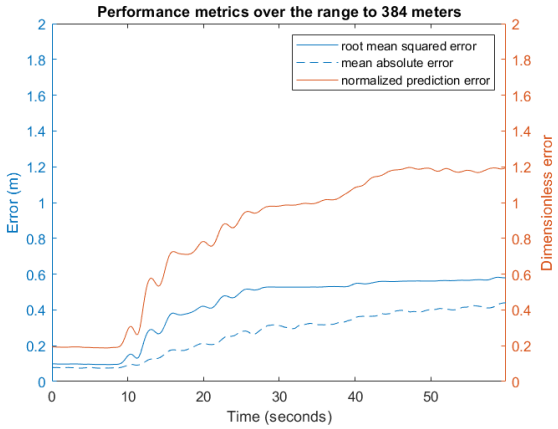

(a) 512 range bins (representing 384 meters)

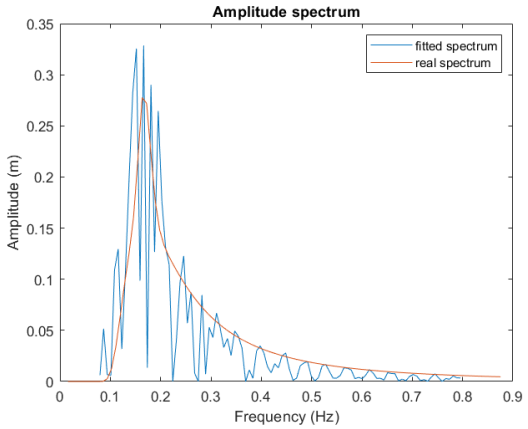

(b) Amplitude spectrum

Figure A.8: Performance metrics for a non-sequential fit with a spatial step size of 2 (1.5 meters) using 256 bins

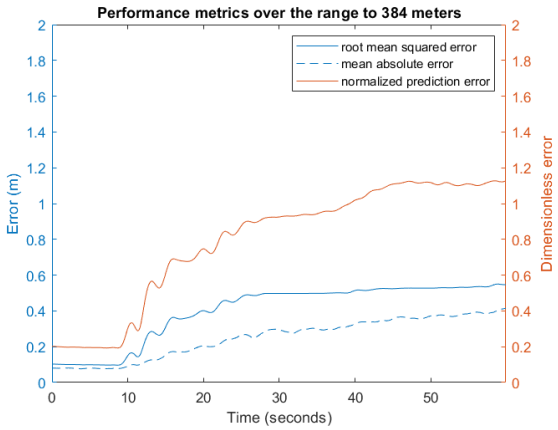

(a) 512 range bins (representing 384 meters)

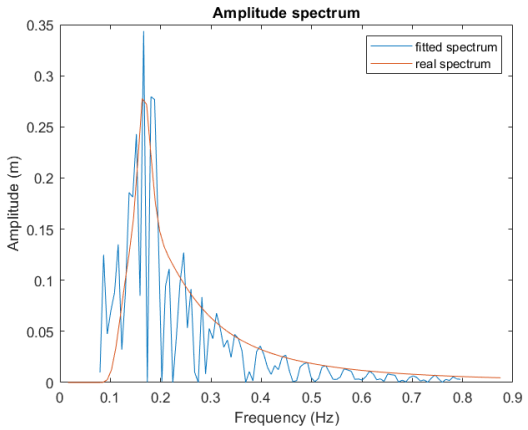

(b) Amplitude spectrum

Figure A.9: Performance metrics for a non-sequential fit with a spatial step size of 4 (3 meters) using 128 bins

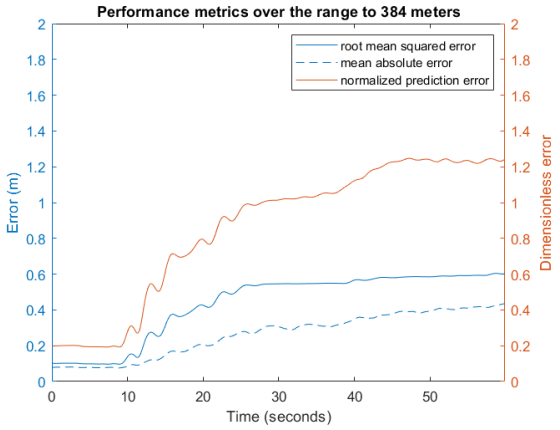

(a) 512 range bins (representing 384 meters)

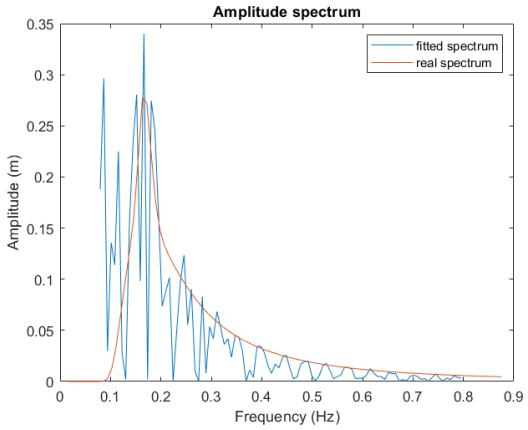

(b) Amplitude spectrum

Figure A.10: Performance metrics for a non-sequential fit with a spatial step size of 8 (6 meters) using 64 bins

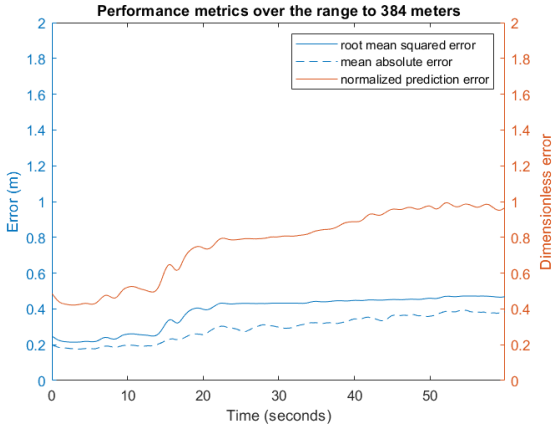

(a) 512 range bins (representing 384 meters)

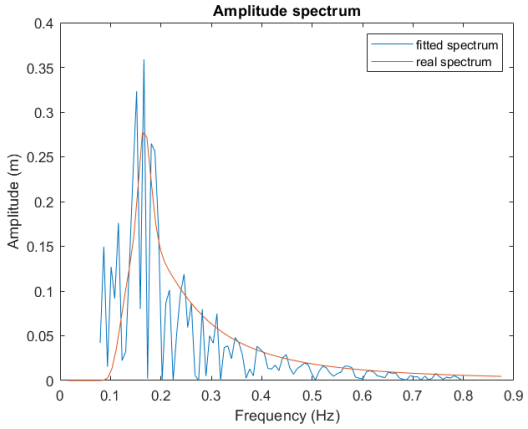

(b) Amplitude spectrum

Figure A.11: Performance metrics for a non-sequential fit with a spatial step size of 16 (12 meters) using 32 bins

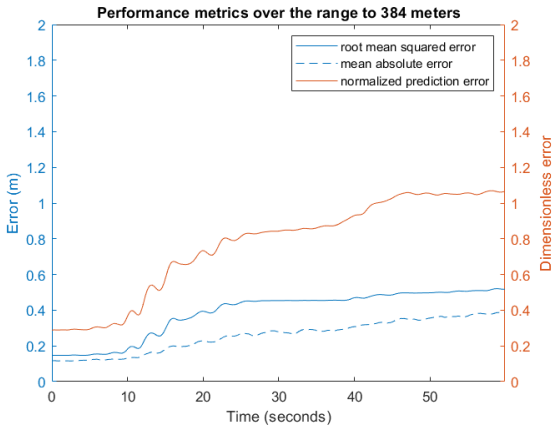

(a) 512 range bins (representing 384 meters)

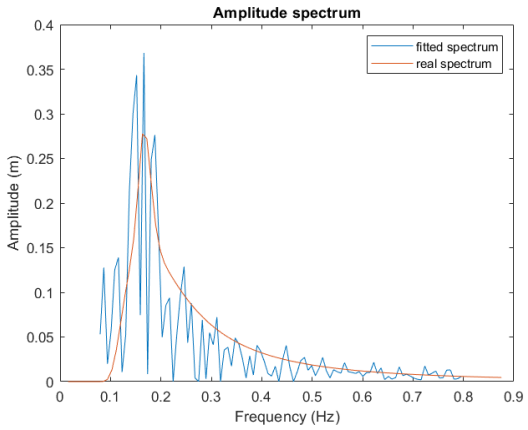

(b) Amplitude spectrum

Figure A.12: Performance metrics for a non-sequential fit with a spatial step size of 32 (24 meters) using 16 bins

A.1.3. Variation in time step size

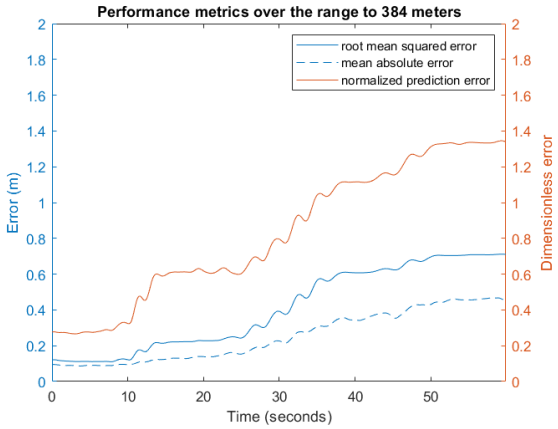

(a) 512 range bins (representing 384 meters)

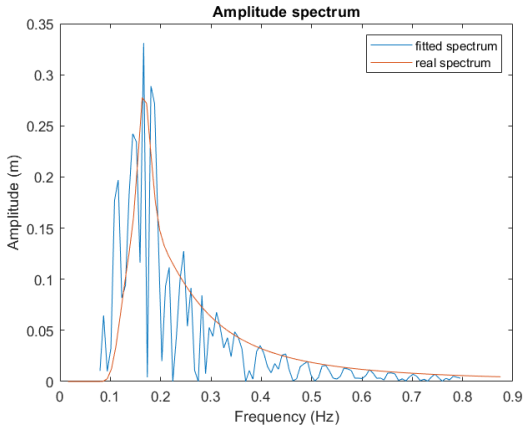

(b) Amplitude spectrum

Figure A.13: Performance metrics for a non-sequential fit with a time step size of 1 (0.1 seconds) using 100 measurements

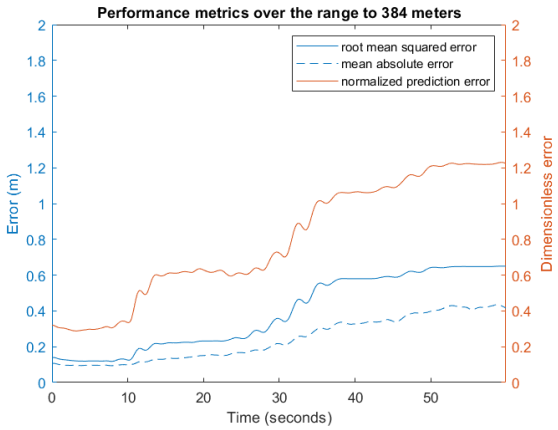

(a) 512 range bins (representing 384 meters)

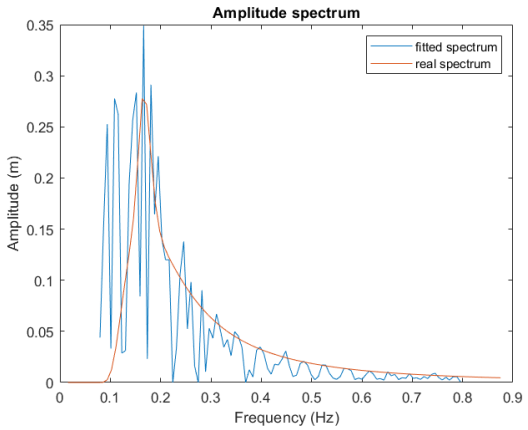

(b) Amplitude spectrum

Figure A.14: Performance metrics for a non-sequential fit with a time step size of 10 (1 second) using 10 measurements

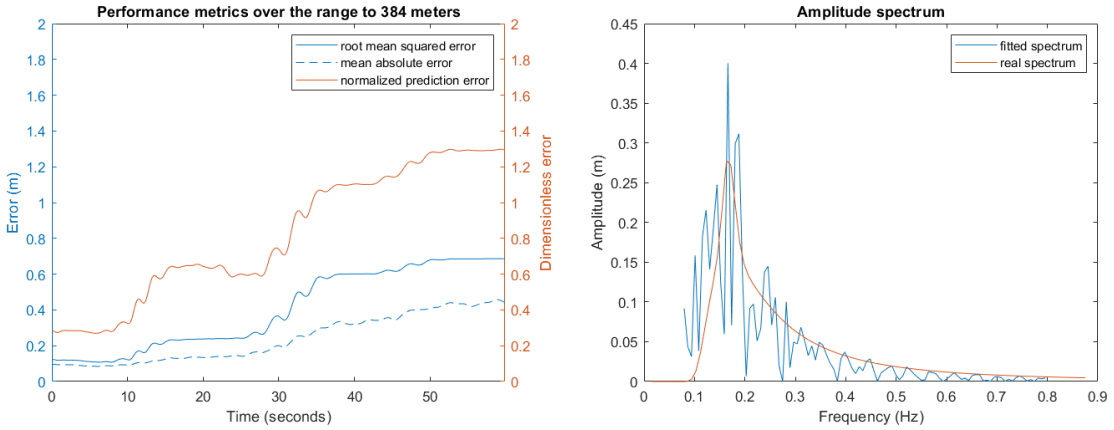

(a) 512 range bins (representing 384 meters) (b) Amplitude spectrum

Figure A.15: Performance metrics for a non-sequential fit with a time step size of 20 (2 seconds) using 5 measurements

B

Multi directional model

B.1. Artificial data

B.1.1. Variation in wave directions

For the following results an artificial sea surface with two wave directions coming from $-\frac{\pi}{8}$ and $\frac{\pi}{8}$ radians incidence angle:

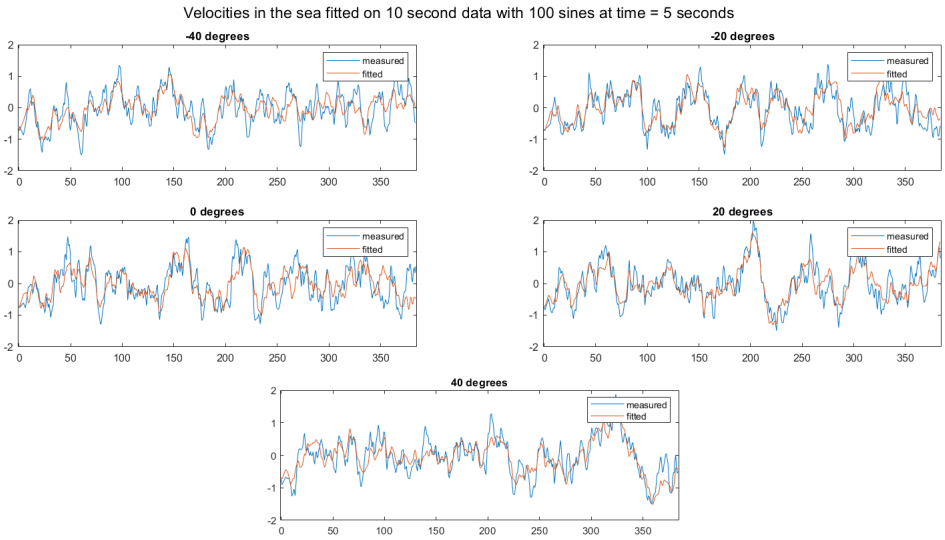

Figure B.1: Velocities along the 5 beams fitted on a long crested sea containing two wave directions

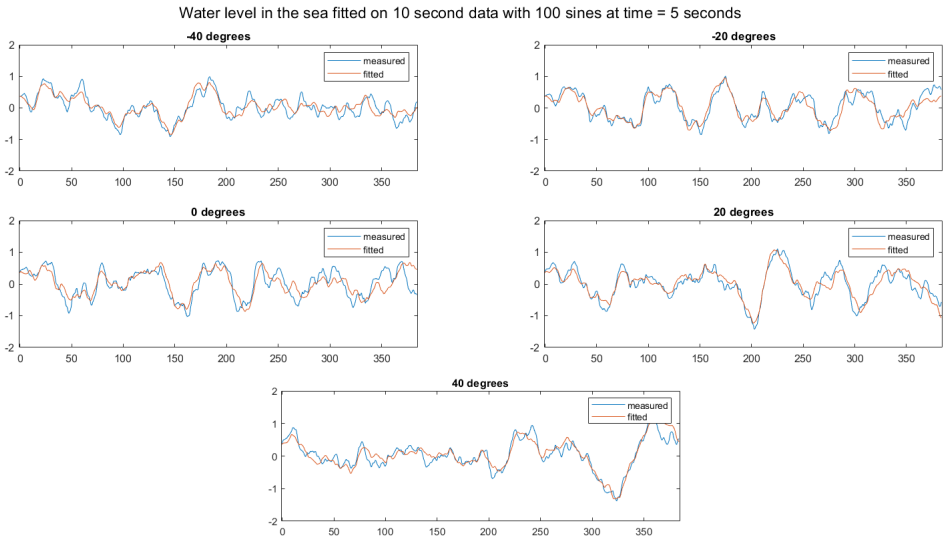

Figure B.2: Water level along the 5 beams fitted on a long crested sea containing two wave directions

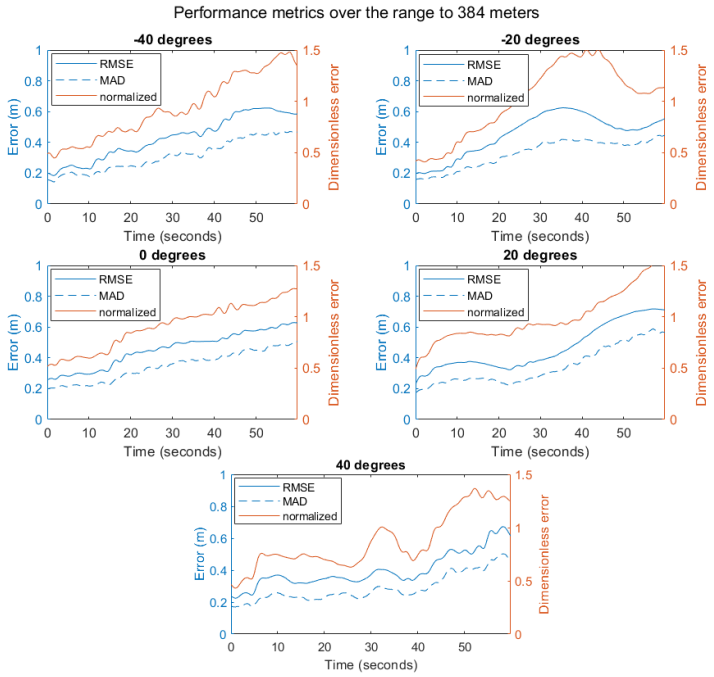

Figure B.3: Performance metrics for a non-sequential fit over the wave directions over the full range of 384 meters from the radar fitted on a long crested sea containing two wave directions

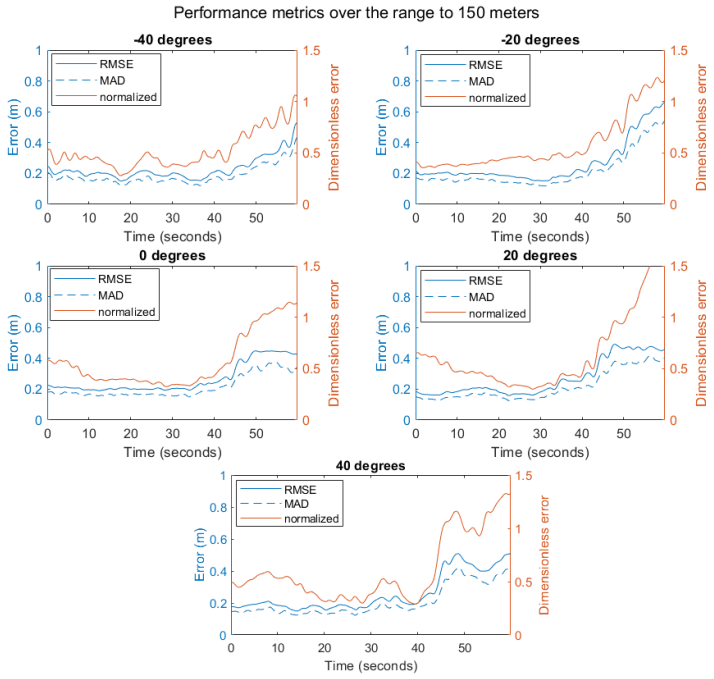

Figure B.4: Performance metrics for a non-sequential fit over the wave directions over a range of 150 meters from the radar fitted on a long crested sea containing two wave directions

For the following results an artificial sea surface with three wave directions coming from $-\frac{\pi}{8}$, 0 and $\frac{\pi}{8}$ radians incidence angle:

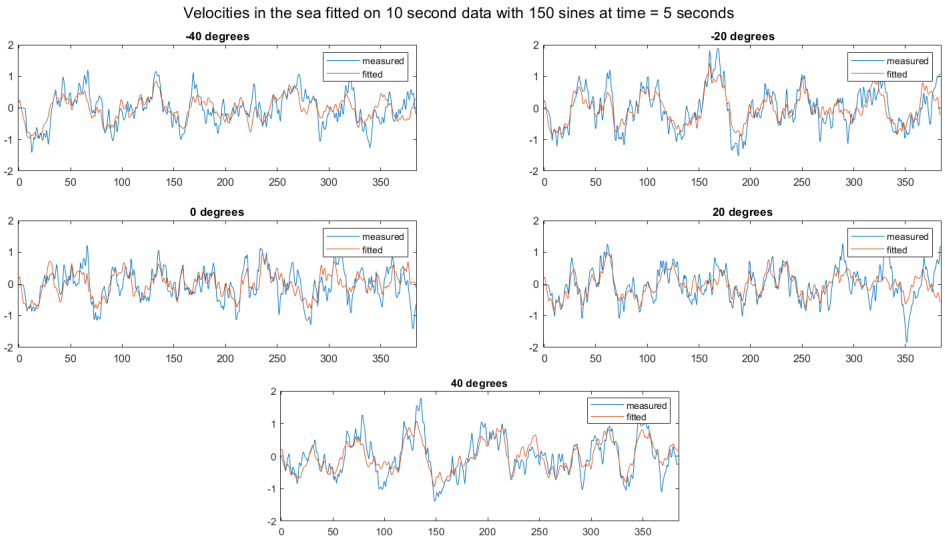

Figure B.5: Velocities along the 5 beams fitted on a long crested sea containing three wave directions

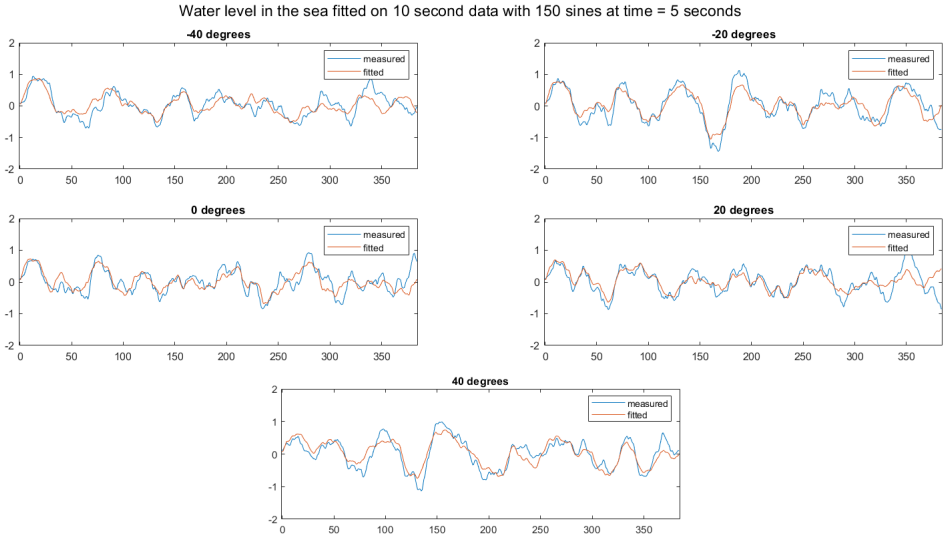

Figure B.6: Water level along the 5 beams fitted on a long crested sea containing three wave directions

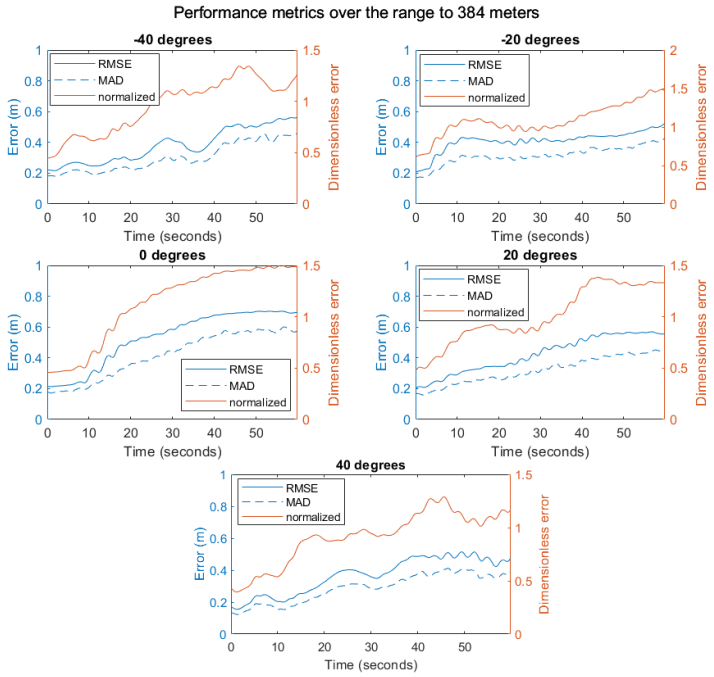

Figure B.7: Performance metrics for a non-sequential fit over the wave directions over the full range of 384 meters from the radar fitted on a long crested sea containing three wave directions

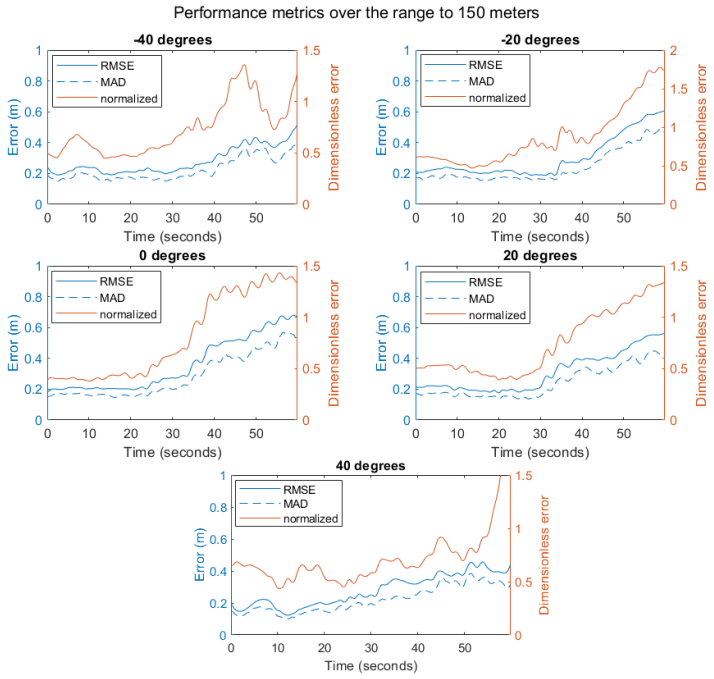

Figure B.8: Performance metrics for a non-sequential fit over the wave directions over a range of 150 meters from the radar fitted on a long crested sea containing three wave directions

B.2. Real data

The results found in figs. B.9 to B.13 are obtained by reducing the timestep between the measured data to 0.2 seconds instead of 0.5 seconds as in the base case presented in chapter 5.

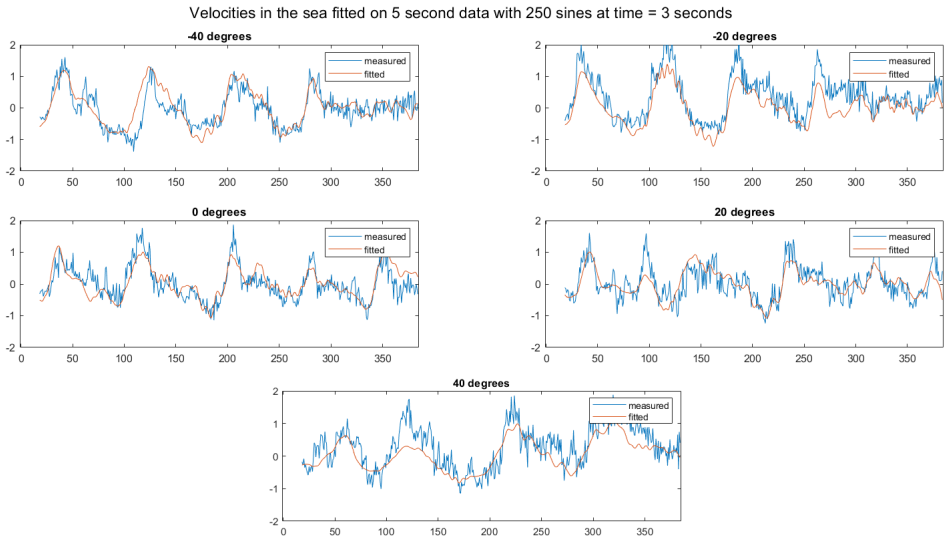

Figure B.9: Velocities along the 5 beams fitted on 5 second data with 0.2 seconds between measurements

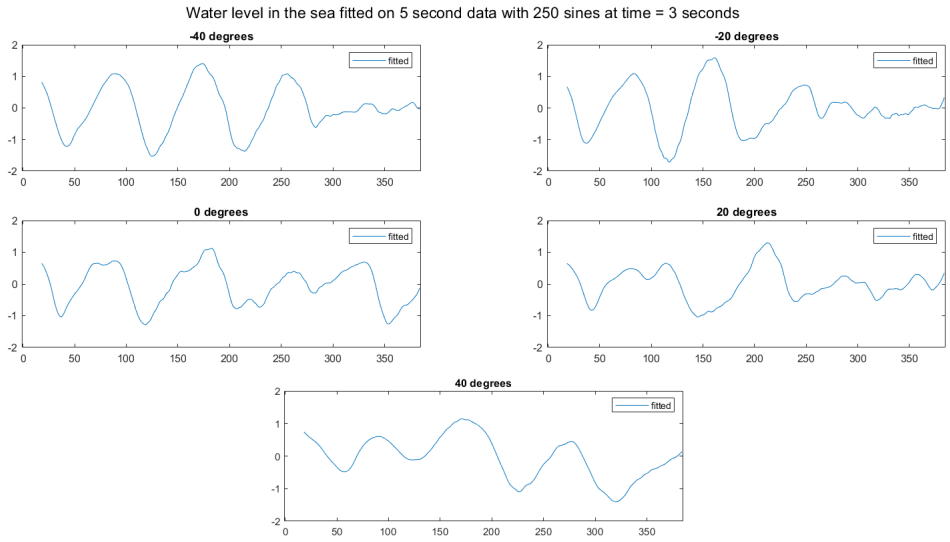

Figure B.10: Water level along the 5 beams fitted on 5 second data with 0.2 seconds between measurements

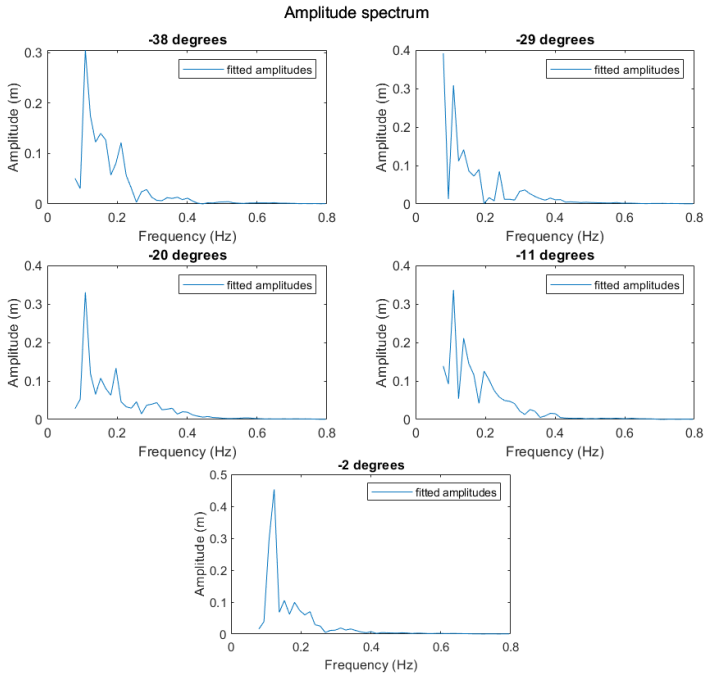

Figure B.11: Amplitude spectrum for a non-sequential fit over the wave directions fitted on 5 second data with 0.2 seconds between measurements

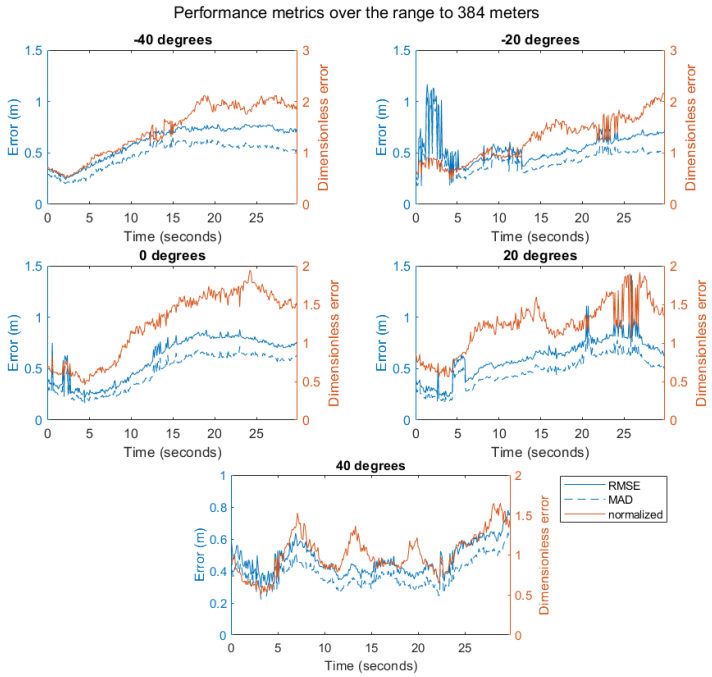

Figure B.12: Performance metrics for a non-sequential fit over the wave directions over the full range of 384 meters fitted on 5 second data with 0.2 seconds between measurements

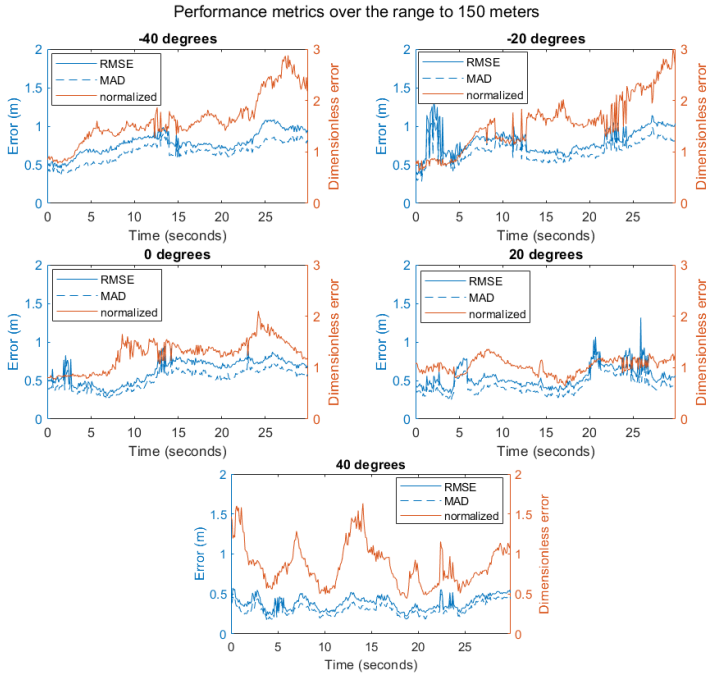

Figure B.13: Performance metrics for a non-sequential fit over the wave directions over a range of 150 meters from the radar fitted on 5 second data with 0.2 seconds between measurements

B.2.1. Variation in wave and current directions

The following experiment has been done using an alternative wave direction centered around 20 degrees incidence angle. These are shown in figs. B.14 to B.18

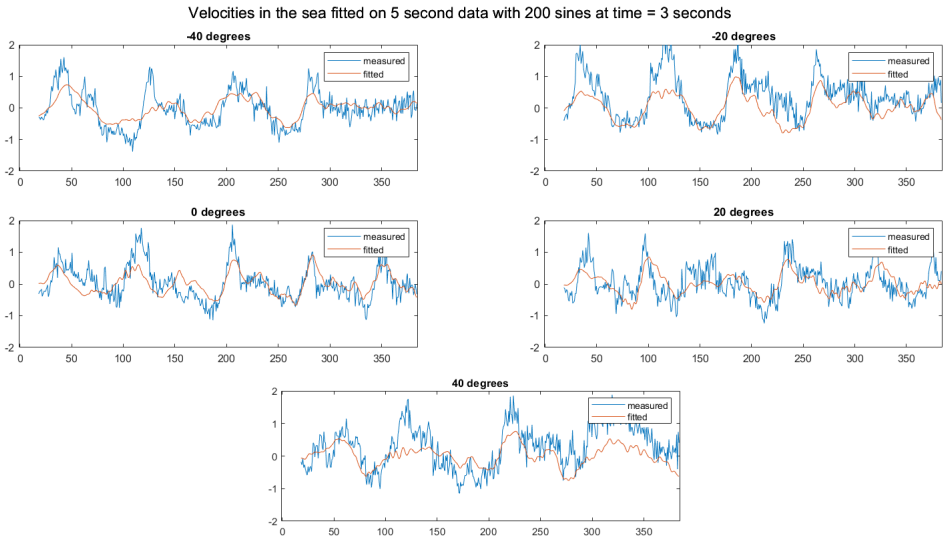

Figure B.14: Velocities along the 5 beams fitted on 5 second data with alternative wave direction

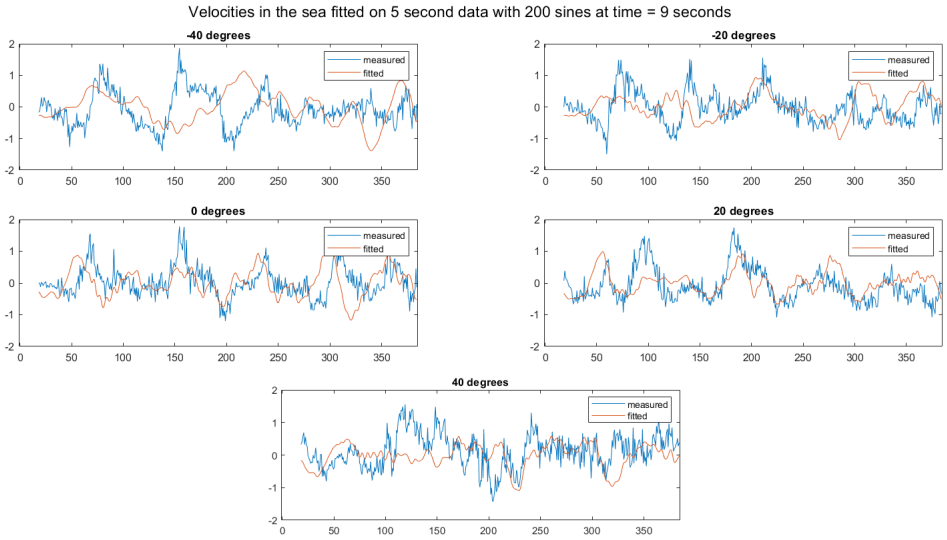

Figure B.15: Velocities along the 5 beams fitted on 5 second data with alternative wave direction

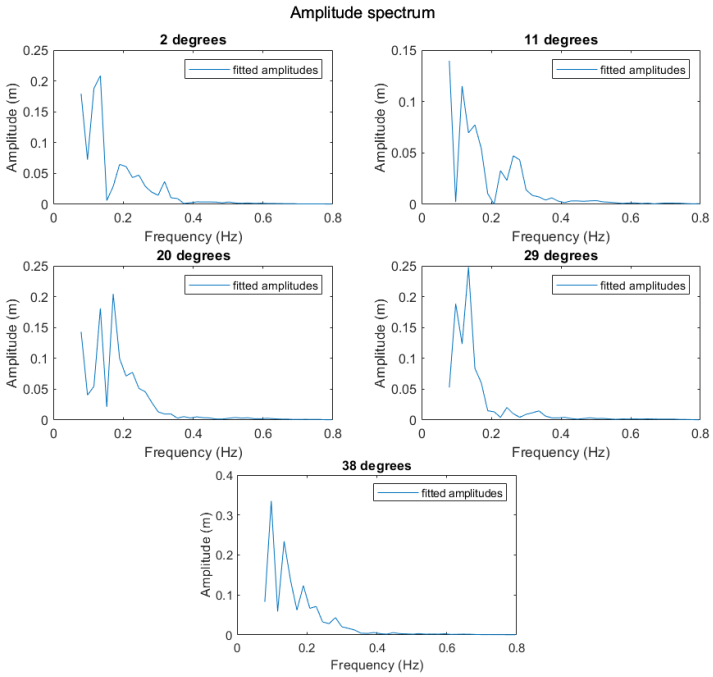

Figure B.16: Amplitude spectrum for a non-sequential fit over the wave directions fitted on 5 second data with alternative wave direction

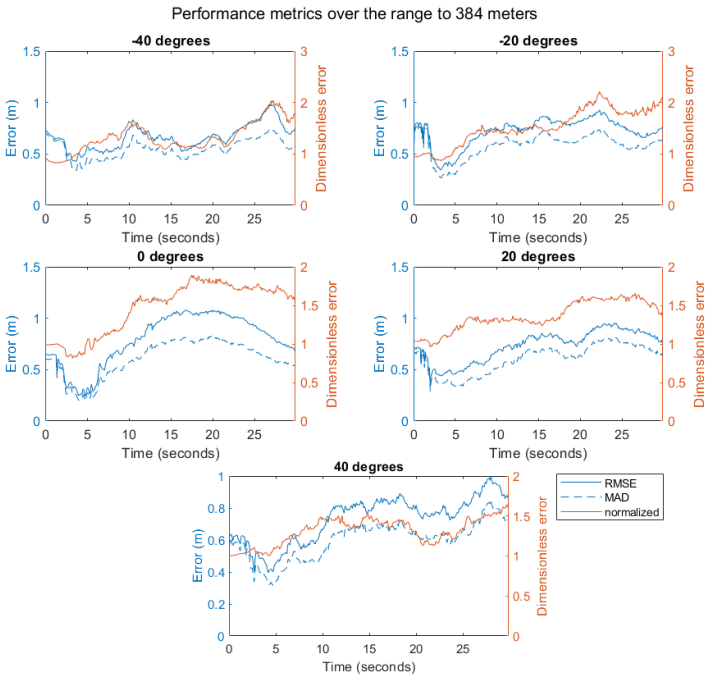

Figure B.17: Performance metrics for a non-sequential fit over the wave directions over the full range of 384 meters fitted on 5 second data with alternative wave direction

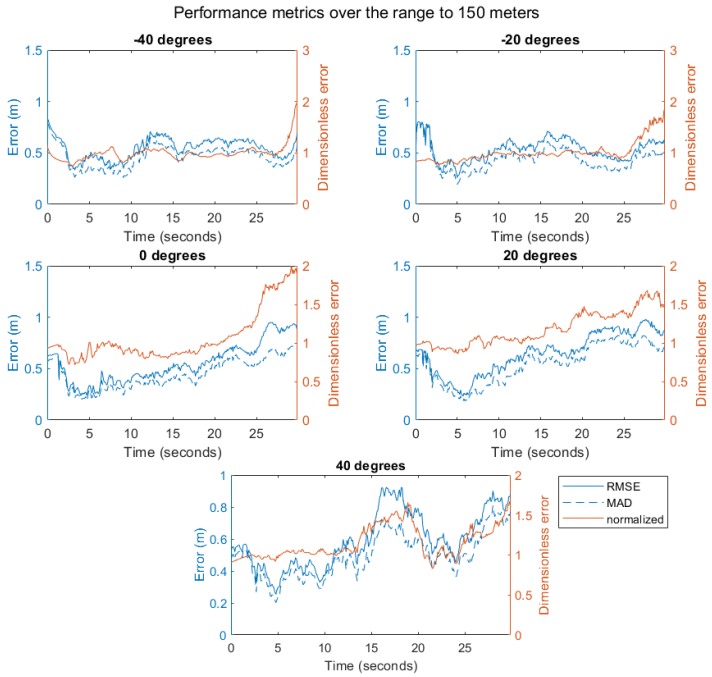

Figure B.18: Performance metrics for a non-sequential fit over the wave directions over a range of 150 meters from the radar fitted on 5 second data with alternative wave direction

The following experiment has been done with an alternative current direction with 20 degrees incidence angle. These are shown in figs. B.19 to B.23

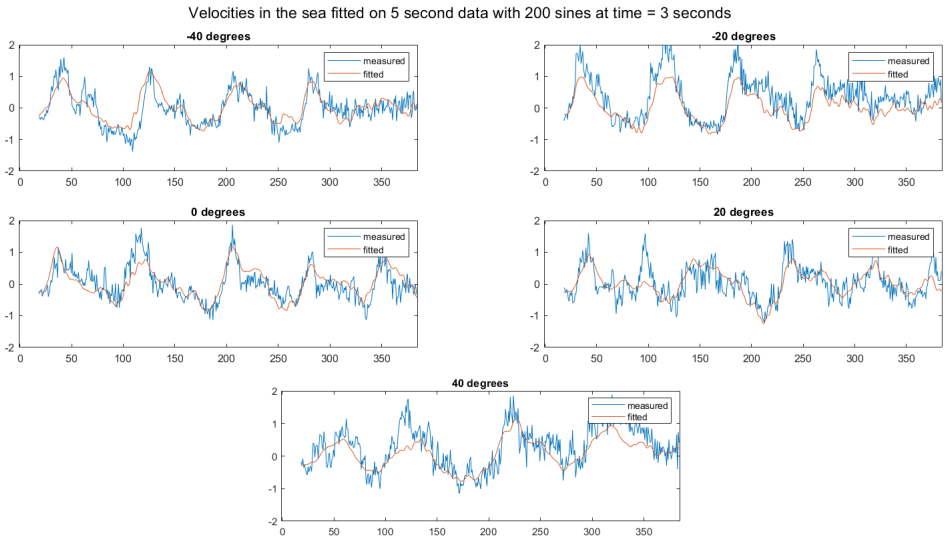

Figure B.19: Velocities along the 5 beams fitted on 5 second data with alternative current direction

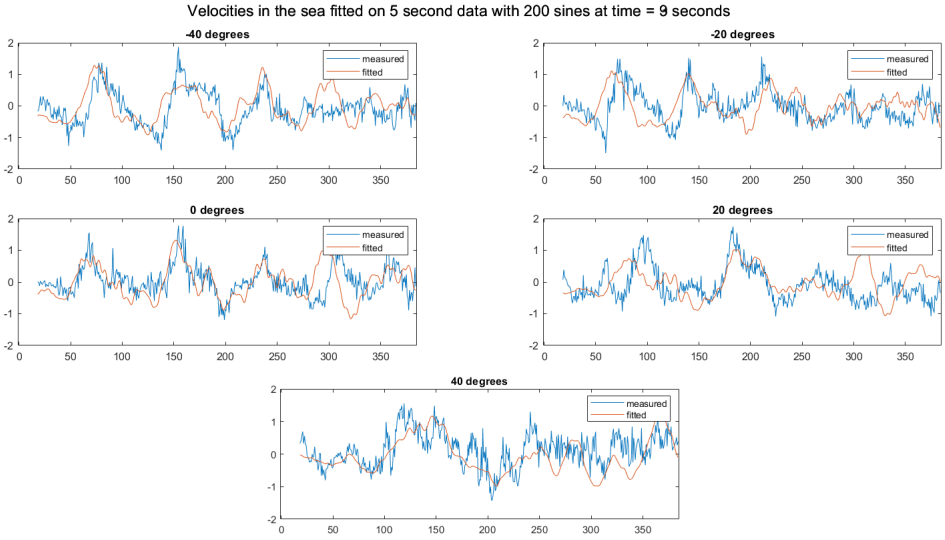

Figure B.20: Velocities along the 5 beams fitted on 5 second data with alternative current direction

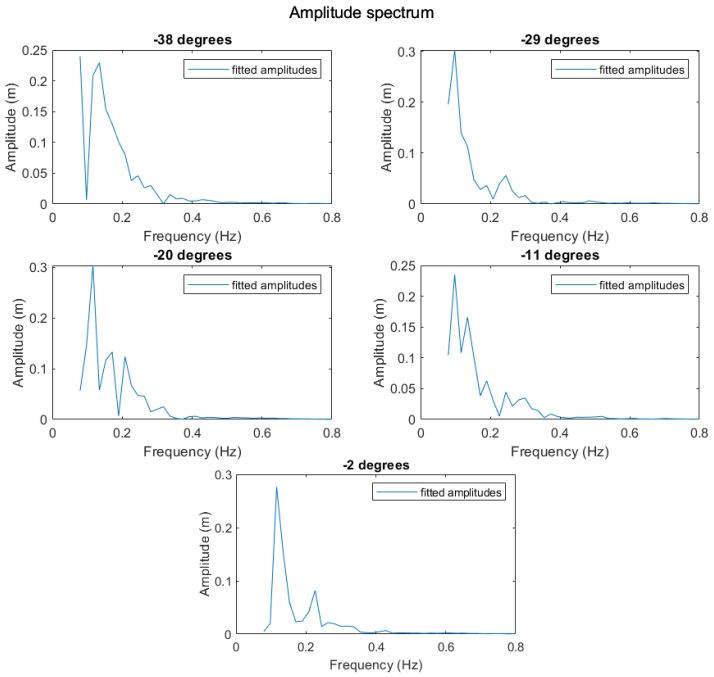

Figure B.21: Amplitude spectrum for a non-sequential fit over the wave directions fitted on 5 second data with alternative current direction

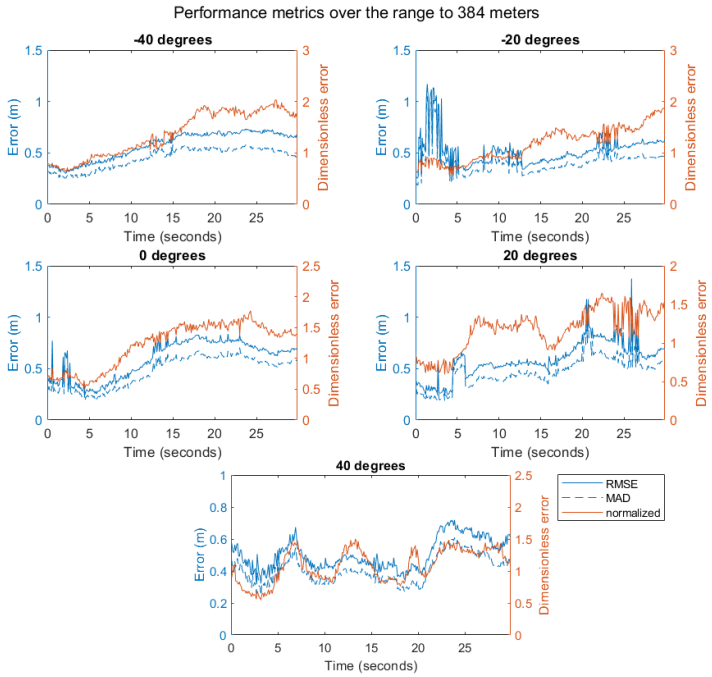

Figure B.22: Performance metrics for a non-sequential fit over the wave directions over the full range of 384 meters fitted on 5 second data with alternative current direction

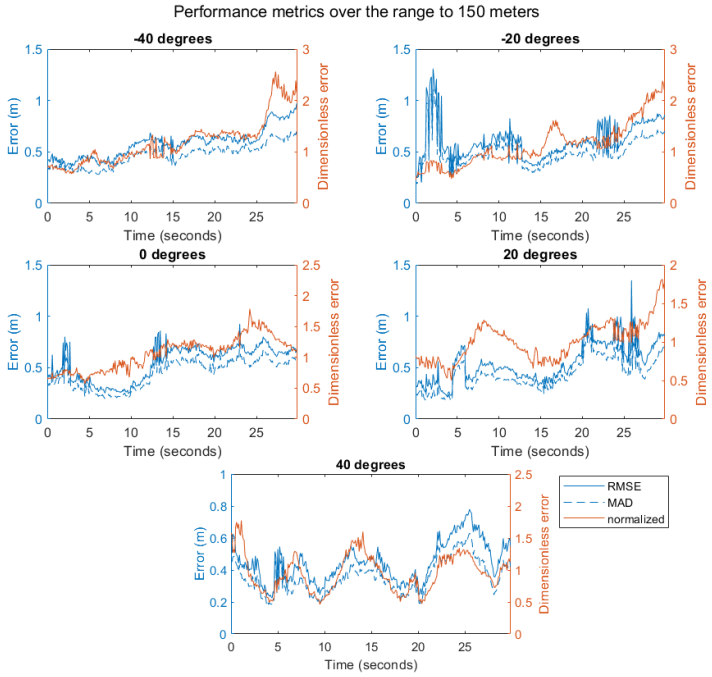

Figure B.23: Performance metrics for a non-sequential fit over the wave directions over a range of 150 meters from the radar fitted on 5 second data with alternative current direction

The following experiment has been done with an alternative current direction with 20 degrees incidence angle and alternative wave direction centered around 20 degrees. These are shown in figs. B.24 to B.28

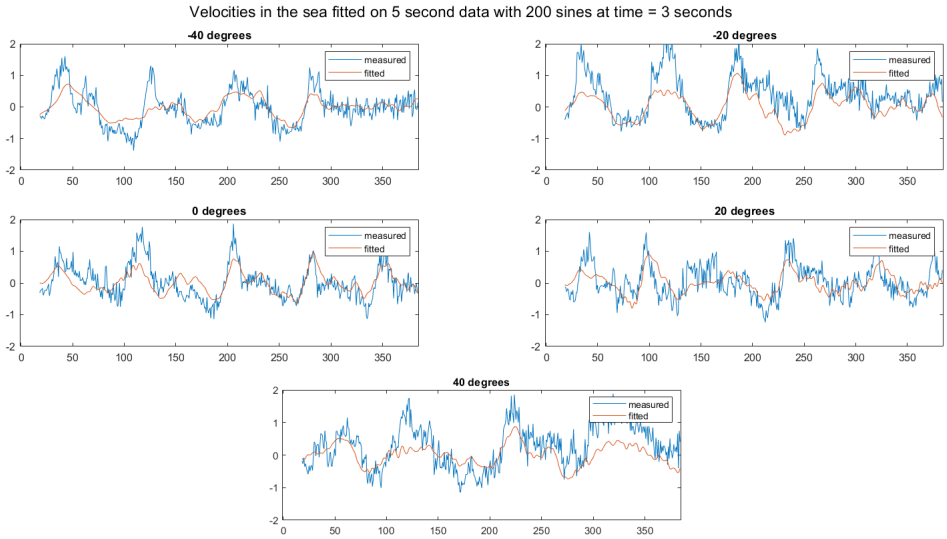

Figure B.24: Velocities along the 5 beams fitted on 5 second data with alternative current and wave direction

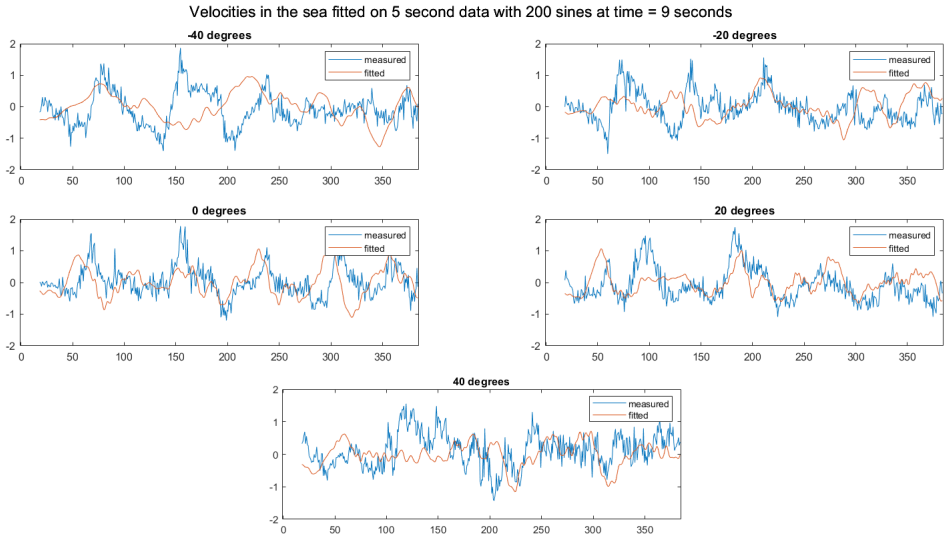

Figure B.25: Velocities along the 5 beams fitted on 5 second data with alternative current and wave direction

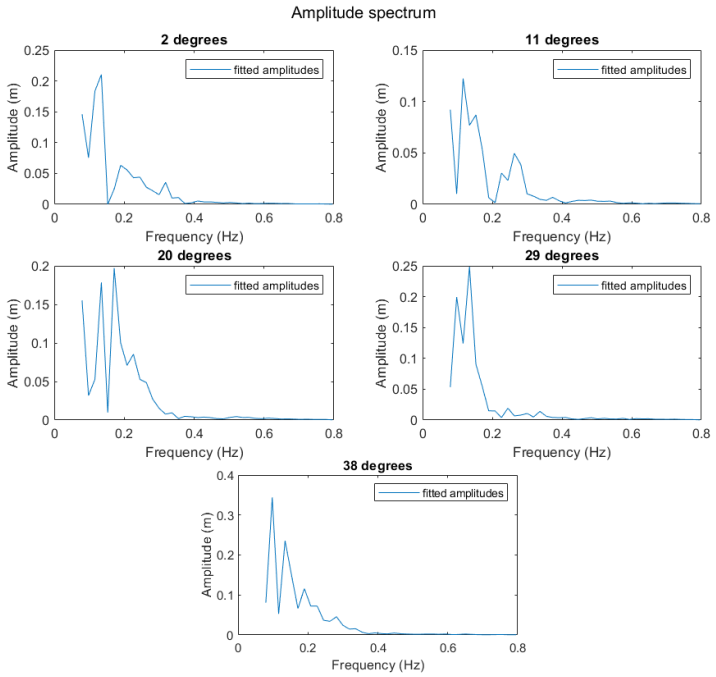

Figure B.26: Amplitude spectrum for a non-sequential fit over the wave directions fitted on 5 second data with alternative current and wave direction

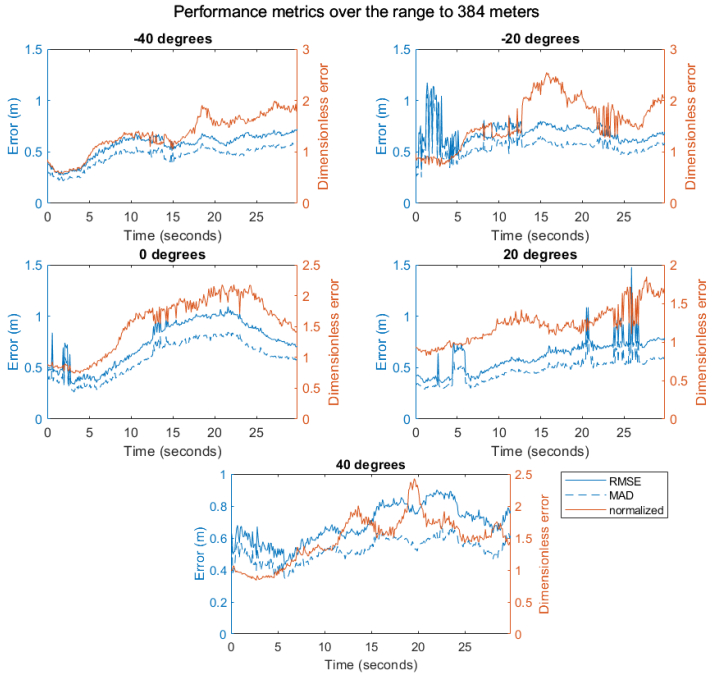

Figure B.27: Performance metrics for a non-sequential fit over the wave directions over the full range of 384 meters fitted on 5 second data with alternative current and wave direction

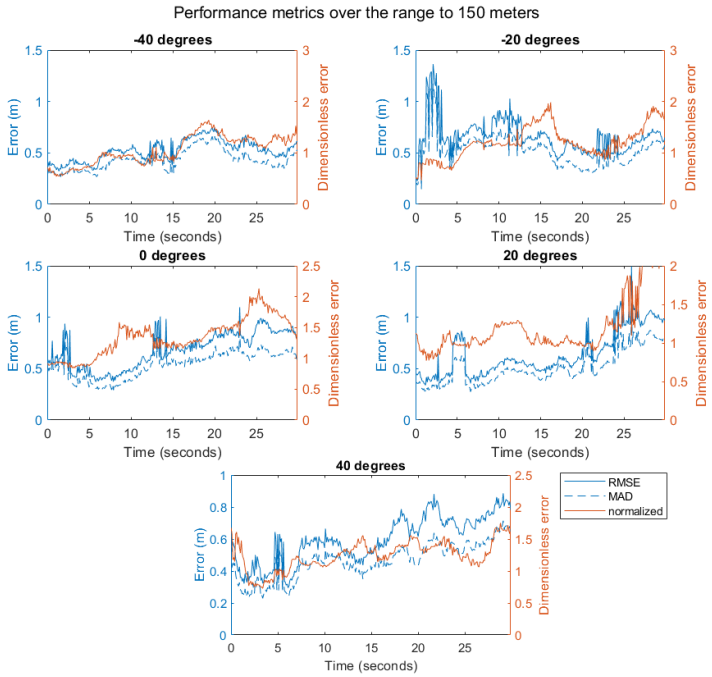

Figure B.28: Performance metrics for a non-sequential fit over the wave directions over a range of 150 meters from the radar fitted on 5 second data with alternative current and wave direction

Bibliography

[1] R. H. Byrd, R. B. Schnabel, and G. A. Shultz. Approximate solution of the trust region problem by minimization over two-dimensional subspaces. *Mathematical Programming*, 40(1):247–263, 1988. ISSN 1436-4646. doi: https://doi.org/10.1007/BF01580735.

[2] C. Eckart. The propagation of gravity waves from deep to shallow water. In *Gravity Waves*, 1952.

[3] K. Hasselmann, T.P. Barnett, E Bouws, H Carlson, D.E. Cartwright, K Enke, J A Ewing, H Gienapp, D E. Hasselmann, P Kruseman, A Meerburg, P. Muller, D.J. Olbers, K Richter, W Sell, and H Walden. Measurements of wind-wave growth and swell decay during the joint north sea wave project (jonswap). *Deut. Hydrogr. Z.*, 8:1–95, 1973.

[4] L. H. Holthuijsen. *Waves in Oceanic and Coastal Waters*. Cambridge University Press, 2007. ISBN 978-0-521-86028-4. doi: https://doi.org/10.1017/CBO9780511618536.011.

[5] IDON. *Noordzee-atlas*. Ministerie van Verkeer en Waterstaat/Rijkswaterstaat directie Noordzee, 2004. ISBN 90-369-3468-0.

[6] B. Kinsmann. *Wind Waves, their generation and propagation on the ocean surface*. Prentice-Hall,Inc., 1965. ISBN 978-981-3228-37-5. doi: https://doi.org/10.1126/science.150.3697.737-a.

[7] G. J. Komen, L. Cavaleri, M. Donelan, K. Hasselmann, S. Hasselmann, and P. A. E. M. Janssen. *Dynamics and Modelling of Ocean Waves*. Cambridge University Press, 1994. ISBN 0-521-47047-1. doi: https://doi.org/10.1017/CBO9780511628955.

[8] Krohne. Tdr & fmcw radar level transmitters principle, 2019. URL `https://instrumentationtools.com/tdr-fmcw-radar-level-transmitters-principle/`.

[9] K. Levenberg. A method for the solution of certain non-linear problems in least squares. *Quarterly of Applied Mathematics*, 2(2):164–168, 1944. ISSN 0033569X, 15524485. URL `http://www.jstor.org/stable/43633451`.

[10] D. Marquardt. An algorithm for least-squares estimation of nonlinear parameters. *Journal of the Society for Industrial and Applied Mathematics*, 11(2):431–441, 1963. doi: https://doi.org/10.1137/0111030.

[11] S.R. Massel. *Ocean Surface Waves, Their Physics and Prediction*. World Scientific Publishing Co. Pte. Ltd, 2018. ISBN 978-981-3228-37-5.

[12] R. Miche. Mouvements ondulatoires des mers en profondeur constanteou décroissante. *Ann. des Ponts et Chaussées Ch. 114*, pages 131–164,270–292 and 369–406, 1944.

[13] W.J. Pierson, J.J. Tuttle, and J.A. Wooley. The theory of the refraction of a short-crested gaussian sea surface with application to the northern new jersey coast. *Proceedings 3rd Conference of Coastal Engineering*, pages 86–108, 1952.

[14] Rijkswaterstaat. Golfhoogte ijgeul1, 2020. URL `https://waterinfo.rws.nl/#!/kaart/golfhoogte/`.

[15] A. Simanesew, K. Trulsen, H.E. Krogstad, and J.C. Nieto-Borge. Surface wave predictions in weakly nonlinear directional seas. *Applied Ocean Research*, 65:79 – 89, 2017. doi: https://doi.org/10.1016/j.apor.2017.03.009.

[16] SureWind, 2020. URL `http://www.surewindmarine.com/`.

[17] A.P. Wijaya. *Reconstruction and deterministic prediction of ocean waves from synthetic radar images*. PhD thesis, University of Twente, Netherlands, 2017.